

G-PROTEIN COUPLED RECEPTOR MEDIATED SIGNALING PATHWAYS IN
CHEMORESISTANT MELANOMA AND OVARIAN CANCER

by

MOLLY KOERTEL ALTMAN

(Under the Direction of MANDI M. MURPH)

ABSTRACT

Cellular signaling pathways are involved in numerous physiological processes such as reproduction, growth, and the development of cancer and chemoresistance. G-protein coupled receptors (GPCRs) are master regulators of many signaling pathways as they are expressed in numerous tissues types throughout the body. GPCRs are being investigated in cancer development particularly through their roles in angiogenesis, metastasis, and inflammation-associated cancer. Growth factors that bind and activate GPCRs to mediate signaling pathways involved in growth and survival include lysophosphatidic acid (LPA).

In our studies, both *in vitro* and *in vivo* methods were used to test the importance of several signaling pathways in chemoresistant cancer cell survival and tumor biology. In our studies, we found that specific Regulators of G-protein signaling (RGS) proteins are involved in modulating growth and survival pathways in ovarian cancer. Specifically, we showed that silencing of RGS10 and RGS17 proteins increases viability of ovarian cancer cells, and we further examined the role of modulating RGS10 expression on cell differentiation, proliferation, and survival pathways.

We also showed that the inhibition of autotaxin the enzyme that produces LPA is a potential therapeutic target for melanoma and how LPA mediated receptor pathways can be manipulated to overcome chemoresistance in cancer. Our most valuable observation was that our novel compounds were able to reduce tumor progression *in vivo* in a primary xenograft model of melanoma in correlation with a reduction in markers of angiogenesis. Our data serves to help better understand signaling pathways involved in the development of chemoresistance.

INDEX WORDS: G-protein coupled receptors, lysophosphatidic acid, chemoresistance, Regulators of G-protein Signaling, angiogenesis, autotaxin, melanoma, ovarian cancer

G-PROTEIN COUPLED RECEPTOR MEDIATED SIGNALING PATHWAYS IN
CHEMORESISTANT MELANOMA AND OVARIAN CANCER

by

MOLLY KOERTEL ALTMAN

B.S., University of Florida, 2006

A Dissertation Submitted to the Graduate Faculty of The University of Georgia in Partial
Fulfillment of the Requirements for the Degree

DOCTOR OF PHILOSOPHY

ATHENS, GEORGIA

2014

© 2014

Molly Koertel Altman

All Rights Reserved

G-PROTEIN COUPLED RECEPTOR MEDIATED SIGNALING PATHWAYS IN
CHEMORESISTANT MELANOMA AND OVARIAN CANCER

by

MOLLY KOERTEL ALTMAN

Major Professor: Mandi Murph
Committee: Shelley Hooks
Brian Cummings
Jason Zastre
James Franklin
Xiaoqin Ye

Electronic Version Approved:

Julie Coffield
Interim Dean of the Graduate School
The University of Georgia
August 2014

DEDICATION

I would like to dedicate this to my family, friends, and teachers that have been instrumental in my growth and development.

To my husband, DJ who has been very patient with me and given me countless hours of encouragement throughout the process of writing my thesis and preparing to defend it. He has offered advice and help when I needed it the most. I will do the same for you when it is your turn very soon. I love you and I am so thankful to have you in my life.

To my younger brother Trent and my two beautiful sisters Bianca and Lillian, thank you for showing me unconditional love and support throughout the many years I have been in school. Having such great siblings has always been a bright spot in my life.

To my parents, Angela and Mark, who have helped to support, encourage, and ground me in my academic and life pursuits.

To my grandparents, Doris and Barry, who had a significant role in my up-bringing and always kept me in their prayers.

Finally, to my high school science teachers who sparked my interest in science and my college biology professor who told me I should look into doing research at the University of Florida. Thank you for encouraging me to pursue a career in science and medicine.

ACKNOWLEDGEMENTS

For the past five years at the University of Georgia, I've had the opportunity to work with a great advisor and mentor, Dr. Mandi Murph. She is an exceptional scientist and teacher. I'm very grateful for her support and patience in training me.

I would like to acknowledge my committee members: Dr. Shelley Hooks, Dr. Brian Cummings, Dr. Jason Zastre, Dr. James Franklin, and Dr. Xiaoqin Ye. Thank you all for the guidance and advisement throughout my time in graduate school. The commitment to helping students in our department become the best scientists that they are capable of being is felt in the time that you all dedicate to teaching. I greatly appreciate having had the opportunity to work with each of you.

One of the most important lessons that I have learned from my graduate studies is how important it is to cultivate collaborations. From inter-department collaborations to building bridges to work with investigators at other institutions, the professors in Pharmaceutical and Biomedical Sciences have been very successful at both. I have seen first-hand how important it is to reach out and work with other investigators and funding-programs in order to further the development and growth of your research. The research that I am completing right now would not have happened without the collaborations that the department has built and fostered. I feel that this mindset to collaborate is very necessary in order to succeed in any field.

Thank you to my lab mates: Ha Nguyen, Wei Jia, Tian Geng, Mihir Patel, Pooya Hoozeindah, Sterling Tran and former students Jada Fambrough, Santosh Patel, and Duy Nguyen. Having you all around in the lab really made my work enjoyable.

I would also like to thank the College of Pharmacy Administrative Staff: Joy Wilson, Mary Eubanks, and Demetrius Smith, all wonderful women who have always been tremendously helpful the entire time I've been at UGA.

Finally, I would like to convey my sincere appreciation to the Stewart Endowment in the College of Pharmacy at UGA, the Alfred P. Sloan Scholar Foundation, the Georgia Cancer Coalition, the College of Pharmacy and the Graduate School at the University of Georgia for their generous financial support.

TABLE OF CONTENTS

	Page
ACKNOWLEDGEMENTS.....	v
LIST OF TABLES.....	ix
LIST OF FIGURES.....	x
ABBREVIATIONS.....	xiii
CHAPTER	
1 INTRODUCTION AND LITERATURE REVIEW	1
2 CELLULAR VIABILITY IS MODULATED BY REGULATORS OF G-PROTEIN SIGNALING RGS10 AND RGS17 IN CHEMORESISTANT OVARIACANCER CELLS.....	31
3 A NON-CANONICAL ROLE FOR RGS10 IN MTOR PATHWAY ACTIVATION THROUGH THE SMALL G-PROTEIN RHEB	56
4 REGULATOR OF G-PROTEIN SIGNALING 5 REDUCES HEYA8 OVARIAN CANCER CELL PROLIFERATION AND EXTENDS SURVIVAL IN A MURINE TUMOR MODEL.....	98
5 TARGETING MELANOMA GROWTH AND VIABILITY REVEALS DUALISTIC FUNCTIONALITY OF THE PHOSPHONOTHIONATE ANALOGUE OF CARBA CYCLIC PHOSPHATIDIC ACID	121
6 IN VITRO CHARACTERIZATION OF A NOVEL INHIBITOR OF AUTOTAXIN.....	151

7	SUMMARY AND FUTURE DIRECTIONS	171
	REFERENCES	187
	APPENDICES.....	207
	Supplementary Figure 3.1. Heatmap of proteomics data in SKOV-3 cells with RGS10 suppression.....	208

LIST OF TABLES

	Page
Table 1.1: Regulators of G-protein Signaling family members and their domain and function.....	24
Table 2.1: Potencies of chemotherapeutics following siRNA treatments in SKOV-3 cells.....	45
Table 4.1: Histological examination of tumor sections by a pathologist.....	109

LIST OF FIGURES

	Page
Figure 1.1: The Hallmarks of Cancer adapted from Hanahan and Weinberg.....	4
Figure 1.2: Production of lysophosphatidic acid (LPA) by the enzyme autotaxin.....	7
Figure 1.3: LPA Induced G-Protein Signaling Pathways Important in Cancer.....	8
Figure 1.4: Regulators of G-protein Signaling Act as GTPases for GPCR Ligand Activated Cellular Activity.....	23
Figure 1.5: Challenges in Drug-Development for Anti-cancer Therapeutics.....	29
Figure 2.1: RGS transcript expression is decreased in cisplatin resistant A2780 cells.....	41
Figure 2.2: RGS expression is decreased in multi-drug resistant HeyA8 ovarian cancer cells...	42
Figure 2.3: Percent cell viability of HeyA8 parental versus HeyA8-MDR cell lines.....	46
Figure 2.4: Cell viability measured in SKOV-3 cells treated with chemotherapeutics.....	47
Figure 2.5: SKOV-3 cell sensitivity to cytotoxic drugs is altered by modulating RGS10 and RGS17 expression levels.....	48
Figure 2.6: Cell viability curves in SKOV3 cells treated with chemotherapeutics.....	49
Figure 2.7: RGS10 alters cytotoxicity of cisplatin in multi-drug resistant HeyA8 cells.....	52
Figure 2.8: Results from BrdU proliferation assay in SKOV-3 cells.....	53
Figure 3.1: Reverse phase protein lysate array (RPPA) in treated SKOV-3 cells.....	71

Figure 3.2: Immunoblot analysis confirms RPPA detection of phospho-4E-BP1.....	73
Figure 3.3: Immunoblot analysis confirms RPPA detection of Total 4E-BP1.....	74
Figure 3.4: Immunoblot experiment results confirm phospho-4E-BP1 in HeyA8 Parental cells.....	75
Figure 3.5: Electropherogram mRNA peaks for RGS10 in SKOV-3 and HeyA8 ovarian cancer cells.....	76
Figure 3.6: Immunoblot analysis of RGS10 expression in HeyA8 and OVCAR-3 cells.....	77
Figure 3.7: Phosphorylation of mTOR is mediated by RGS10 reduction in SKOV-3 cells.....	78
Figure 3.8: Phosphorylation of 4E-BP1 is mediated by RGS10 reduction in SKOV-3 cells.....	80
Figure 3.9: INK-128 an mTOR inhibitor impedes phosphorylation in HeyA8 cells.....	81
Figure 3.10: INK-128 an mTOR inhibitor impedes phosphorylation in OVCAR-3 cells.....	82
Figure 3.11: Modulating RGS10 affects activated RheB in SKOV-3 cells.....	83
Figure 3.12: Co-immunoprecipitation with RGS10 and Rheb shows co-localization.....	84
Figure 3.13: Reducing the expression of RGS10 enlarges ovarian cancer cells via the mTOR pathway.....	88
Figure 3.14: Reducing the expression of RGS10 has marginal effects on cell size in HeyA8 parental cells.....	89
Figure 3.15: The effects of RGS10 reduction is modulated by the selective mTOR inhibitor INK-128 in SKOV-3 cells.....	90
Figure 3.16: Reducing the expression of RGS10 affects proliferation in HeyA8 parental cells.....	91

Figure 3.17: Reducing the expression of RGS10 doesn't affect proliferation in SKOV-3 cells.....	92
Figure 3.18: Our model for RGS10 involvement with Rheb and mTOR pathway activation.....	97
Figure 4.1: RGS5 inducible expression in HeyA8-MDR cells reduces proliferation.....	111
Figure 4.2: Expression of RGS5 in ovarian tumors did not significantly reduce the rate of growth, but did increase the overall survival time of mice bearing such tumors.....	113
Figure 4.3: Mice bearing RGS5-expressing ovarian tumors displayed less frequent tumor ulcerations.....	114
Figure 4.4: RGS5-expressing ovarian tumors increase the number of CD31-positive vessel-like structures.....	116
Figure 5.1: Thio-ccPA 18:1 reduces the viability of B16F10 cells in vitro.....	134
Figure 5.2: Cell line comparison of viability by thio-ccPA 18:1.....	135
Figure 5.3: The LPA3 receptor mediates viability in A375 and MeWo melanoma cells.....	138
Figure 5.3: Knockdown of the LPA3 receptor induces cell death in A375 melanoma cells.....	140
Figure 5.5: Inhibition of the LPA3 receptor using siRNA knockdown or LPA3 antagonists reduces the viability of MeWo melanoma cells.....	142
Figure 5.6: Thio-ccPA 18:1 reduces metastatic melanoma lesions in murine lungs.....	144
Figure 5.7: A subset of melanomas express high levels of the LPA3 receptor and ATX.....	145
Figure 6.1: Autotaxinab inhibits tumor progression in a melanoma mouse model.....	164
Figure 6.2: Autotaxinab inhibits angiogenesis and serum autotaxin levels.....	165
Figure 6.3: Immunofluorescence staining of Ki-67 positive cells in MeWo tumors treated with autotaxinab.....	166

ABBREVIATIONS

- ABC: ATP-binding cassette
- AKT: serine/threonine kinase; Ak strain thymoma
- ATX: Autotaxin
- BRAF: v-raf murine sarcoma viral oncogene homolog B
- DNMTs: DNA Methyl-transferases
- EDG: Endothelial differentiation gene
- EGFR: Endothelial Growth Factor Receptor
- ERK: Extracellular signaling-Regulated Kinase
- FRET: Fluorescence Resonance Energy Transfer
- GAP: GTPase accelerating protein
- GDP: Guanosine Diphosphate
- GDI: Guanine Dissociation Inhibitor
- GEF: Guanine Exchange Factor
- GGL: γ -like domain
- GTP: Guanosine Triphosphate
- GPCR: G-protein Coupled Receptor
- HDAC: Histone deacetylase
- HER: Heregulin
- LPA: Lysophosphatidic acid
- MAPK: Mitogen-activated Protein Kinase

MDR: Multi-drug Resistance

MEK: MAPK/ERK Kinase

PDZ: postsynaptic density protein (PSD95), Drosophila disc larger tumor suppressor (Dlg1), and zonula occludens-1 (zo-1)

PGP: P-glycoprotein

PH: Pleckstrin-homology domain

PLC: Phospholipase C

RAF: Rapidly Accelerated Fibrosarcoma

RAS: Rat Sarcoma

RBD: Ras-binding domain

RGS: Regulator of G-protein Signaling

CHAPTER 1

INTRODUCTION AND LITERATURE REVIEW

Introduction

The need to survive is innate in all of us, including cancer cells which have developed extraordinary means to evade growth suppression. Since pioneering studies in 1909 that isolated what is now known as oncogenic Rous sarcoma virus (RSV), the modern field of cancer has grown immensely (Weinberg 2007a). Despite the wealth of literature on the etiology of cancer and diversity within the field, the exact mechanisms behind how a normal cell transforms into a cancerous cell and develops into a chemoresistant tumor are not fully understood. A major challenge to the treatment of many cancers, including ovarian cancer and melanoma, is overcoming drug resistance that occurs in the majority of patients. Cancer patients that were once sensitive to commonly administered anti-cancer drugs relapse with tumors that are insensitive to these first-line chemotherapeutics. Patients with refractory ovarian tumors and advanced staged malignant melanoma have dismal outcomes. Understanding the molecular biology of a solid tumor and the evolutionary mechanisms behind chemoresistance is critical to developing therapeutic strategies to overcome this clinical problem.

Ovarian Cancer

Ovarian cancer is often described as the “silent killer” because many women are not diagnosed until the advanced stages of the disease because symptoms are ignored.

Ovarian cancer has the highest mortality among gynecological cancer, and ovarian cancer is the fifth most common cancer among women in the United States (Siegel et al 2013). Early intervention improves the survival rate of patients with the disease to 90%, the standard treatment regiment for ovarian cancer includes surgical debulking of the tumor followed by chemotherapy. If treated in time, at least 70% of ovarian cancers will respond to a combination of platinum- and taxane- based chemotherapy after cytoreductive surgery (Bast et al 2009). However, a major challenge to the treatment of ovarian cancer is over coming chemoresistance that inevitably develops over time in the majority of patients. Drug resistance occurs not only in cancer cells but other eukaryotes and prokaryotes as well. Resistance can be toward multiple drugs or just a single agent, chemoresistance is defined as concurrent resistance to several unrelated drugs that do not have a common mechanism after initial exposure to one drug (Tannock 2001, Tredan et al 2007). My research is focused on understanding the tumor biology of ovarian cancer and what happens when pathways involved in the development of chemoresistance are modulated in ovarian cancer.

Melanoma

Discovering what signaling pathways can be targeted to develop new therapeutics for advanced stage malignant melanoma is another area of my research. In the United States, melanoma rates are on the rise and despite research efforts, it is often a fatal metastatic cancer (Siegel et al 2013). Recently, G-protein coupled receptors (GPCRs) are being investigated as targets for therapeutics in melanoma, however, not much is known about their mutational status in cancer. Lysophosphatidic acid (LPA) a growth

stimulating factor and autotaxin (ATX) the enzyme that produces LPA, and their receptors are being looked at as targets for cancer therapy (Altman et al 2010). Although initially promising, inhibitors of the MEK/RAF pathways that were developed to treat malignant melanoma are failing because patients are developing resistance to these drugs because of mutations to specific GPCRs such as *GRM3*. (Wagle et al 2011).

The common thread between these different cell types is their ability to divide rapidly, a characteristic not seen in other mammalian somatic cells. With cancer cells there also exists a complex interplay of factors in the development of multi-drug resistance involving the tumor's microenvironment, the physiochemical properties of the chemotherapeutic agents that are administered to cancer patients, immunological host response and epigenetic changes in individual cancer cells (Tannock 2001, Tredan et al 2007). It is important to understand how these factors contribute to the development of chemoresistance in cancer cells.

The Hallmarks of Cancer

Understanding the hallmarks of cancer can give insight into the processes behind tumor development and chemoresistance. The hallmarks of cancer cell lineage as outlined by Hanahan and Weinberg (depicted in **Figure 1.1**) include: sustaining proliferative signaling, evading growth suppressors, avoiding cell death, unlimited potential for replication, inducing angiogenesis, and activating tissue invasion and metastasis (Hanahan and Weinberg 2011, Spencer et al 2006). Additional processes behind tumorigenesis now include deregulating cellular energetics, evasion of immune destruction, genome instability and mutations, and tumor-promoting inflammation among

the cancer hallmarks. Several strategies have been expanded to target cancer cells undergoing these cellular alterations (Hanahan and Weinberg 2011). Several of these hallmarks will be discussed in greater detail.

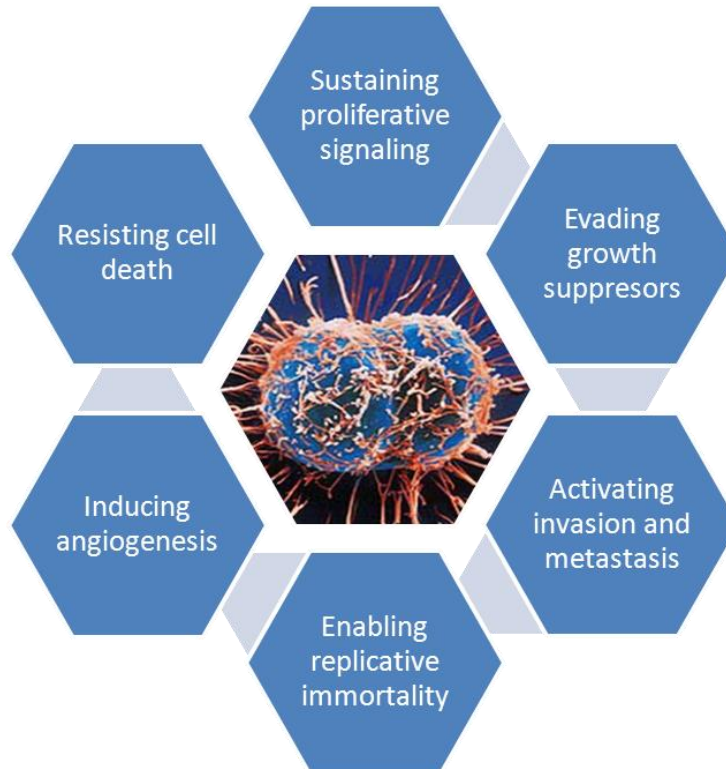


Figure 1.1. The Hallmarks of Cancer adapted from Hanahan and Weinberg. This illustration includes the six hallmark capabilities originally proposed in their 2000 perspective. Cell (2011).

Sustaining proliferative signaling

The ability of cancer cells to sustain chronic proliferative signaling is highly dependent on growth factors. Initiation factors involved in sustaining tumor growth and other physiological processes include lysophosphatidic acid (LPA) and sphingosine-1-phosphate (S1P) (Murph and Mills 2007). LPA is found at normal levels in the bloodstream and is involved in essential physiological processes including wound healing, the production of angiogenic factors, and ion channel regulation (Murph et al 2006). Biologically, women have a marginally higher amount of LPA in their serum than men. In cancer, LPA is found abundantly in the peritoneal ascitic fluid of ovarian cancer patients and the serum of women with other gynecological cancers as well as in patients with multiple myelomas (Murph and Mills 2007).

LPA is considered to be a bioactive lysophospholipid that exerts its effects through promoting proliferation, migration and survival. As both an autocrine and paracrine signaling molecule, LPA circulates in the blood and is generated from phospholipid precursors of membranes and secreted by platelets (**Figure 1.2**). The secreted lysophospholipase D enzyme, autotaxin (ATX) produces LPA from extracellular membrane lysophospholipids (Liu et al 2009a). Autotaxin was named after its first discovery as an autocrine motility factor. Expressed widely in mammalian tissues, ATX mRNA is detected at the greatest levels in the ovary, intestines, lung, lymph nodes, brain, and spinal cord (Perrakis and Moolenaar 2014). A membrane-derived lipid mediator, LPA is involved in a number of regulatory functions that mediate angiogenesis, neuronal and reproductive development (Ye et al 2002, Ye 2008).

Specifically, LPA receptors are involved in a number of physiological responses in cellular signaling and they play a role in the pathological development of many diseases including cancer, pulmonary fibrosis, and diabetes (Blaho and Hla 2011). LPA binds multiple GPCRs of the eight member endothelial differentiation gene (Edg) family. The effects of LPA on cellular proliferation are thought to be mediated by cell surface Edg receptors and subsequent activation of G-proteins (Hurst et al 2008). LPA receptor genes have been cloned for *lpa₁* and subsequent LPA receptors, LPA1/EDG-2, LPA2/EDG-4 and LPA3/EDG-7 have been identified in mammals. LPA1 and LPA2 activate the PTX-insensitive G_q and G_{12/13}, and PTX-sensitive G_{i/o}. In contrast LPA3 stimulates G_{q/11/14} and G_{i/o} but not G_{12/13}. Many of the G-protein mediated pathways activated by LPA stimulation are thought to contribute to cancer development (as depicted in **Figure 1.3**) including G_i, G_q, and G_{12/13} (Hurst et al 2009, Yu et al 2008).

Activation of LPA receptors results in a broad array of intracellular events such as increases in inositol phosphates and intracellular calcium, inhibition of adenylyl cyclase, and initiation of kinases such as protein kinase C and many other signaling pathways (Ye et al 2002). The aberrant expression of LPA receptors that are hypersensitive to growth factors and constitutively active G-proteins contribute to sustained proliferative growth in tumors. Investigating these signaling components has illuminated regulators of G-protein signaling (RGS) proteins, which terminate active G-protein signaling, as moderators of chemoresistance in ovarian cancer (Hooks et al 2010, Hurst et al 2009). Additionally, targeting specific LPA receptors expressed in melanoma has proved to be a viable anti-cancer therapeutic strategy (Altman et al 2010). These topics will be further discussed in detail in later chapters.

Many receptors are often dysregulated in cancer by unknown mechanisms. For instance, atypical autocrine activation of the endothelin 1 (ET1) axis by LPA is recognized as a common mechanism underlying the advancement of various solid tumors, including ovarian cancers (Bagnato et al 1995, Kamrava et al 2005). Endothelin 1 receptor activates G-proteins that are involved in numerous signaling pathways responsible for gene transcription, cell survival, proliferation, migration, epithelial-to-mesenchymal transition (EMT), neovascularization, and promoting chemoresistance (Capaccione and Pine 2013, Rosano et al 2013).

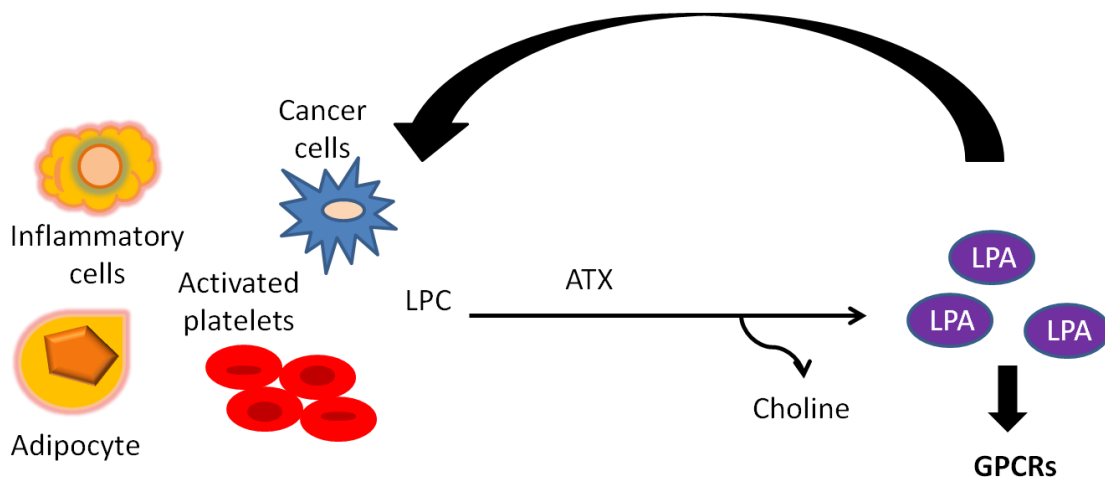
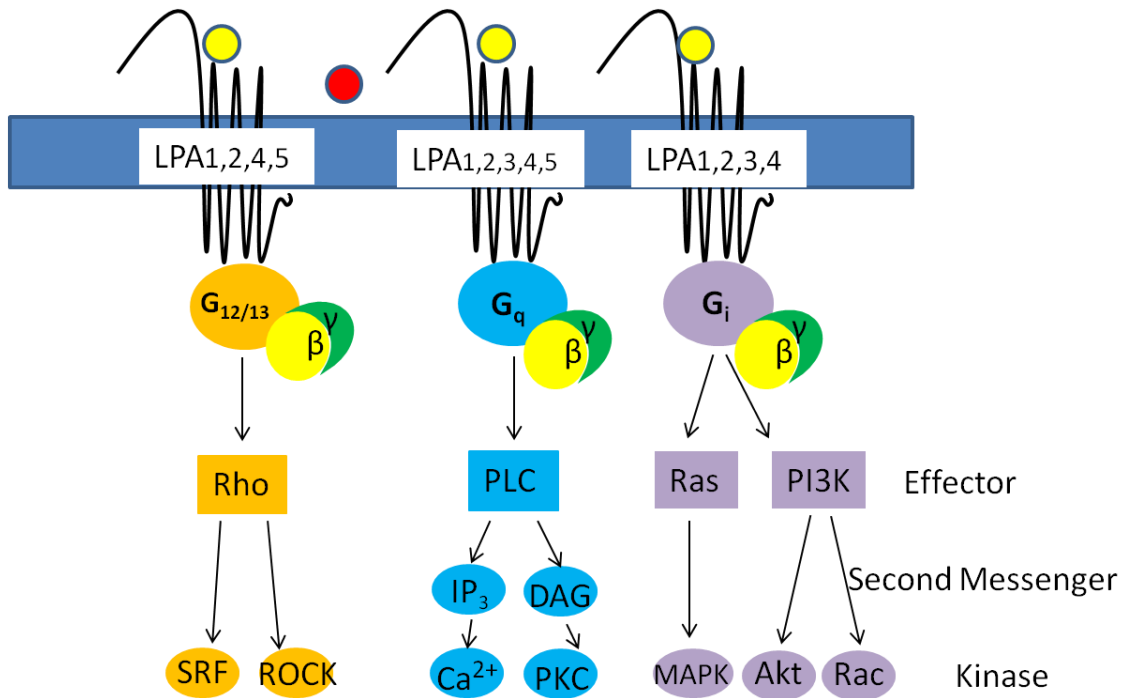


Figure 1.2. Production of lysophosphatidic acid (LPA) by the enzyme autotaxin.

Autotaxin and LPA are secreted by membrane cells and tissues. ATX hydrolyzes lysophospholipids such as lysophosphatidylcholine (LPC) to produce bioactive LPA. Levels of LPA function in a feedback loop and LPA acts on its own GPCRs (adapted from Liu et al. Cell Cycle, 2009).



Cellular Functions ie. Growth, Proliferation, Survival & Migration.

Figure 1.3. LPA Induced G-Protein Signaling Pathways Important in Cancer.

LPA acts on its own GPCRs through at least three distinct classes of heterotrimeric G-proteins: G_q, G_i, and G_{12/13} to activate multiple downstream cellular pathways and produce its biological effects. The downstream pathways include the RAS-ERK pathway through G_i and G_q; PI3-AKT pathway through G_i; PKC-GSK3β-β-catenin through G_q; Rho-CDC42 pathway through G_i which produce expression of multiple transcription factors that induce cell proliferation, growth, and production of prosurvival cytokines.

Evading growth suppressors

The survival promoting activity of LPA has been detected in several cancer cell lines including ovarian cancer and melanoma (Gupte et al 2011b, Oyesanya et al 2010). LPA is able to inhibit the transcriptional activity and quantity of the tumor suppressor p53 by activating LPA1 and/or LPA3 receptors. Subsequently, LPA exerts its effects through $G\alpha_i$ initiation of the phosphoinositol 3-kinase (PI3K) signaling cascade to facilitate nuclear export and proteosomal degradation of p53 in lung carcinoma cells (Murph et al 2007). Diminished levels of p53 protein results in decreased p53-mediated transcription and reduced caspase-3 activity which consequently leads to evasion of apoptosis, increased cell survival, maturation, and proliferation in chondrocytes (Hurst-Kennedy et al 2010). These observations may translate to other cell types that express levels of specific LPA receptors including melanoma cells which express higher levels of LPA1 and LPA3 receptors.

Inducing angiogenesis

Angiogenesis is the process by which endothelial cells create new blood vasculature networks and it is a vital process for sustained growth and development in the human body. In its normal state angiogenesis is tightly synchronized and spurs new blood vessels in orderly matrices. In cancers such as ovarian cancer and melanoma, angiogenesis is deregulated and it is a primary step in the direction of a more aggressive phenotype. Vascular endothelial growth factor (VEGF) is a secreted cytokine that signals cells to stimulate the growth of new blood vessels otherwise known as the process of vasculogenesis. Part of the vascular repair system, VEGF is able to restore the oxygen

supply to tissues when blood circulation is inadequate (Jin et al 2009). The normal function of VEGF is to create new blood vessels during development, injury or exercise, and new blood vessels to bypass blocked vessels. The pathological effects of the over-expression of VEGF contribute to vascular leakiness and disease (Weis and Cheresh 2005).

Autotaxin is another proangiogenic factor that stimulates human endothelial cells to form tubules and tumors to become more hyperemic (Clair et al 2003). An increase in VEGF enhances autotaxin expression in ovarian cancer cells resulting in more circulating LPA. Consequently, the cells also produce more LPA and VEGF receptors as well (Ptaszynska et al 2008). This corresponds to a positive feedback loop between autotaxin and growth factors involved in angiogenesis such as LPA which also stimulates VEGF production (Ptaszynska et al 2008).

RGS5 in angiogenesis

Greater RGS5 expression has been identified in tumors with high angiogenic potential. It is noted that higher RGS5 expression is also observed during ovarian angiogenesis (Silini et al 2012). In the process of pathological angiogenesis which is seen throughout tumor progression in many different cancers, RGS5 is temporally regulated and directly associated with vessel remodeling during tumor-induced neovascularization (Mitchell TS 2008). Interestingly, contrary to its role in angiogenesis, it is known RGS5 can hinder chemo-attractant receptors and control cellular processes such as migration and adhesion. GPCR signaling is thought to be inhibited by the up-regulation of RGS5 in the course of vascular maturation. RGS5 causes pericytes to be

less receptive to chemokine signaling through its GTPase accelerating protein (GAP) activity (Cho et al 2003, Mitchell TS 2008).

Angiogenesis and lymphanogenesis in melanoma

Numerous studies have shown that angiogenesis performs a vital function in lymphatic and hematological metastasis in melanoma. Primary cutaneous melanomas that are more malignant in nature are well vascularized and this is coupled to lymphatic metastasis and reduced survival. Tumor lymphanogenesis and elevated levels of VEGF have been prognostic of metastasis to the lymph nodes in melanoma (Mansfield and Markovic 2013). Lymphanogenesis is the process in which new lymphatic vessels are formed and it is linked to worse prognosis in cancer patients. Researchers have looked at the effects of LPA in inducing lymphanogenesis, metastasis, and chemokine production (Mu et al 2012).

Previous studies have shown growing evidence for investigating the autotaxin-lysophosphatidic acid affiliation in angiogenesis and lymphanogenesis. A study in zebrafish showed that embryonic silencing of LPA₁ resulted in a defect in embryonic lymph vessel development (Lee et al 2008b). Another study in mice showed that ATX through producing LPA is vital for vascular development (Tanaka et al 2006). In addition, researchers were able to show that LPA induced the production of IL-8, a proangiogenic chemokine found in ovarian cells and granulosa-lutein cells. LPA was able to exert its effects through the NF- κ B pathway both in *in vitro* and *ex vivo* model systems (Mu et al 2012). These studies provide rationale for further research into this signaling axis.

Chemoresistance in cancer

Chemoresistance in cancer is two-fold and can be attributed to both acquired and intrinsic mechanisms of tumor cell survival after exposure to chemotherapy. Examples of acquired mechanisms include: genetic mutations, gene amplifications, or epigenetic changes that alter genes involved in the cell cycle and DNA repair processes (Tannock 2001). These mechanisms can also manipulate the uptake, metabolism, or export of drugs from individual cells. In addition, some intrinsic properties of the tumor microenvironment that affect both drug penetration and drug permeability include: cell adhesion, pH, hypoxia, blood flow, nutrient supply, abnormal vasculature, ion-channels, membrane transporters, and receptors all of which can contribute to the development of multi-drug resistance in cancer (Damiano et al 2001, Minchinton and Tannock 2006). Currently, there are no completely successful pharmaceuticals that are able to avoid the onset of chemoresistance in cancer patients which presents a major clinical problem.

Selective pressure

The role of selective pressure is another important factor in tumorigenesis and the development of chemoresistance. Cells in the human body undergo mutations that provide them with a selective growth advantage that leads to their aberrant propagation (Ovens and Naugler 2012). The appearance of invasive behavior in cancer is critical to survival but not clearly understood because of its multifaceted nature. Model simulations predict that inhospitable tumor microenvironment conditions such as hypoxia and heterogenous ECM drive selective pressures on the tumor toward the selection of

aggressive cancer cell clones that result in a more malignant phenotype (Anderson et al 2006).

The genetic composition of a cancer cell may recognize its invasive potential through clonal expansion fueled by characterized selective forces in the microenvironment. Clonogenic or cancer stem cells are able to generate progeny that regenerate a tumor after it has been exposed to chemotherapy (Dean et al 2005, Minchinton and Tannock 2006). Selective conditions in the microenvironment will cause mutational inactivation of nonessential genes while eliminating mutations in essential survival genes through natural selection. Ultimately, this could give rise to a molecular signature comprised of genes required for survival and reproduction in the genomes of cancer cells (Ovens and Naugler 2012).

Through a series of bioinformatic data mining approaches, a signature was discovered corresponding to chemoresistance in serous epithelial ovarian carcinoma cells exposed to cisplatin, which also correlated with vincristine- and paclitaxel-resistance. Among the specific transcripts looked at there was a decrease in regulators of G-protein signaling (RGS) proteins, in particular RGS5, RGS10 and RGS17 (Hooks et al 2010). The role of RGS proteins in the tumor biology of ovarian cancer and their contribution to growth and survival signaling pathways are areas of research that need further study.

Growth factors facilitating chemoresistance

In cancer progression, as discussed earlier growth factors such as VEGF are critical in promoting angiogenesis. In the development of solid tumors, cancer cells that produce VEGF are able to grow and metastasize. Over-expression of VEGF and HIF-1 α

has been associated with a poor prognosis in ovarian cancer and breast cancer patients (Saponaro et al 2013, Shao et al 2012). Particularly, these tumors have an aberrant vascular network with new vessels that supply blood and nutrients to the tumor as well as leaky vessels that make drug delivery to the primary site difficult (Tredan et al 2007).

The homeostatic regulation of tissue growth and angiogenesis is disrupted within solid tumors affecting the delivery of anti-cancer drugs to the primary site (Brown and Wilson 2004). Tumor cells have the capacity to more aggressively proliferate than the cells that form blood capillaries; the rapid proliferation of tumor cells forces vessels apart. As a result, normal vascular architecture is destroyed which leads to irregular blood flow creating a population of cells distant from the blood vessels. These distal cell populations that are in close contact with one another and in high cell concentrations are particularly resistant to treatment due to their intrinsic cell adhesion properties (Carmeliet and Jain 2000).

The composition and structure of the ECM can reduce the speed of molecules moving inside the tumor (Minchinton and Tannock 2006, Tredan et al 2007). Ultimately, these characteristics of the tumor microenvironment regulate the delivery of anticancer drugs to cells that are located distal from operating blood vessels. Especially recognized in aggressive malignancies like ovarian cancer, cancer cells that are distant from blood vessels are subject to decreasing amounts of oxygen, decreasing drug concentration, nutrients and energy. Therefore, these cancer cells develop mechanisms that allow them to survive under these conditions (Brown and Wilson 2004, Minchinton and Tannock 2006).

Problems with inadequate drug penetration

A major shortcoming in anticancer drug treatment, inadequate drug penetration of chemotherapeutic agents into solid tumors is a significant obstacle restricting their therapeutic benefit. In cancer treatment, the problem of drug penetration deals with the ability of the drug to reach its target site at effective concentrations and drug permeability deals with the biological properties of the cellular membrane and the pharmacokinetics of the drug that allow for its passage through the cell membrane (Minchinton and Tannock 2006). Many anticancer drugs like cisplatin can be sequestered by macromolecules decreasing their intracellular accumulation (Sancho-Martinez et al 2012, Zastre et al 2007).

The physiochemical properties of drugs control their rate of diffusion through tissue and affect drug penetration and permeability potential in solid tumors; they include molecular weight, shape, polarity and aqueous solubility of the drug (Garattini 2007). Drug penetration also relies on how the drug is metabolized in the body and free drug is removed. These metabolic processes that affect drug permeability involve both specific and non-specific binding to tissue elements and mechanisms of uptake and retention in tumor cells (i.e. drug receptors and membrane transporters). For an anticancer drug to be successful, the drug needs to be able to circulate throughout the tumor vasculature, cross vessel walls, and pass throughout the tumor tissue to reach and effectively kill proliferating cancer cells (Tredan et al 2007).

Receptor pathways implicated in chemoresistance

Hundreds of distinctive isoforms of the different membrane receptors exist in the human body. Nearly half of all the drugs on the market today target GPCRs (Conn et al 2009). Drugs that target GPCRs have varied selectivity and affinity to cross talk with other growth factor receptors. This diversity lends to the role of GPCRs in the development of resistance to a majority of pharmacological drugs on the market (Lappano and Maggiolini 2011). Prolonged signaling downstream of activated GPCRs through constitutively active G-proteins plays a role in amplifying survival signaling in cancer. RGS proteins are able to terminate G-protein signaling downstream of GPCRs (Hooks et al 2010). The complex interplay of aberrant receptor activation and altered levels of regulatory proteins such as RGS proteins greatly influences the properties in normal cells to shift toward a balance that favors the survival of cancer cells and the development of chemoresistance.

Receptor signaling pathways are involved in the development of cancer and multi-drug resistance. Multifaceted crosstalk between G-protein coupled receptors and growth factor receptors coordinates the regulation of numerous downstream signaling molecules that are recognized in cancer growth, angiogenesis and metastasis (Lappano and Maggiolini 2011). Many growth factors such as LPA and enzymes such as ATX are responsible for the transactivation of epidermal growth factor receptor (EGFR) or Heregulin (HER) receptor through agonist stimulation of G-protein coupled receptors. The functional expression of GPCRs and EGFR are key factors to contributing to the malignant progression of colon, lung, breast and ovarian cancers (Cotton and Claing 2009, Lappano and Maggiolini 2011). These receptors are implicated in the development

of chemoresistance in breast and ovarian cancer and poor patient prognosis (Liu et al 2009b, Oyesanya et al 2010). In addition, some RGS proteins are found to be significantly down-regulated in multi-drug resistant ovarian cancer cells (Hooks et al 2010).

There are additional pathways that are able to contribute to the development of chemoresistance in cancer. The Hedgehog (HH) pathway contributes to normal stem cell maintenance and has been implicated in cancer stem cell regeneration in solid tumors. The Patched (PTC) receptor and G-protein coupled receptor Smoothed (SMO) are the key receptors that mediate the HH signal transduction cascade (Lappano and Maggiolini 2011). Closely related to HH, the WNT- β -catenin signaling pathway contributes to tumor formation most likely through PI3K and AKT survival pathways involved in a number of different cellular processes (Cotton and Claing 2009). Crosstalk between HH- and WNT-receptor mediated pathways is thought to be involved in regulating cellular responses to stimuli and has been linked to cancer development and progression. Given the mounting evidence linking HH- and WNT-associated G-protein coupled receptors to tumor development and progression, further *in vitro* and *in vivo* studies are necessary to develop therapeutic inhibitors of these pathways (Lappano and Maggiolini 2011).

G-protein coupled receptors are expressed in numerous tissue types making them a desirable receptor family to target for therapeutics. Particularly, evidence is accumulating to support GPCR involvement in cancer development particularly through their roles in angiogenesis, metastasis, and inflammation-associated cancer. The ability of GPCRs to crosstalk with growth factor receptors like the EGFR when transactivated by a receptor agonist like LPA is significant to both of their roles in cancer progression

(Lappano and Maggiolini 2011). In the following sections, the importance of G-protein coupled receptors and RGS proteins in signaling pathways will be discussed in more detail.

G-protein Coupled Receptors

GPCRs: a brief history

The G-proteins are guanosine di- or tri-phosphate (GDP or GTP, respectively) binding proteins, for which they get their name. GPCRs are 7 trans-membrane associated receptors (e.g. Rhodopsin) that are members of the largest family of membrane receptors. In 1950, Sutherland was the first to study hormones reacting with a “receptor” that would give rise to the concept of transmembrane signaling. Sutherland’s discovery of cyclic AMP and adenylyl cyclase is what many researchers note as the historical beginning of the study of G-protein coupled receptors (Hardman et al 1971). Rodbell and Birnbaumer suggested that an intermediate transducer had to exist to link discrete receptors to a common effector such as adenylyl cyclase; they collaborated to identify the heterotrimeric G-proteins (Birnbaumer & Rodbell, 1969; Rodbell et al., 1971). Ross and Gilman purified the regulatory subunits through their studies examining hormone sensitive adenylyl cyclase interactions with unknown regulatory components (Ross and Gilman 1977). They discovered that the hydrolysis of GTP allowed heterotrimeric G-proteins to pair receptors to the activation or inhibition of enzymes or ion-channels to allow hormones to modulate physiological and cellular functions (Higashijima et al 1987, Sternweis et al 1981).

2012 Nobel Prize winners in Chemistry, Lefkowitz and Kobilka were the first to theorize that there was a superfamily of receptors that included other seven helix bundle proteins that had a similar transmembrane structure as rhodopsin, one of the oldest membrane receptors, and these proteins were G-protein coupled receptors (Lefkowitz et al 1989). Structural variations to the receptors are situated in the loops in the extracellular and cytoplasmic sides of the membrane (Birnbaumer 2007). These distinctions specify ligand binding and downstream G protein specificity. GPCRs are involved in a number of physiological responses in cellular signaling, and they play a role in the pathological development of many diseases because they are expressed in many different tissues and organ systems such as the CNS, reproductive system, and cardiovascular system (Callihan et al 2011, Marinissen and Gutkind 2001).

Primarily, GPCRs can act as guanine nucleotide exchange factors (GEFs). When a ligand binds to the GPCR, conformational changes take place in the receptor that cause subsequent changes in G-protein activity, which is done by a protein family termed GEFs that exchange GDP for GTP (Cotton and Claing 2009). G-proteins act as switches that cycle between active (GTP bound) and inactive (GDP bound) states regulating the feedback and sensitization of numerous signaling pathways. The general mechanism of the activation of effector proteins associated with G protein-coupled receptors include: 1) the binding of ligand (e.g. hormone) induces a conformational change in the receptor; 2) the activated receptor binds to the $G\alpha$ subunit ; 3) the activated receptor causes conformational changes in $G\alpha$ triggering dissociation of GDP; 4) the binding of GTP to $G\alpha$ triggers dissociation of $G\alpha$ both from the receptor and from $G\beta\gamma$ dimer; 5) Ligand dissociates from the receptor; $G\alpha$ binds to the effector protein; 6) The protein has an

inherent GTPase activity that promotes the hydrolysis of GTP to GDP and causes $G\alpha$ to dissociate from the effector and reassociate with $G\beta\gamma$ reforming the inactive heterotrimeric G-protein coupled receptor complex (Bohm et al 1997). $G\beta\gamma$ works to stabilize the association of GDP with $G\alpha$ after the GTPase reaction happens (Tesmer et al 1997).

G-proteins in signal transduction

More than a dozen different G-protein effectors have been identified including a variety of enzymes and ion channels. G-proteins can act on a variety of effectors including phospholipase C and A_2 , to cause opening or closing of transmembrane channels for K^+ , Na^+ , and Ca^{2+} as well as numerous downstream signaling events including mitogen-activated protein kinase (MAPK) phosphorylation, and other cellular effects (Cotton and Claing 2009). Stimulation of multiple G-proteins which include the four major classes of $G\alpha$ subunits: $G\alpha_i$, $G\alpha_s$, $G\alpha_{q/11}$, and $G\alpha_{12/13}$ results from binding of ligand to a G-protein coupled receptor (Willars 2006). Specifically, $G\alpha_s$ subunits are involved in activating adenylyl cyclase in cAMP production; $G\alpha_i$ inhibit cAMP and are blocked by pertussis toxin; $G\alpha_q$ stimulate PLC β activation leading to the production of DAG and IP3 to stimulate calcium mobilization and PKC; and $G\alpha_{12/13}$ subunits are involved in small G-protein Rho activation (Birnbaumer 2007).

More researchers are recognizing that $G\beta\gamma$ dimers can act as an additional signaling arm of mammalian activated heterotrimeric G-proteins by stimulating phospholipase C β and IP3 formation ultimately leading to calcium mobilization from the mitochondria. In addition, $G\beta\gamma$ dimers have been shown to interact with the

glucocorticoid receptor (GR) and G $\beta\gamma$ dimers have been implicated in the regulation of endocytosis in the inhibition of intrinsic GTPase activity. G $\beta\gamma$ dimers are also mediators of downstream effectors like RAS and they can trigger AKT-mediated signals (Birnbaumer 2007).

The small G-proteins: Ras and Rho

The class of G-proteins described as “small” G-proteins are monomeric GTPases that resemble the G α subunits which share Ras gene homology with heterotrimeric G-protein complexes. Examples include the Rho-family of GTPases that are a main division of the Ras superfamily of small (~21 kDa) GTPases (Rossman et al 2005). Rho proteins much like Ras can function as binary molecular switches in response to binding GDP or GTP. Activated Rho-GTP transduces signals to downstream effectors. This pattern of signal transduction by Rho-family proteins is involved in cell-cycle progression, gene transcription, actin cytoskeleton regulation, growth and cell survival. Abnormal regulation of Ras and the Rho-family GTPases cause malignancy (Rossman et al 2005). Common among mammalian tumors are oncogenic mutations in *H-ras*, *N-ras*, and *K-ras* genes. These mutations impair the intrinsic GTPase activity of Ras proteins and cause them to be constitutively activated resulting in aberrant signaling to downstream effectors in the absence of stimuli (Castellano and Santos 2011).

Regulators of G-protein signaling (RGS)

Regulators of G-protein signaling (RGS) are known as GTPase Accelerating proteins (GAPs) specific for G α of heterotrimeric G-proteins. There are at least 30

mammalian forms all characterized by a 130 amino acid RGS core domain. The presence of an RGS domain causes at least a 50-100 fold increase in GTPase activity (McCoy and Hepler 2009). The first RGS protein to be described in the literature was Sst2p that repressed the pheromone-induced mating response in yeast *S. cerevisiae* by binding to the yeast G α protein, Gpa1 (Apanovitch et al 1998, Dohlman et al 1998). Since that time, RGS proteins have been shown in structure studies to bind to switch regions of G α , a G α subunit, and lock the structure into the transition state for the GTPase activity (Willars 2006). Stabilization of the transition state of the GTPase reaction stimulates the hydrolysis of GTP to GDP depicted in **Figure 1.4**; allowing G α to reassociate with G $\beta\gamma$ dimer and subsequently inactivating it.

RGS Domains of Interest

Most recently, some 37 genes have been identified within the human genome encoding proteins containing an RGS or RGS like domain. These RGS domains contain specific sequences that give the RGS proteins their precise activity. RGS proteins are classified into eight distinct sub-families A-H with secondary abbreviations for their function (Hollinger and Hepler 2002a, Willars 2006). The four main families of RGS proteins and their domains are listed in **Table 1.1**. Some additional domains that RGS proteins may have include: PDZ binding domain, PTB, phosphotyrosine-binding domain; RBD, Ras-binding domain; GGL, G γ -like domain; TM, transmembrane domain; DH, Dbl-homology domain; PH, Pleckstrin-homology domain (Kimple et al 2011).

An example of one of the smaller RGS proteins, RGS10 is comprised of only 167 amino acids that contain only one binding motif comprised of a 120-amino-acid RGS domain containing a conserved cysteine residue for palmitoylation (Hollinger and Hepler 2002b). In comparison, RGS14 contains an RGS domain as well as adjacent Ras binding and GoLoco domains which confer its activity as an effector antagonist and guanine nucleotide dissociation inhibitor. RGS14 has GAP activity against $G\alpha_{i/o}$ subunits, and act as guanine nucleotide dissociation inhibitors for $G\alpha_i$ through a C-terminal GoLoco motif

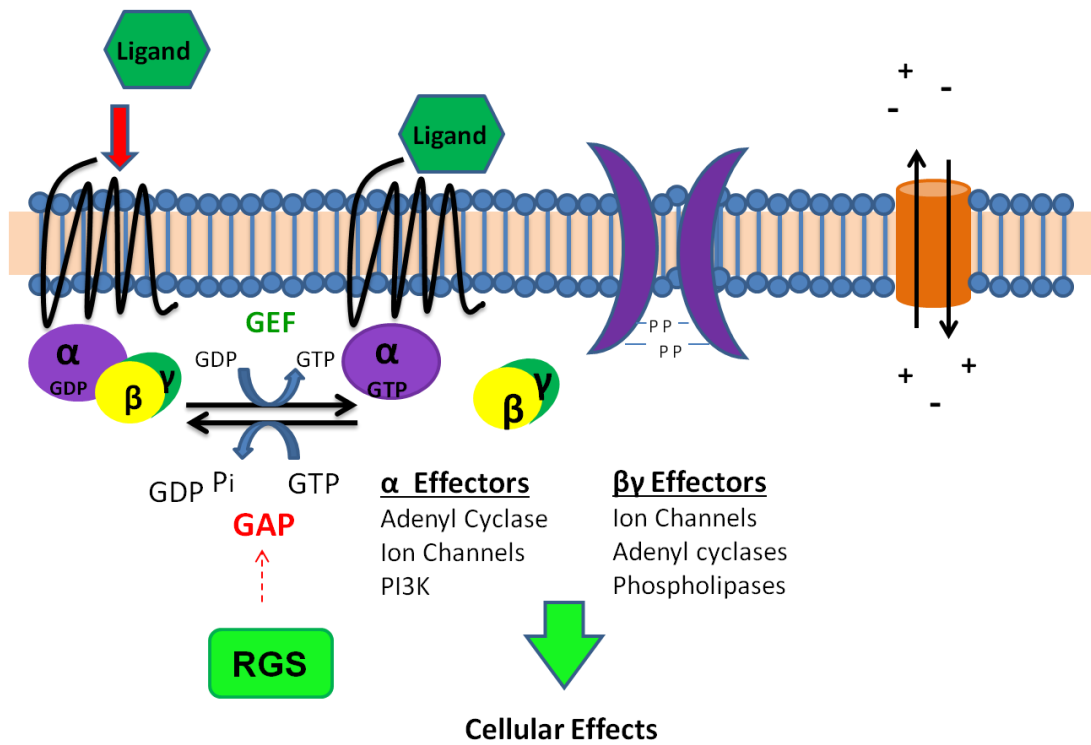


Figure 1.4. Regulators of G-Protein Signaling act as GTPases for GPCR ligand-activated cellular activity.

Table 1.1 Regulators of G-protein signaling family members and their domains and function.

<i>Sub-Family</i>	<i>RGS member</i>	<i>Domains</i>	<i>Function</i>
A/RZ	RGS17	N-terminal Cys region, RGS Box	Reduce $G\alpha_i$ signaling; involved in cell migration.
B/R4	RGS2, RGS5	RGS Box	Establishes important negative feedback circuits in vasoconstrictive hormone signaling in vascular smooth muscle mediated by 7TM receptors. Accelerates GAP activity by directly binding GPCR.
C/R7	RGS11	GGL domain	Binds $G\beta_5$ via $G\gamma$ -like domain, involved in membrane anchoring.
D/R12	RGS10	RGS Box	Reduce $G\alpha_i$ signaling; involved in cell migration.
D/R12	RGS12, RGS14	Ras-binding domain (RBDs), GoLoco motif, PDZ and PTB domains	Bind peptides and are involved in recruitment of pore-forming subunits of ion-channels. Coordinates signal transduction from receptor and/or non-receptor tyrosine-kinases and both monomeric and heterotrimeric G-protein subunits. Via GoLoco motif can act as GDIs.

domain. The GoLoco domain binds selectively to inactive G α subunits and prevents GDP release and subsequently limits G-protein activation. The presence of both a GoLoco and RGS domain within RGS14 permits for interaction with two G α subunits and binding may definitely be co-operative (Zhao et al 2013).

Additional roles for RGS proteins

In more recent studies, RGS proteins are being investigated in additional roles aside of being negative regulators of GPCR-mediated signaling. Some of these additional roles for RGS proteins include acting as Rho-A specific guanine nucleotide exchange factors (RGS-GEFs) and the ability for RGS12 to serve as a signaling axis between tyrosine kinases and G-proteins of both the G-alpha and Ras superfamilies (Siderovski and Willard 2005). Specifically, PDZ-RhoGEFs contain two additional domains that elicit their effects via their dbl-homology (DH) and pleckstrin homology (PH) domains. DH domains aid in the exchange of GDP for GTP on monomeric G-proteins and the PH domains help to anchor Rho-GEFs to other signaling molecules and cause their subcellular localization. These findings point toward RGS proteins being involved in GAP-independent functions in undefined cellular processes including their function as scaffolding proteins and non-canonical functions in the nucleus (Sethakorn et al 2010).

Recently, the mechanism by which RGS proteins target the nucleus and their nuclear function in protein synthesis has become more intensely studied by researchers. Eukaryote initiation factors (eIFs) control mRNA translation and protein synthesis. The eIF2 creates a complex with GTP and the initiation factor Met-tRNA with the 40s

ribosomal subunit that is necessary for protein synthesis. Several of the RGS domain proteins (RGS2, RGS4, RGS6, RGS10, and RGS16) are proposed to have the inherent ability to localize to the nucleus. It is theorized that their ability is through nuclear targeting motifs or passive diffusion with the exception of areas outside the RGS domain that would prohibit them from entering the nucleus (Sethakorn et al 2010).

Many RGS proteins are involved in signal transduction and downstream phosphorylation events that can lead to MAP Kinase cascade signaling and various cellular effects. For example, the finding that RGS3 co-localizes with several Smads including Smad4 led to investigating the potential for RGS3 to regulate TGF- β signaling and cellular effects (Yau et al 2008). The cytokine TGF- β is responsible for cell growth, survival, and cellular phenotype is mainly controlled by the phosphorylation of specific Smads (R-Smad/Smad4) required for recruitment to the nucleus and gene transcription. In earlier studies, a truncated version of RGS3 was found to localize to the nucleus when transfected into CHO cells. Other examples of RGS proteins localizing to the nucleus include RGS10 endogenous expression in Neuroglia cells and ectopic and endogenous expression of RGS2 and RGS10 in COS7 cells (Sethakorn et al 2010).

RGS10

Specifically, RGS10 is of interest in our studies looking at signaling pathways involved in proliferation and chemoresistance in ovarian cancer. RGS10 has been extensively studied in the brain and to some extent in osteoclast formation in bone diseases. RGS10 expression is enriched in many regions within the brain such as the striatal regions and the dentate gyrus granule cells, unlike, RGS5 that is expressed at

lesser amounts in the brain (Gold et al 1997). RGS10 is also dominantly expressed in osteoclasts and the RGS10-null mutation results in a severe osteopetrosis phenotype in mice, characterized by shortened limbs and stature. In a study using RGS10 null mice, researchers found that the loss of RGS10 impairs the RANKL-induced RGS10/calmodulin-[Ca²⁺]_i oscillation-calcineurin-NFATc1 signaling pathway in osteoclast differentiation (Yang and Li 2007). These studies clarify a role of RGS10 in differentiation and development.

RGS5

A member of the R4 subfamily, RGS5 is also of interest in our studies looking at the functional role of RGS proteins in ovarian cancer. RGS5 in addition to its RGS domain has an amino terminus that aids with sub-cellular localization. There are also transcript variants of RGS5 that lack the amino terminus causing its inability to act at the cell membrane (Bansal et al 2007). The physiological function of RGS5 is not well characterized because of the lack of transgenic mice models with altered RGS5 gene expression (Cho et al 2003). There is robust expression of RGS5 in mural cells of angiogenic vessels particularly within the pericytes of both capillaries and arterioles. In mice, the expression of RGS5 reflects the abundance of tyrosine kinase receptor for platelet-derived growth factor beta (PDGFR β) and its ligand PDGF. Mice embryos that don't have either the PDGF receptor or the ligand lack Rgs5 and pericytes (Bansal et al 2007). These studies clarify a role for RGS5 in vascular development and angiogenesis.

Research Rationale

In the United States alone, millions of patients are diagnosed each year with some form of cancer (Jemal et al 2013). This presents a serious economic and emotional burden to the average American. Especially, since most cancers like ovarian cancer are not diagnosed until the later stages of the disease which are particularly difficult to treat. In an effort to develop new cancer therapies, the process of drug development is taking an increasing amount of time and money to develop a single drug with limited success. There is a tremendous need for basic science, drug discovery screening, and testing compounds in vitro and in vivo for efficacy and toxicity in cancer model systems both in industry and academia; the drug development pipeline is depicted in **Figure 1.5**. There lacks an adequate picture of the cellular processes behind why the majority of patients become resistant to drug therapy.

The goal of this thesis research was to characterize signaling pathways that mediate chemoresistance in two different cancers: melanoma and ovarian cancer. My research focused on understanding the novel role RGS proteins have in mechanisms that are behind chemoresistance in ovarian cancer and on studies to further characterize a novel therapeutic target for melanoma. Ultimately, my goal was to improve knowledge of signaling pathways to aid in targeted patient therapy and to help develop potential new multi-component therapeutic strategies.

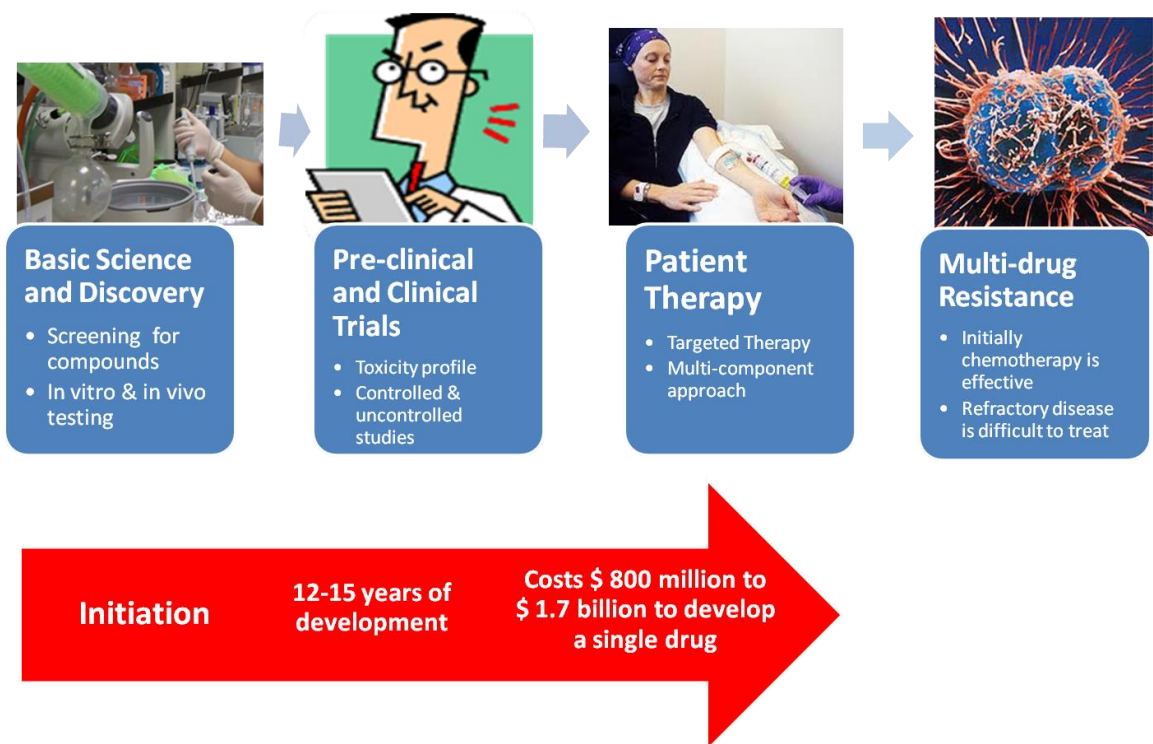


Figure 1.5. Challenges in Drug-Development for Anti-cancer Therapies.

Research Objectives

- 1) Determine whether modulating specific RGS protein expression affects the viability of ovarian cancer cells treated with first-line chemotherapeutics.
- 2) Determine whether modulating specific RGS protein expression affects cellular proliferation in ovarian cancer cells.
- 3) Determine the contribution of silencing RGS10 to cellular survival signaling pathways.
- 4) Determine the contribution of RGS5 modulation to tumor biology and progression in an *in vivo* model of ovarian cancer.
- 5) Determine the effects of novel autotoxin inhibitors using *in vitro assays* in melanoma and other cancer cell lines.
- 6) Determine the effects of novel autotoxin inhibitors in tumor growth in an *in vivo* melanoma model.

CHAPTER 2
CELLULAR VIABILITY IS MODULATED BY REGULATORS OF G-PROTEIN
SIGNALING RGS10 AND RGS17 IN CHEMORESISTANT OVARIAN CANCER
CELLS

Introduction

Chemoresistance is a substantial problem in ovarian cancer and prevents a cure until the mechanisms behind it can be uncovered. Patients with refractory ovarian tumors have poor prognoses and any improvement in long-term outcomes will require a better understanding of the process. In defining why ovarian cancer cells become resistant to platinum and taxane drugs, the answers may elucidate therapeutic targets and diagnostic tools that predict drug responsiveness. Through a series of bioinformatic data mining approaches, we discovered a signature corresponding to chemoresistance in serous epithelial ovarian carcinoma cells exposed to cisplatin, which also correlated with vincristine- and paclitaxel-resistance. Leading among the transcripts involved was a significant decrease in Regulators of G protein Signaling (RGS) proteins, in particular RGS10 and RGS17. Thus, my research project sought to better understand the functional consequence of altering RGS proteins and their role in tumor biology and cellular survival pathways. The data presented in this chapter was produced from experiments performed or assisted by Molly Altman. Work in this chapter contributed to the

publication entitled “Regulators of G-Protein Signaling RGS10 and RGS17 regulate chemoresistance in ovarian cancer” (Hooks et al 2010).

Ovarian cancer

Ovarian cancer has the highest mortality among gynecological cancer, and ovarian cancer is the fifth most common cancer among women in the United States. The disease is more common in industrialized nations; for example in the U.S., females have a 1.4% to 2.5% (1 out of 40-60 women) lifetime chance of developing ovarian cancer but in underdeveloped nations the risk is less (Jemal et al 2010). More than half of the deaths from ovarian cancer occur in women between 55 and 74 years of age, indicating that older women are at the highest risk for the disease, although germ-line ovarian cancer can affect young girls. Moreover, one quarter of ovarian cancer deaths occur in women between 35 and 54 years of age (Jemal et al 2010).

The exact causes of ovarian cancer are unknown, however, there are risk factors associated with developing the disease such as age, a family history of cancer, and hormone exposure to estrogen without progesterone (Bast et al 2009). Ovarian cancer is termed the “silent killer” because many women do not realize they have cancer until they develop a more advanced stage of disease. Often times there are symptoms in the earlier stages of disease and these symptoms are overlooked because they resemble gastrointestinal symptoms, which could be related to other medical conditions and unrelated to cancer.

Early surgical and first-line chemotherapeutic treatment of ovarian cancer improves the survival rate of patients with the disease to 90%. The standard treatment

regimen for ovarian cancer includes surgical debulking of the tumor followed by chemotherapy. If caught in time, at least 70% of ovarian cancers will respond to a combination of platinum- and taxane- based chemotherapy after cytoreductive surgery (Bast et al 2009).

Chemoresistance in ovarian cancer

However, a major challenge to the treatment of ovarian cancer is over coming multi-drug resistance or chemoresistance that inevitably develops over time in the majority of patients. Chemoresistance is the specific resistance developed by tumor cells against the action of therapeutic agents that makes current cancer treatment refractory (Tannock 2001). Therefore, finding ways to resensitize cancer cells to chemotherapy or developing novel derivatives of chemotherapeutic drugs are major goals of cancer treatment development.

An initiation factor that enhances ovarian cancer cell survival includes lysophosphatidic acid (LPA) which functions by activating multiple LPA receptors or G-protein coupled receptors (GPCRs) which regulate intracellular signaling cascades (Hooks et al 2010). Lysophosphatidic acid (LPA) and sphingosine-1-phosphate (S1P) are considered to be bioactive lysophospholipids. LPA and S1P are membrane-derived lipid mediators that are involved in a number of regulatory functions (Ye 2008). They are generated from phospholipid precursors of membranes and secreted by platelets. It has been implicated that LPA's effect on cellular proliferation is mediated by cell surface G protein-coupled receptor(s) also known as Edg receptors (Hurst et al 2008).

G protein-coupled receptors (GPCRs) are 7 trans-membrane associated receptors that are members of the largest family of membrane receptors. They are involved in a number of physiological responses in cellular signaling and they play a role in the pathological development of many diseases. GPCRs are guanine nucleotide exchange factors (GEFs) that when bound by a ligand are responsible for conformational changes in the receptor and subsequent changes in G-protein subunit activity (Cotton and Claing 2009).

A critical regulator of GPCR intracellular signaling activation includes GTPase accelerating proteins (GAPs) or Regulators of G-protein signaling (RGS) proteins which blunt the signal. There are over 20 human RGS proteins in the family and many of these have unknown roles in specific GPCR pathway deactivation (Hurst et al 2009). Preliminary data has demonstrated that ovarian cancer cells endogenously express RGS proteins that function to suppress LPA signaling.

Multi-drug resistance is a significant problem in treating refractory ovarian cancer patients and cellular mechanisms involved in chemoresistance need to be further investigated (Hooks et al 2010). Ovarian cancer is characterized by rapid and uncontrolled proliferation of cancer cells within the developing tumor. Based on preliminary studies, we predict that suppressed expression of RGS proteins is a major molecular mechanism that allows ovarian cancer cells to resist treatment with chemotherapeutics by enhancing cell survival and blunting drug-toxicity. The following sets of experiments tested the hypothesis that specific RGS proteins function to regulate ovarian cancer survival signals. We hypothesized that decreasing RGS proteins promotes

chemoresistance by enhancing survival signaling in the presence of first-line chemotherapeutic drug treatment in serous epithelial ovarian carcinoma.

Materials and Methods

Cells and Reagents

We purchased SKOV-3 cells from American Type Culture Collection (Manassas, VA). These cells were maintained in McCoy's 5A medium (Mediatech, Inc., Manassas, VA.) supplemented with 10% FBS (PAA Laboratories, Inc., Etobicoke Ontario, Canada). Both the parental and the MDR-HeyA8 cell line, a taxane-resistant line generated by the long-term exposure to paclitaxel, were kind gifts from Dr. Isaiah J. Fidler (Department of Cancer Biology, University of Texas M.D. Anderson Cancer Center, Houston, TX) and are presented elsewhere (Kamat et al 2007). MDR-HeyA8 cells are maintained in RPMI 1640 medium with 300 ng/mL paclitaxel with 15% FBS and HeyA8 cells are maintained in RPMI medium with 15% FBS. Lysophosphatidic acid (18:1,1-oleoyl-2-hydroxy-sn-glycero-3-phosphate) was purchased from Avanti Polar Lipids, Inc. (Alabaster, AL) and reconstituted in 0.1% fatty acid free BSA immediately prior to use. Cisplatin, docetaxel, paclitaxel and vincristine were purchased from Sigma-Aldrich (St. Louis, MO). siRNA was purchased from Ambion (Austin, TX). RGS plasmids were purchased from the UMR cDNA Resource Center (Rolla, MO).

Bioinformatics

Gene expression profiling data were acquired through the NCBI Gene Expression Omnibus (GEO) DataSets. The datasets GSE7556 (Buys et al 2007), GSE15709 (Li et al

2009) and GSE2058 (unpublished) were downloaded and mined using Microsoft Excel prior to further analysis. Hierarchical clustering analyses was performed using Cluster developed by the Eisen lab and the display of hierarchical clustering graphs utilized TreeView (Eisen et al 1998) as previously described (Murph et al 2009). Visual representation of the data into box plots was done with GraphPad Prism 5 (Graph-Pad Software, Inc., La Jolla, CA).

RGS Gene Modulation

SKOV-3 cells were simultaneously plated and transfected using siPORT NeoFX transfection reagent (Ambion, Austin, TX) according to the manufacturer's protocol for reverse transfection. Cells were transfected in parallel with RGS-targeted siRNA and negative control (RISC-free) or scrambled siRNAs for each experiment. The siGENOME RISC-free siRNA is a suitable negative control because it will not be taken up by the RNA-Induced Silencing Complex (RISC). A transfection mix containing 10 nM siRNA and 2 μ L siPORT NeoFX reagent in OptiMem (Invitrogen) was added to each well of a 24-well plate, followed by 30,000 cells in normal growth medium. Cells and transfection mix were incubated for 24 hours at 37°C at which point the media was changed to fresh SKOV-3 growth medium and/or cells were re-plated into either 96-well or 12-well plates. Assays were performed and samples taken for transcript expression analysis 72 h after transfection. Knock-down experiments using siRNA in HeyA8 cells were performed using Dharmacon ON-TARGET*plus* SMARTpools (Thermo Scientific, Lafayette, CO) and transfected using Dharmafect reagent, according to the manufacturer's recommended protocols.

Cellular viability assays

Approximately 5,000 SKOV-3 cells were seeded in triplicates in 96-well plates in 10% FBS DMEM and allowed to attach for 24 hours prior to gene manipulation or treatment with the indicated concentrations of cisplatin, vincristine, paclitaxel or docetaxel for 48 hours. After 48 hours in the presence of chemotherapy, a cell viability assay was conducted by removing all media from the 96-well plate and replacing it with serum free media containing CellTiter-Blue® reagent (Promega Corporation, Madison, WI) as previously described (Hasegawa et al 2008) and measured using SpectraMax M2 model microplate reader (Molecular Devices, Sunnyvale, CA).

Assessment of Active Cell Proliferation via BrdU Incorporation Assay

Approximately 5,000 SKOV-3 cells were plated into 96-well plates in the presence of 10% fetal bovine serum. The plated cells were incubated for 18 h at 37°C in 5% CO₂ and then transfected with siRNA for RISC-free or RGS10. Transfected cells were incubated for an additional 24 h prior to treatment with BrdU, a thymidine analogue. Incorporation of BrdU is a measure of cellular proliferation and is measured by fluorescent intensity. For BrdU cells were pulse treated for 1 h with a BrdU analog. Cells were then stained according to the protocol provided by the manufacturer (Millipore, Billerica, MA). Plates were scanned using Cellomics ArrayScan (Thermo Fisher) and the number of cells was automatically captured. Representative images are shown. Each condition had 6 replications and 8 fields per well were analyzed using high content scanning software. The data was retrieved from the manufacturer's software and results were plotted with GraphPad Prism.

Quantitative real-time PCR

For HeyA8 parental and multi-drug resistant cells, mRNA was isolated using Trizol reagent (Invitrogen) and quantified prior to cDNA synthesis. The cDNA was synthesized using a Superscript II kit (Invitrogen) and a Mastercycler Pro (Eppendorf AG, Hamburg, Germany). Following cDNA synthesis, quantitative real-time polymerase chain reaction was performed using Superscript III kit for RT-PCR (Invitrogen) and Master Mix containing Power SYBR Green reagent (Applied Biosystems, Foster City, CA). Transcript expression was assessed using a 7900HT Real-Time PCR System from Applied Biosystems (now Life Technologies, Carlsbad, California). Reactions were normalized using the housekeeping gene GAPDH and calculations were performed according to the $\Delta\Delta CT$ method. Primers used were based on algorithm-generated sequences from Primer Bank ([http:// pga.mgh.harvard.edu/primerbank/](http://pga.mgh.harvard.edu/primerbank/)).

RGS10 Forward: GACCCAGAAGGCGTGAAAAGA,

RGS10 Reverse: GCTGGACAGAAAGGTCATGTAGA,

RGS17 Forward: CAGAGGAAGTCT TGTCCTGGT,

RGS17 Reverse: CAAGCAAGCCAGAAAAGTAGGT,

GAPDH Forward: GCCAAGGTCATCCATGACAACCT,

GAPDH Reverse: GAGGGGCCAT CCACAGTCTT.

Statistical analysis

Experimental data was analyzed for statistical differences using an analysis of variance (ANOVA) followed by Bonferroni's Multiple Comparison test or Tukey's test

between groups, where indicated. * $p < 0.05$ ** $p < 0.01$ and *** $p < 0.001$ indicate the levels of significance. Error bars are standard error of the mean.

Results

Analysis of RGS expression changes in ovarian cancer models of chemoresistance

We have recently demonstrated that RGS proteins significantly suppress LPA signaling in ovarian cancer cells (Hurst et al 2008, Hurst and Hooks 2009) and that LPA mediates AKT activation (data not shown but included in the original paper within the appendix) and survival signals in cancels (Hurst and Hooks 2009, Murph and Mills 2007). Given these connections, we explored possible roles for RGS proteins in ovarian cancer chemoresistance. To determine whether altered RGS expression correlates with acquired chemoresistance, we assessed RGS expression in multiple datasets downloaded from the NCBI Gene Expression Omnibus DataSets that contain whole-genome expression data in cultured ovarian cancer cell lines before and after acquired chemoresistance. Dataset GSE15709 describes changes in gene expression in parental chemo-sensitive A2780 cells and A2780 cells resistance to cisplatin using quintuplicate sample (Li et al 2009). In the initial study, Nephew and colleagues chronically treated drug-sensitive cells with increasing concentrations of cisplatin. Following multiple rounds of clonal selection of increasingly resistant cells, they generated a multi-drug resistant cell line. Analysis of changes in RGS gene expression revealed that several RGS transcripts-RGS2, RGS3, RGS5, RGS10, RGS12, RGS16, and RGS17 were decreased in chemoresistant cells. These RGS transcripts were sufficient to distinguish between parental and resistant cell lines in hierarchical clustering analysis of expression data. To select RGS probes

distinguishing chemo-resistant from parental cells, we first applied Welch's t-test to all of the probes contained within the array for RGS transcripts. The result was then visualized with a heatmap after hierarchical clustering. This supervised approach revealed a clear correlation between decreases in selected RGS transcripts and the cisplatin-resistant phenotype (**Figure 2.1A**). We further compared the level of expression from individual RGS transcripts in parental A2780 and cisplatin-resistant cells using GSE15709 and determined that RGS2, RGS5, RGS10, and RGS17 were significantly lower in resistant cells than in parental cells (**Figure 2.1B**, *** $p < 0.001$, * $p < 0.05$). Multiple probes for RGS5 and RGS10 were present on the array, distinguished in the figure as RGS5 and RGS5', and RGS10 and RGS10'.

To further confirm that expression of these RGS transcripts is reduced in drug resistant cancer cells, we directly measured expression of RGS transcripts in parental Hey-A8 ovarian cancer cells and taxane-resistant derivatives of this cell line (commonly referred to as Multi-drug resistant or MDR-HeyA8 cells), although they retain cisplatin sensitivity (**Figure 2.3**). RNA was isolated from both cell lines, and transcript expression was quantified using real time RT-PCR as described in the methods. We again found that RGS2 was decreased in the HeyA8 MDR cell line; however, no change was observed in RGS5 expression (**Figure 2.2**). Taken together, these data show that RGS2, RGS10, and RGS17 transcripts are commonly down-regulated in acquired chemoresistance in three distinct ovarian cancer cell lines resistant to three distinct chemotherapeutics, while RGS5 was down-regulated in two of the models. This suggests that these RGS proteins have a broad role in cell survival in the presence of multiple chemotherapeutic agents.

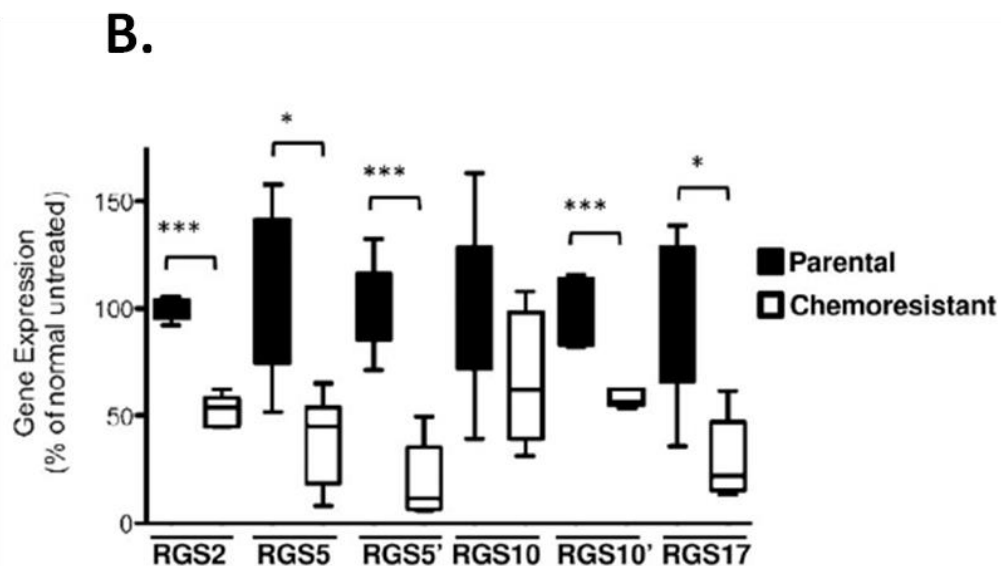
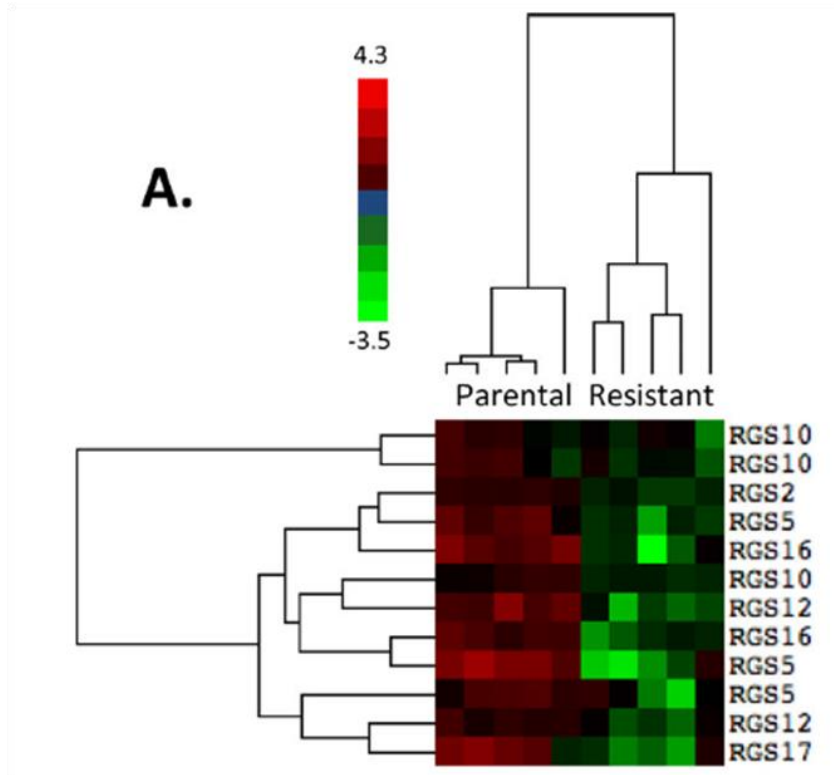


Figure 2.1. RGS transcript expression is decreased in cisplatin resistant A2780 cells. (A) A hierarchical clustering heat map is shown depicting changes in RGS expression between parental A2780 cells (n = 5) and chemoresistant (resistant) A2780 cells (n = 5). As indicated in the side bar, red coloring represents a high level of comparative expression and green indicates a lower level (range 4.3 to -3.5). (B) A box plot depicts the expression levels of multiple RGS transcripts in parental and drug resistant A2780 cells exposed to long-term cisplatin. RGS2, 5, 10, and 17 were significantly down regulated in repeated datasets and are presented here. Where multiple probes for the same gene were included on the microarray chip, these are distinguished with ('). *p < 0.05, ***p < 0.001 between groups, parental vs. chemoresistant cells.

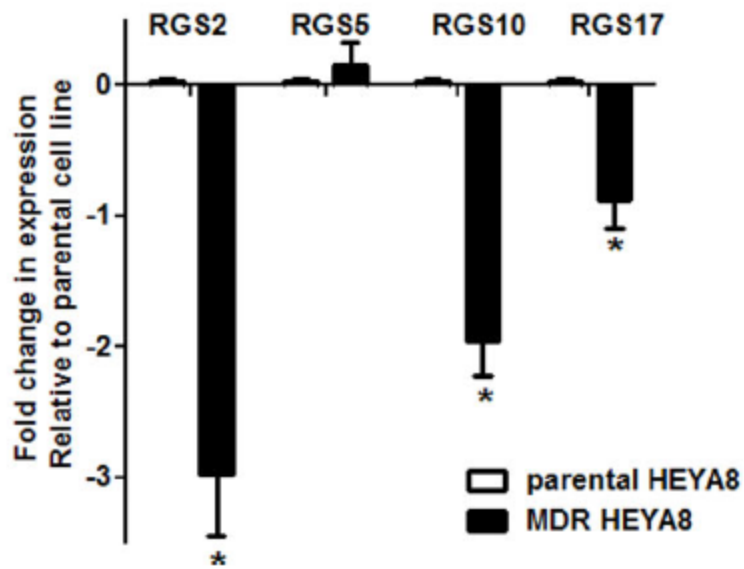


Figure 2.2. RGS expression is decreased in multi-drug resistant HeyA8 ovarian cancer cells. RGS expression is decreased in paclitaxel-resistant HeyA8 cells compared to parental HeyA8 cells. RNA was isolated from parental and MDR-HeyA8 cells as described, and the expression of RGS2, RGS5, RGS10 and RGS17 transcripts was normalized to *b2*- microglobulin as an internal standard prior to the comparison between parental and multi-drug resistant HeyA8 cells. The fold change in expression relative to vehicle controls was calculated by the $2^{-\Delta\Delta C_t}$ method. * $p < 0.05$, normalized control vs. RGS groups.

Cisplatin treatment lowers expression of RGS10 and RGS17 in ovarian cancer cells

The above analysis suggests a correlation between acquired chemoresistance and decreased expression of RGS2, RGS5, RGS10 and RGS17 transcripts. Lower expression observed in chemoresistant cancer cells could reflect acutely down-regulated RGS transcripts or selection for cells expressing reduced RGS transcripts. To determine if exposure to chemotherapeutics acutely causes inhibition of RGS transcripts, we treated SKOV-3 ovarian cancer cells with cisplatin for 24 and 48 hours, isolated RNA, and quantified RGS transcript expression. Cells were treated with 100 μ M cisplatin, which

represents approximately an IC80 dose, as determined by cell viability dose response curves (**Figure 2.4**).

Expression of RGS10 and RGS17 was reduced following a 48 h exposure to cisplatin (* $p < 0.05$). Significant reductions in transcript levels were RGS10, and RGS17 transcripts were significantly reduced in the MDR-HeyA8 cell line also observed just 24 hours after cisplatin treatment (data not shown included in publication). To assess whether the changes were transient, we further determined the level of transcript expression after treatment with 100 μ M cisplatin for 48 hours as described above, followed by removal of the drug and growth in fresh media for an additional 48 hours. Surprisingly, RGS10 and RGS17 transcript levels remained significantly lower two days following removal of the drug as compared to control cells, suggesting persistent effects on RGS expression following cisplatin exposure (data not shown included in publication) (Hooks et al 2010).

To determine the effects of more chronic exposure, we also treated cells with IC30, IC50, and IC80 doses of cisplatin for 72 and 96 hour incubations. Unfortunately, exposure times greater than 48 hours using an IC80 dose led to significant cell death, and treatment of cells with lower doses did not have a significant effect on RGS10 and RGS17 transcript expression (data not shown). No significant changes were observed in RGS2 or RGS5 expression following cisplatin exposure, and changes in RGS10 and RGS17 were not consistently observed following exposure to therapeutic doses of vincristine or docetaxel (data not shown).

RGS10 and RGS17 expression levels regulate the cytotoxicity of chemotherapeutics

We next determined if directly inhibiting RGS expression could recapitulate the observed loss of chemosensitivity. For the following experiments, we focused on RGS10 and RGS17 because they were down-regulated in three independent models of chemoresistance, and, unlike RGS2, they selectively deactivate G_i family G-proteins (Heximer et al 1997, Mao et al 2004), which are known to regulate survival pathways (Hurst and Hooks 2009, Long et al 2005a, Nunn et al 2006). To determine if the loss of RGS10 and/or RGS17 expression could be directly linked to a change in sensitivity to chemotherapeutics, we determined the effect of siRNA mediated knock-down of RGS10 and/or RGS17 on cell viability in the absence or presence of chemotherapeutics. Transfection of siRNA duplexes targeted at RGS10 and RGS17 resulted in 75-85% reduction of each respective transcript whether transfected alone or in combination (**Figure 2.5A**). We first assessed changes in cell viability mediated by changes in RGS expression levels in the absence of any chemotherapeutic drug. Reduced expression of either RGS10 or RGS17 resulted in significantly higher cell viability 72 hours after siRNA transfection (**Figure 2.5B**).

We further assessed the ability of RGS10 and RGS17 levels to affect cell death induced by three cytotoxic chemotherapy agents: the platinum compound cisplatin, the taxane compound docetaxel, and vincristine. Platinum and taxane compounds are used in first-line chemotherapy regimens in ovarian cancer (paclitaxel usage in ovarian cancer is an FDA-approved labeled indication while docetaxel is off-label for this indication).

Table 2.1. Potencies of chemotherapeutics following siRNA treatments in SKOV-3 cells

	Scrambled siRNA	RGS10 siRNA	RGS17 siRNA
Vincristine Potency (nM IC ₅₀ +/- SEM)	5.85 +/- 1.3	12.8 +/- 2.9	58 +/- 8.7
Docetaxel Potency (nM IC ₅₀ +/- SEM)	0.886 +/- 0.432	10.7 +/- 3.7	85 +/- 23
Cisplatin Potency (μ M IC ₅₀ +/- SEM)	10.4 +/- 1.1	23.0 +/- 1.2	27.9 +/- 1.2

Vincristine is used for other tumor types (acute lymphoblastic leukemia, Hodgkin's lymphoma, multiple myeloma, etc.), but was included in the analysis to determine how broad the effects of RGS proteins were. SKOV-3 cells display low sensitivity to cisplatin, requiring micromolar doses for significant cell death. In contrast, these cells are highly sensitive to vincristine and docetaxel (**Figure 2.4**). Cell viability was determined following 48 hour treatment with 100 μ M cisplatin, 100 nM vincristine, or 100 nM docetaxel in cells transfected with either negative control siRNA, RGS10 siRNA, RGS17 siRNA or both RGS siRNA constructs. The percent cell viability (normalized to cell number in the absence of drug, to account for the effect on overall cell growth as shown above) was significantly higher in cells with reduced RGS10 or RGS17 expression levels (**Figure 2.5C**). Dose response curves show that lowering either RGS10 or RGS17 transcript levels resulted in a decrease in the potency of cisplatin, vincristine, and docetaxel (**Figure 2.6A-C**). The potencies of these three chemotherapeutic agents following siRNA treatment in SKOV-3 cells are contained in **Table 2.1** (Hooks et al 2010).

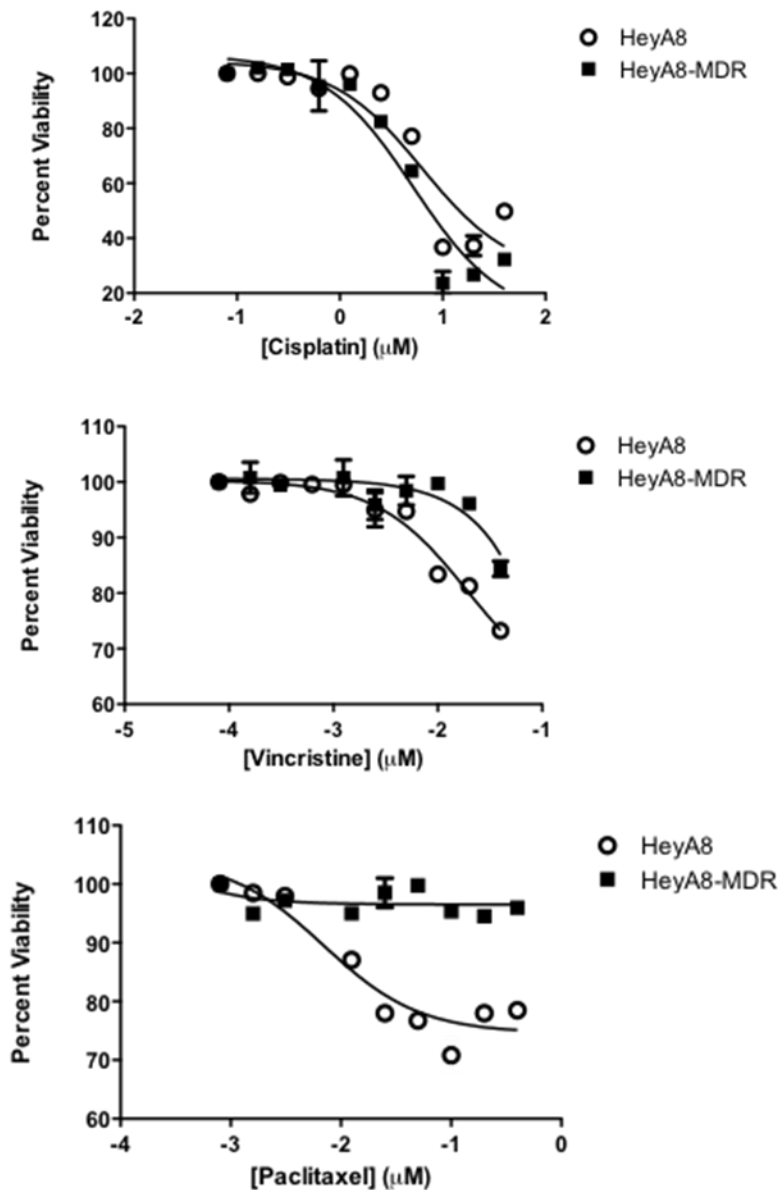


Figure 2.3. Percent cell viability of HeyA8 parental versus HeyA8-MDR cell lines.

Hey A8 and HeyA8-MDR cells were plated into 96 well plates for drug treatments at 5,000 cells per well. Cells were treated with concentrations of cisplatin, vincristine, and paclitaxel for 48 hours. After 48 hours, the media was removed and replaced with serum-free media containing cell-titer blue reagent. Plates were read approximately 8 hours later and absorbance was read and percent viability was calculated using the untreated control cells absorbance readings. All data was graphed in GraphPad Prism.

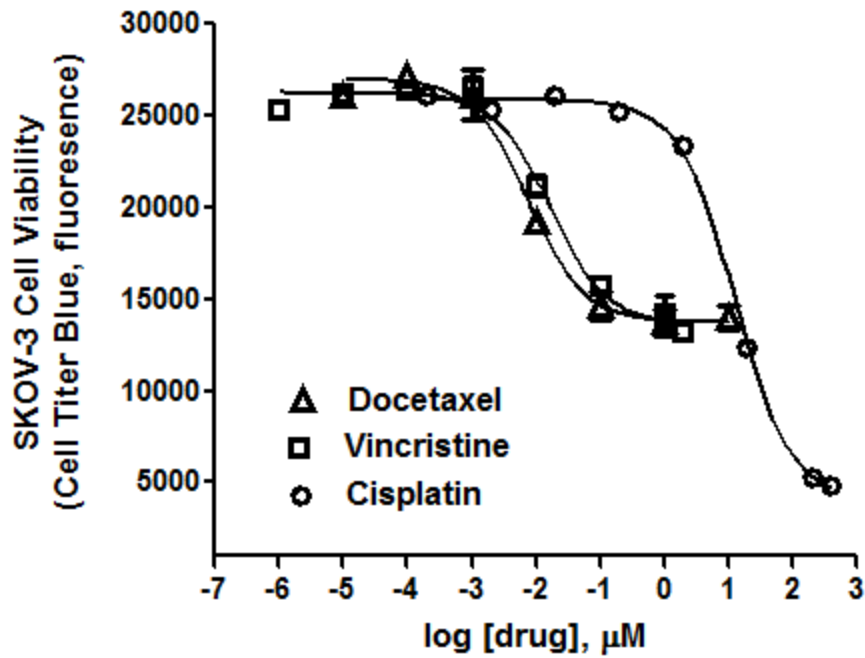


Figure 2.4. Cell viability measured in SKOV-3 cells treated with chemotherapeutics. Potency of Docetaxel, vincristine, and cisplatin was determined after 48 hours of drug treatment using cell titer blue metabolic viability assays. Drug concentrations are graphed in log μM doses.

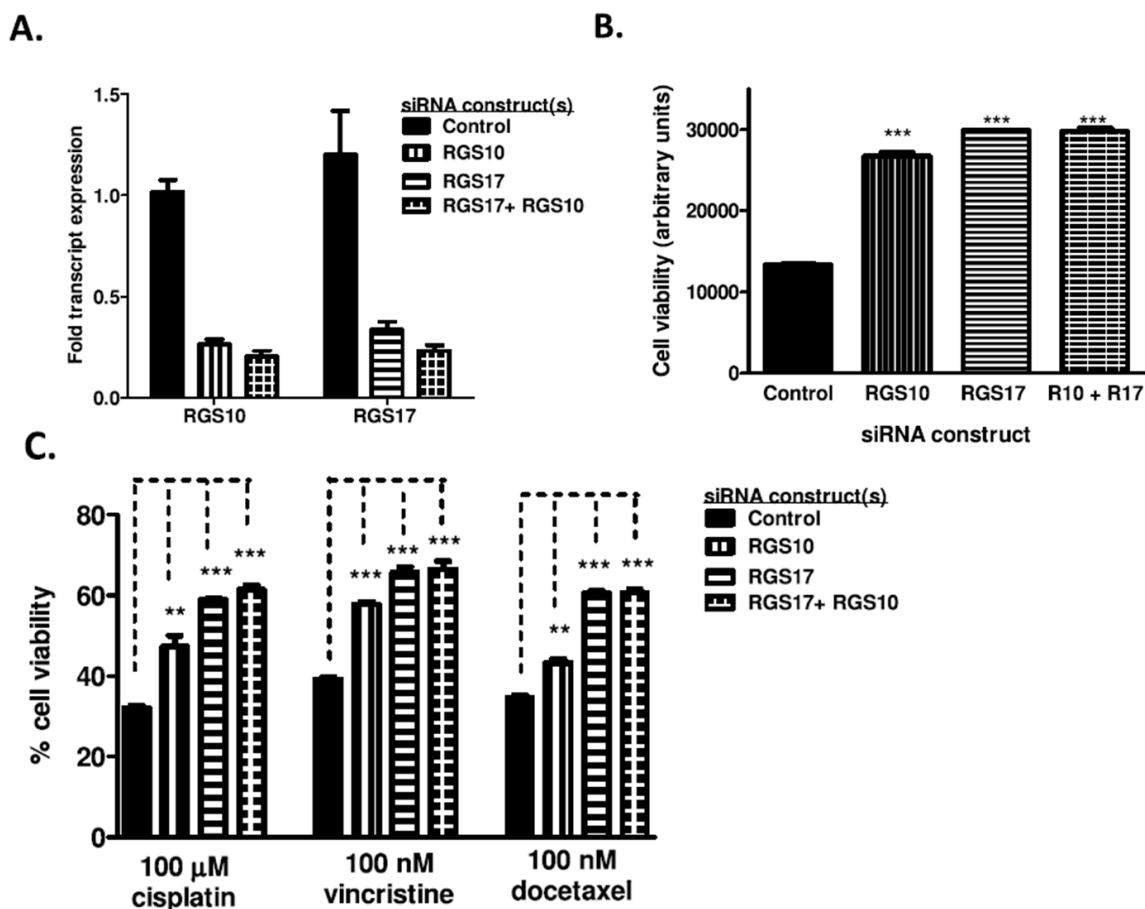


Figure 2.5. SKOV-3 cell sensitivity to cytotoxic drugs is altered by modulating RGS10 and RGS17 expression levels. (A) Transcript levels of RGS10 and RGS17 were determined using quantitative RT-PCR 72 hours after transient transfection with the indicated siRNA constructs. RGS transcript levels were normalized to GAPDH transcripts and reported relative to negative control-siRNA treated cells. (B) Overall cell viability was determined in SKOV-3 cells 48 hours following siRNA transfection in the absence of drug using CellTiter-Blue colorimetric cellular metabolism assays. (C) Cytotoxic drugs were added to cells at the indicated doses 24 hours after siRNA transfection, and cell viability was determined 48 hours after addition of drug. Data are shown normalized to cell viability in the absence of drug (100%). *: $p < 0.05$, **: $p < 0.01$, ***: $p < 0.001$.

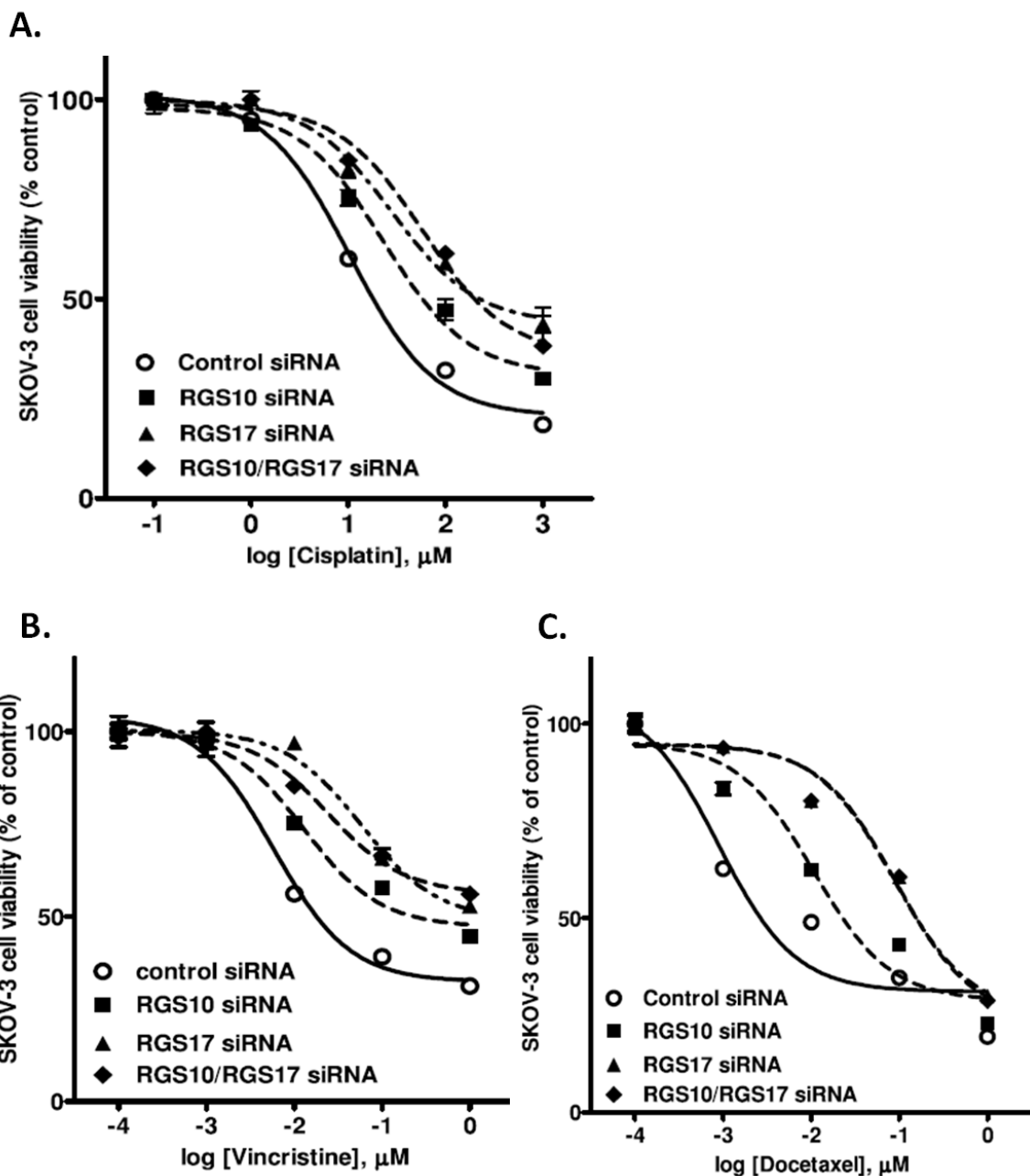


Figure 2.6. Cell viability curves in SKOV3 cells treated with chemotherapeutics. (A-C) siRNA-mediated knock-down of RGS10 or RGS17 alone or in combination resulted in a right-shifted dose response curve of cisplatin (A), vincristine (B), or docetaxel (C) toxicity in SKOV-3 cells.

Simultaneous knock-down of RGS10 and RGS17 did not markedly enhance the effect of individual knock-downs. These data suggest that ovarian cancer cells may have survival signals which are normally blunted by endogenous RGS10 and RGS17 expression. Notably, the fold decrease in RGS10 and RGS17 transcript expression achieved following siRNA treatment that led to this increase in cell survival is comparable to that observed following cisplatin exposure, indicating that cisplatin exposure itself may reduce the sensitivity of SKOV-3 cells to cisplatin by inhibiting RGS10 and RGS17 expression.

We next performed the reciprocal experiment by over-expressing either RGS10 or RGS17 in SKOV-3 cells, with the expectation that this may increase the potency of cisplatin-induced cell death. Indeed, in some experiments RGS10 and RGS17 over-expression did enhance chemotherapeutic potency, but the effect was not consistent, varying with transfection efficiency (data not shown). It is possible that the endogenous levels of RGS10 and RGS17 are sufficiently high to provide near- maximal GAP activity, such that only extremely high levels of transient transfection produce a significant change in activity levels. Nonetheless, the decrease in cytotoxicity of chemotherapeutics following RGS10 or RGS17 knock-down clearly indicate that the suppression of these proteins promotes cell survival and suggest a decrease in the expression levels of RGS10 or RGS17 are sufficient to lower ovarian cancer cell sensitivity to chemotherapeutic cytotoxicity.

MDR-HeyA8 sensitivity to cisplatin cytotoxicity is regulated by RGS10 expression

To confirm that our observation that direct suppression of RGS expression by siRNA decreases sensitivity to chemotherapeutic drug induced cytotoxicity was not specific to SKOV-3 cells, we also determined the effect of RGS knock-down on cell viability, cell proliferation, and cell death in Hey-A8 cells. RGS10 siRNA resulted in selective loss of RGS 10 transcript (**Figure 2.7A**). However, in our hands RGS17 siRNA resulted in non-selective knock-down in HeyA8 cells, unlike the selective effects seen in SKOV-3 cells. Thus, we report here the effects of only RGS10 siRNA. Transient siRNA transfection resulted in approximately 80% knock-down of RGS10 transcript MDR-HeyA8 cells and the effects on cell viability and death were strikingly similar to those observed in SKOV-3 cells. Knock-down of RGS10 transcript resulted in a small but significant and reproducible increase in cell viability (**Figure 2.7B**). Further, the relative cell viability in the presence of micromolar doses of cisplatin (normalized to that seen in the absence of drug) was significantly higher with RGS10 siRNA knock-down (**Figure 2.7C**). Also similar to results in SKOV-3 cells, we confirmed that RGS10 knockdown blunts cell death stimulated by a 10 μ M dose of cisplatin (data not shown), while it has no effect on cell proliferation in SKOV3 cells, as measured by BrdU incorporation (**Figure 2.8**). Thus, RGS10 knockdown has similar effects in SKOV-3 cells and MDR-HeyA8 cells.

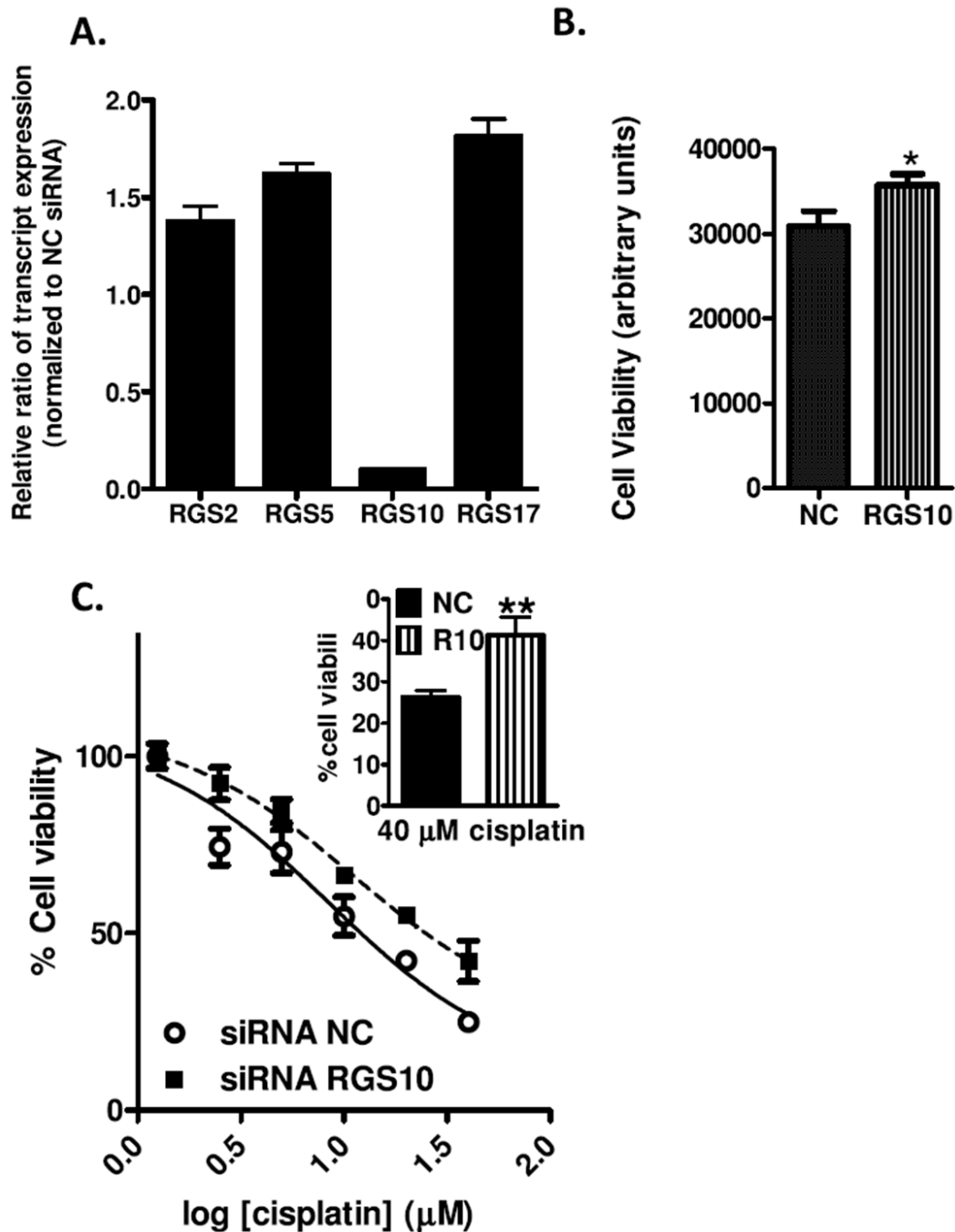


Figure 2.7. RGS10 alters cytotoxicity of cisplatin in multi-drug resistant HeyA8 cells. (A) RT-PCR indicates selective knock-down of RGS10 48 hours following transfection of MDR-HeyA8 cells with RGS10 siRNA. (B) siRNA mediated knock-down of RGS10 results in increased cell growth as determined by viability assays. *: $p < 0.05$ (C) Cisplatin was added at the indicated doses 24 hours after siRNA transfection, and cell viability was determined 48 hours after drug treatment. Data are shown normalized to cell viability in the absence of drug (100%). Inset: Relative cell viability of RGS10 siRNA transfected MDR-HeyA8 cells is significantly higher than control transfected cells in the presence of 40 μM cisplatin. **: $p < 0.01$.

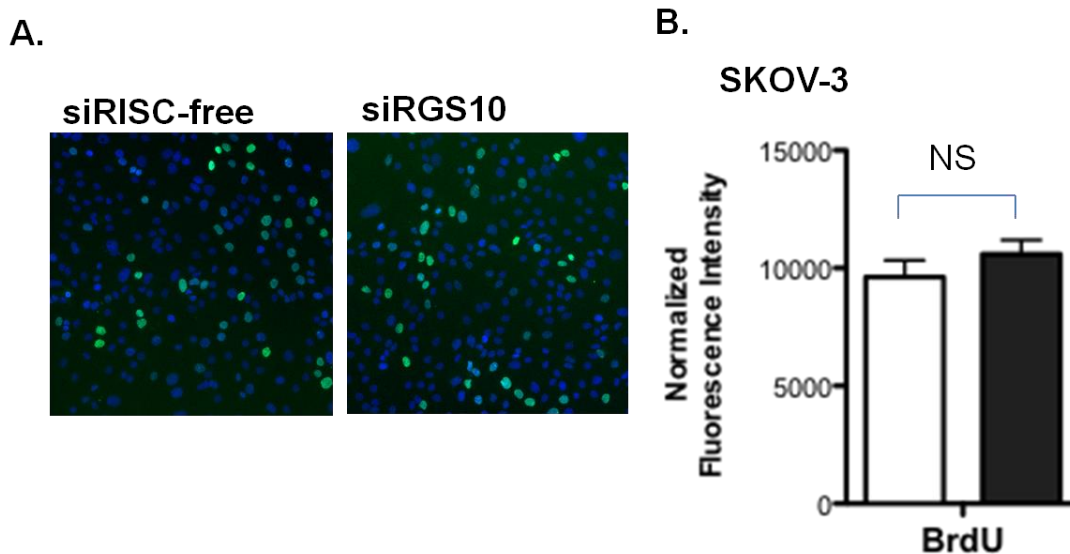


Figure 2.8. Results from BrdU proliferation assay in SKOV-3 cells. A. Images taken with cellomics machine of SKOV-3 cells transfected with Negative non-targeted siRNA after BrdU treatment and siRNA for RGS10 48 hours following transfection. B. SKOV-3 cells transfected with siRNA for RGS10 after BrdU treatment. Cells were also pretreated with BrdU a thymidine analogue, incorporation of BrdU is a measure of cellular proliferation. The average fluorescent intensity in each field in each siRNA condition is shown for BrdU. N=2 independent experiments with 6 wells per condition and >7 fields per well. Error bars are standard error of the mean (SEM).

Discussion

Chemoresistance is a formidable obstacle to treating patients that become refractory and resistant to first-line anti-cancer drugs. Patients that relapse have a poor prognosis and strategies to overcome resistance are greatly needed to further understand the mechanisms underlying chemoresistance in ovarian cancer. Our collaborative study is the first to implicate certain RGS proteins, specifically RGS10 and RGS17, in the development of chemoresistance in ovarian cancer.

Herein, we discussed in this thesis chapter is the characterization of the cellular survival response to chemotherapeutic drugs when RGS protein expression is modulated in SKOV-3 and HeyA8 MDR ovarian cancer cell lines. We first set out to characterize the expression patterns of RGS10 and RGS17 in these cell lines as well as the effects of reduced RGS expression on cell viability in the presence of first-line chemotherapeutic drugs. In addition, our collaborators on this work observed the ability of RGS10 and RGS17 to blunt activation of the survival factor AKT (data not shown) (Hooks et al 2010). Taken together this data proposes that reduced expression of RGS proteins confers cancer cells the ability to survive in the presence of chemotherapy.

The mechanisms by which cancer cells become resistance to first-line chemotherapeutics such as paclitaxel and cisplatin are not clearly understood. Our collaborative work is the first to suggest that RGS10 and RGS17 are able to moderate endogenous survival pathways. RGS proteins are known as GAPs specific for $G\alpha$ of heterotrimeric G-proteins. There are at least 30 mammalian forms all characterized by a 130 amino acid RGS core domain. The presence of an RGS domain causes at least a 50-100 fold increase in GTPase activity (McCoy and Hepler 2009). The importance of RGS

proteins in mediating the strength and duration of survival signals makes them essential proteins for many physiological effects. Reduced RGS expression can have profound effects in the cardiovascular and respiratory systems (Labuda et al 2013, Qin et al 2012).

Lacking well characterized functional domains outside of the RGS domain, RGS10 and RGS17 are among the smallest of the RGS proteins. Both RGS10 and RGS17 have sites for palmitoylation which control their subcellular localization (Mao et al 2004). In the clinic, RGS17 has been shown in expression databases to decrease with advanced disease staging in ovarian cancer (Rhodes et al 2004). In contrast there are studies that show overexpression of RGS17 in human lung and prostate cancer promotes tumor cell proliferation (James et al 2009). Before our studies, RGS10 expression changes have not been reported in ovarian cancer. These observations point toward the effects of RGS expression as cell-type dependent.

Our study was driven by whole-genome expression changes reported for acquired chemoresistance in ovarian cancer. The changes in RGS transcripts that were observed overlapped with previously published LPA-induced transcriptome data that identified transcripts that were regulated after LPA treatment in OVCAR-3 and SKOV-3 cells (Buys et al 2007, Murph et al 2009). This is not surprising because LPA is known to induce activation of G-proteins upon binding to GPCRs.

Although there is support for the involvement of LPA survival pathways in the connection between RGS proteins and chemoresistance, there are discrepancies in our data that suggest LPA agonist activation of GPCRs is not the complete story. We and our collaborators have observed inconsistencies in LPA-induced activation of AKT and other downstream phosphorylation events that will be discussed in chapter 3.

CHAPTER 3

A NON-CANONICAL ROLE FOR RGS10 IN MTOR PATHWAY ACTIVATION THROUGH THE SMALL G-PROTEIN RHEB¹

¹ Altman, MK., Murph, MM., To be submitted to *Molecular Cancer*.

Abstract

The regulator of G-protein signaling 10 (RGS10) is a GTPase activating protein that accelerates the hydrolysis of GTP and therefore inactivates G alpha subunits, ultimately terminating signaling. We previously demonstrated that the absence of RGS10 enhances ovarian cancer cell survival and facilitates chemoresistance, yet the molecular mechanism regulating this outcome was evasive. Herein, we report activation of the mTOR pathway is significantly enhanced following RGS10 suppression in ovarian cancer cells. Knockdown of RGS10 resulted in a significant increase of activated Rheb, a GTPase protein that shuttles between its GDP- and GTP-bound forms to activate mTOR. Immunoblotting experiments and reverse phase protein lysate arrays indicate that knockdown of RGS10 results in an increase in the phosphorylation of mTOR (Ser-2448) and the eukaryotic translation initiation factor 4E binding protein 1 (4E-BP1) at Thr-37/46 residues. Since this occurs in the absence of any agonist stimulation, we propose that RGS10 is antagonizing mTOR signaling through the small G-protein Rheb. Phosphorylation of mTOR and 4E-BP1 by RGS10 suppression is inhibited or abolished only after exposing cells to temsirolimus or INK-128, respectively.

Furthermore, suppressing RGS10 increases cell size and further enlargement is achieved by agonist stimulation (via lysophosphatidic acid) and reversed by mTOR inhibition. Nascent protein synthesis increased somewhat among cells with reduced RGS10 expression. Since 4E-BP1 phosphorylation is a hallmark of aggressive cancer phenotypes, our data suggests that RGS10 suppression mediates this effect through an increase in RheB-GTP and thus a gain in the activation of mTOR signaling in ovarian cancer cells.

Introduction

Regulators of G protein signaling (RGS) proteins are GTPase activating proteins (GAPs) that accelerate the hydrolysis of GTP from G alpha protein subunits, thus inactivating these proteins and preventing continued signaling. More specifically, the RGS10 protein increases the hydrolysis of GTP from the activated forms of $G\alpha_{i3}$, $G\alpha_o$ and $G\alpha_z$, but not $G\alpha_s$ (Hunt et al 1996). The classical model of cellular signaling through seven transmembrane, G protein-coupled receptors (GPCRs) along the plasma membrane asserts that RGS proteins attenuate heterotrimer-linked, G-protein signaling initiated as a result of receptor activation due to extracellular agonist binding; therefore, they control the master switch which regulates the signal duration.

There are at least 30 RGS and RGS-like, domain-containing proteins; among these, the RGS10 protein has a very basic structure. Although it is not the smallest RGS protein, the RGS10 protein has little more than the common 120 amino acid RGS domain containing a conserved cysteine residue for palmitoylation (Hollinger and Hepler). Its lack of structural complexity enhances the enigmatic nature of the protein and provides no clues to its role in regulating cellular signaling. In addition, RGS10-deficient mice are viable (Lee et al , Yang and Li), which implies its role affects signal modulation and it is not absolutely essential for life. However, since the gene is broadly conserved across species, including human, Rhesus monkey, dog, cow, mouse, rat and chicken, it suggests an influential role for RGS10 in biological systems.

Non-traditional roles for RGS proteins aside from acting primarily as a GAP for G-proteins include acting as guanine nucleotide exchange factors (RGS-GEFs) and the ability for RGS12 to serve as a signaling axis between tyrosine kinases and G-proteins of

both the G-alpha and Ras superfamilies (Siderovski and Willard 2005). Many RGS proteins are involved in signaling transduction and downstream phosphorylation events that can lead to MAP Kinase cascade signaling and various cellular effects (Sambi et al 2006).

Recent studies are investigating how RGS proteins target the nucleus and their nuclear function. Presently, it is known that many RGS proteins have the capability to localize to the nucleus. Examples include RGS10 endogenous expression in Neuroglia cells and ectopic and endogenous expression of RGS2 and RGS10 in COS7 cells. Several RGS domain proteins (RGS2, RGS4, RGS6, RGS10, and RGS16) are proposed to have the inherent ability to localize to the nucleus. It is theorized that their ability is through nuclear targeting motifs or passive diffusion with the exception of areas outside the RGS domain that would prohibit them from entering the nucleus (Sethakorn et al 2010). Their function while in the nucleus is still not fully understood, however, because of intense study there are several functions of RGS proteins in the nucleus currently known that include; acting as scaffolding proteins in transcription binding complexes with CREB and RGS protein involvement in protein synthesis (Sethakorn et al 2010).

One example of nuclear functioning of RGS proteins includes RGS2 acting to regulate protein synthesis. Eukaryote initiation factors (eIFs) control mRNA translation and protein synthesis. The heterotrimeric GTPase, eIF2 creates a complex with GTP and the initiation factor Met-tRNA with the 40s ribosomal subunit that is necessary for protein synthesis. A pentameric guanine nucleotide exchange factor (GEF) protein, eIF2B acts to exchange GDP for GTP on the eIF2 complex. In a yeast two hybrid study it was shown that eIF2B epsilon has a surface interaction area that binds RGS2 and

prevents the exchange of GDP for GTP. Functionally this results in reduction of translation efficiency and the inhibition of protein synthesis (cite 48 in RGS non-canonical paper Sethakorn, 2010). The function of RGS2 in protein synthesis is attributed to the 37 amino acid binding sequence that is conserved among other RGS proteins at the N-terminus of the RGS domain and may confer similar functioning in other RGS proteins as well.

The mammalian (or mechanistic) target of rapamycin (mTOR) is a serine/threonine-protein kinase in the phosphatidylinositol 3-kinase(PI3-K)/Akt signaling pathway, signal integrator and thus a master regulator of cell physiology. It forms the catalytic subunit of two intracellular complexes, mTORC1 (mTOR-Raptor-GβL) and mTORC2 (mTOR-Rictor-GβL), which regulate the processes of growth, survival and protein translation. The mTORC1 complex phosphorylates the eukaryotic translation initiation factor 4E binding protein 1 (4E-BP1). Through the phosphorylation of 4E-BP1, mTOR is thus able to govern cell growth. In addition, mTOR is also a crucial upstream activator of Akt, which allows it to affect cell survival and proliferation.

A chief regulator of protein synthesis downstream of mTORC1, 4EBP1 is a cap-binding protein that negatively regulates eIF4E translation initiation (Hsieh et al 2012). When 4EBP1 becomes phosphorylated by mTORC1, it is removed from eIF4E which allows the formation of the translation initiation complex at the 5' end of mRNAs. Inhibition of mTOR signaling has shown promise as a cancer therapeutic in several different cancer types. A specific mTORC1 inhibitor, INK128 inhibits cancer cell migration and decreases the expression of the four main pro-invasion genes (Mazzoletti et al 2011).

In more recent years, highly sophisticated inhibitors are being used to target proteins that are involved in key translational complexes. Rapamycin and its analogues temsirolimus and everolimus are inhibitors of mTOR that rapidly prevent the activity of mTORC1 and causes a progressive shutdown of mTORC2. Inhibition of mTOR signaling has shown promise as a cancer therapeutic in several different cancer types. A specific mTORC1 inhibitor, INK128 inhibits cancer cell migration and decreases the expression of the four main pro-invasion genes (Guo and Kwiatkowski 2013, Weinberg).

Rheb, the Ras homolog enriched in brain protein, is a member of the small GTPase superfamily of monomeric proteins. The structure of Ras includes two switch regions (I and II) within Ras that are greatly altered when Ras cycles between GTP and GDP-bound form. An effector of Ras, PI3-K binds to switch region I when Ras is GTP-bound (Tee et al 2005). Rheb functions to bind and activate mTOR (Long et al) and it is essential for coupling all upstream signals including growth factors to the activation of mTORC1 (Efeyan and Sabatini 2010, Goorden et al 2011). A well-characterized regulator of Rheb is the tuberous sclerosis complex 2 (TSC2) protein (Zhang et al), which inhibits Rheb using its GAP activity (Tee et al). TSC2 is also a known tumor suppressor that forms a complex with TSC1 and negatively regulates mTORC1. Thus, Rheb stimulates the phosphorylation of mTOR and 4E-BP1, ultimately regulating cell growth (Inoki et al). There is also evidence that Rheb activation of mTOR is effected by mutations to critical residues in the switch regions of the protein. These observations suggest that Rheb is only able to activate mTOR when in its GTP-bound state (Tee et al 2005). This further strengthens our finding that RGS10 is able to elicit effects on mTOR signaling presumably as an effector antagonist for the small GTPase Rheb (GDI?).

We have recently shown that the suppression of RGS10 expression is involved in mediating chemoresistance in ovarian cancer cells (Hooks et al). In this study we demonstrated that chemotherapy-induced cell toxicity is significantly altered by RGS10 reduction, allowing the cells to survive at much higher drug concentrations. Furthermore, the suppression of RGS10 expression observed in our system occurs through epigenetic modulation via histone de-acetylation in tumorigenesis and DNA methylation in chemoresistance (Ali et al). Taken together, our previous studies imply that cancer cells have the ability to epigenetically modify RGS10 protein expression during toxic conditions in order to survive. However, the specific molecular mechanism explaining how RGS10 is able to influence cell signaling affecting survival pathways was previously unknown. In addition, it was unclear whether RGS10 had any other specific purpose as an antagonist or exists exclusively as a GAP for G alpha protein subunits to terminate signaling events.

Herein we have identified that RGS10 affects mTOR activity in the absence of agonist-induced cell signaling. The RGS10 protein regulates mTOR signaling through its effects on Rheb, because in the absence of RGS10 there is a significant increase in activated Rheb bound to GTP. Furthermore, when RGS10 is suppressed, this causes mTOR phosphorylation and subsequent phosphorylation of 4E-BP1, which ultimately enhances cell growth.

Experimental Methods

Materials

Ascites-isolated SKOV-3 ovarian cancer cells were purchased from American Type Culture Collection (Manassas, VA) and cultured at 37° C in the presence of 5% CO₂ in DMEM medium supplemented with 10% fetal bovine serum (FBS) and antibiotics (Mediatech Inc., Manassas, VA). HeyA8 cells were kindly gifted from Dr. Isaiah J. Fidler (The University of Texas M.D. Anderson Cancer Center, Houston, TX) and cultured in RPMI medium supplemented with 10% FBS (Mediatech). Isolated on the ovary, OVCAR-3 were purchased from the American Type Culture Collection and cultured in RPMI supplemented with 10% FBS. INK-128 and temsirolimus were purchased from Cayman Chemical (Ann Arbor, MI). Lysophosphatidic acid (LPA, 18:1, 1-oleoyl-2-hydroxy-sn-glycero-3-phosphate) was purchased from Avanti Polar Lipids, Inc. (Alabaster, AL) and reconstituted in 0.1% fatty acid free BSA immediately prior to use.

Reverse Phase Protein Lysate Array

SKOV3 cells were seeded into 6-well plates at 150,000 cells/well and incubated overnight prior to transfection with siRNA for 48 h. Cells were treated with LPA for the times indicated prior to 20 min incubation with occasional agitation on ice for lysis in 150 µl of buffer (1% Triton X-100, 50mM HEPES, pH 7.4, 150mM NaCl, 1.5mM MgCl₂, 1mM EGTA, 100mM NaF, 10mM Na pyrophosphate, 1mM Na₃VO₄, 10% glycerol, containing freshly added protease and phosphatase inhibitors from Roche Applied Science Cat. #04693116001 and 04906845001). Cells were then scraped and

collected in microcentrifuge tubes before centrifugation at 14,000 rpm for 10 min at 4°C, after which the supernatant was collected. The BCA assay was used to determine protein concentration. Lysates were mixed with 4X SDS sample buffer and samples were boiled for 5 minutes and stored at -80°C. The reverse phase protein lysate array was performed as previously described (Liu et al , Tibes et al).

Reducing RGS10 expression

SKOV3 and HeyA8 ovarian cancer cells were plated in 6-well dishes at 120,000 cells/well and 100,000 cells/well, respectively. The plated cells were incubated for approximately 18 h at 37°C in 5% CO₂ and then transfected with siRNA using RISC-free (negative control) and RGS10 Dharmacon SmartPools (Thermo Scientific, Pittsburg, PA), following manufacturer's recommended protocol. In other experiments requiring transfection in a 96-well plate, 100 nM concentration of siRNA and 0.25 µL of Dharmafect 1 transfection reagent (Thermo Scientific) were used per well. Transfection medium was replaced with DMEM medium with 10% FBS after 8 h. Transfected cells were incubated for another 30 h and all assays were performed approximately 48 h post-transfection. In other experiments, stable cell lines were created with shGFP vector and shRNA for RGS10 in HeyA8 Parental cells using SureSilencing shRNA Plasmid for Human RGS10 (SABiosciences, Qiagen, Valencia, CA). HeyA8 cells were transfected with shRNA constructs using Fugene (Promega, Madison, WI) at a 3:1 plasmid to transfection reagent ratio.

Immunoblotting

Transfected cells were incubated for an additional 24 h and then serum-starved overnight. After 48 h post-transfection, specified conditions were treated with LPA (10 μ M) for 30 min. The cells were lysed in buffer containing protease/phosphatase inhibitor cocktail (Cell Signaling Technology, Danvers, MA) and processed for SDS-PAGE. After transferring the denatured proteins to nitrocellulose, blots were probed with primary antibodies for either phospho-mTOR (Ser2448) XP Rabbit mAb #5536, phospho-4E-BP1 (Thr37/46) #2855, β -Actin (8H10D10) Mouse mAb #3700 (all from Cell Signaling Technology) or RGS10 #H-159 (Santa Cruz Biotechnology, Dallas, TX) overnight at 4°C. Briefly, phospho-mTOR and phospho-4EBP1 were diluted 1:1000 in 5% w/v BSA in 1X TBS-T and incubated at 4°C overnight with constant gentle agitation. The following day blots were washed with TBS-T and probed with anti-rabbit HRP conjugated and anti-mouse HRP conjugated secondary antibodies (Amersham ECL detection kit, GE Health Life Sciences, Piscataway, NJ). Secondary antibodies were diluted in either anti-rabbit 1:6000 or anti-mouse 1:10,000 in 2.5% milk TBS-T and incubated for approximately 90 min. Protein bands were quantified using Image J (National Institutes of Health, Bethesda, MD) and normalized to actin.

Evaluation of RGS10 Expression

RNA was collected from cells using TRIzol® Reagent (Life Technologies, Grand Allen, NY) according to manufacturer's protocol. Afterward, RNA was quantified using a NanoDrop2000 Spectrophotometer (Thermo Scientific) and then reverse-transcribed into cDNA using iScript™ cDNA Synthesis Kit (Bio-Rad, Hercules, CA). Following

cDNA synthesis, the cDNA template was then used in a PCR reaction with primers for RGS10 and ImmoMix (Bioline USA Inc., Taunton, MA). The following primers were used for RGS10 forward: 5'- AAC CGC ACC CTC TGA TGT TC -3' and reverse: 5'- GGC TGT AGC TGT CGT ACT TCA -3'; β 2-microglobulin forward: 5'- GTG GCC TTA GCT GTG CTC G -3' and reverse: 5'- ACC TGA ATG CTG GAT AGC CTC -3' based on algorithm-generated sequences from Primer Bank (Wang and Seed). To quantify PCR results and visualize peaks, the PCR products were then loaded into an Agilent DNA 1000 chip in gel-dye matrix and analyzed using the Agilent 2100 Bioanalyzer System and software (Agilent Technologies, Santa Clara, CA), which automatically generated peaks.

Rheb Activation Assay

SKOV-3 cells were plated in 10 cm dishes at a density of approximately 400,000 cells per dish and incubated overnight at 37°C. The cells were transfected with siRGS10, siRISC-free, pcDNA, and RGS10 plasmid as indicated. After 48 hours, the culture media was removed and cells were rinsed with ice-cold PBS and 1 mL of ice-cold lysis buffer containing protease and phosphatase inhibitors was added to each dish. Plates were placed on ice for 10-20 minutes with agitation every 5 min. Lysates were cleared by centrifugation for 10 minutes at 12,000 x g at 4°C. The protein supernatant was collected and stored at -80°C until quantified by BCA assay. Cells were then treated following the manufacturer's instructions from a RheB activation assay kit (NewEast Biosciences, Malvern, PA). Following standard protocol for electrophoresis, approximately, 20 μ L/well of the pull-down supernatant was loaded onto a polyacrylamide gel (17%) and

protein bands were resolved by immunoblotting on a nitrocellulose membrane. Proteins were detected by ELC using SuperSignal West Pico Chemiluminescent Substrate (Thermo Scientific).

Immunofluorescence

SKOV-3 cells were seeded in a 96-well plate at a density of 3,000 cells per well. After 24 h, cells were transfected with siRGS10 or siRISC (negative control) as indicated. After 30 h, cells were treated with either temsirolimus or INK-128 for approximately 16 or 18 h, respectively, and then pulse treated with lysophosphatidic acid (LPA) for 30 min at a concentration of 10 μ M per well. After pulse treatment with LPA, cells were fixed with 50 μ L of 3.7% formaldehyde in PBS for 15 min. The cells were then washed once with 50 μ L of PBS and permeabilized with 50 μ L of 0.1% Triton X-100 in PBS for 15 min. After permeabilization, cells were washed twice with 50 μ L PBS prior to exposure to 50 μ L of the Whole Cell Stain Solution (Thermo Scientific, Rockford, IL) for 1 h in the dark at room temperature. Subsequently, cells were washed twice with 50 μ L of PBS and then treated with 50 μ L of DAPI in PBS (1:2000) for 20 min. After 20 min, DAPI was aspirated, 50 μ L of PBS was added to each well, and the plate was sealed for high-throughput scanning using the Cellomics ArrayScan VTI High Content Analysis Reader (Thermo Fisher Scientific, Waltham, MA).

Quantification of Cell Size and Number

Plates were analyzed using images taken by the Cellomics ArrayScan (Thermo Fisher). Each condition had at least three replicates, and ≥ 5 fields were analyzed per well

using high content screening analysis software. The automated software determined the average cell colony perimeter and the number of valid cells per well. The collected results of cell size were graphed with GraphPad Prism (LaJolla, CA) and normalized to each untreated condition. The assessment of cell count was measured as previously described (Jia et al).

Assessment of Active Cell Proliferation

Approximately 4,000 HeyA8 and 5,000 SKOV-3 cells were plated into 96-well plates in the presence of 10% fetal bovine serum. The plated cells were incubated for 18 h at 37°C in 5% CO₂ and then transfected with siRNA for RISC or RGS10. Transfected cells were incubated for an additional 24 h prior to treatment with etoposide, nacodazole, aphidicolin, paclitaxel or BrdU, where indicated. For the BrdU treatment, cells were pulse treated for 1 h with a BrdU analog, whereas all other conditions were treated with drugs for approximately 4 h. Cells were then stained according to the protocol provided by the manufacturer (Millipore, Billerica, MA). Plates were scanned using Cellomics ArrayScan (Thermo Fisher) and the number of cells was automatically captured. Representative images are shown. Each condition had 6 replications and 8 fields per well were analyzed using high content scanning software. The data was retrieved from the manufacturer's software and results were plotted with GraphPad Prism.

Evaluation of Nascent Protein Synthesis

Approximately 4,000 HeyA8 and 5,000 SKOV-3 cells were plated into 96-well plates with methionine-free medium for 18 h prior to siRNA transfection and another 24

h incubation. The Click-iT® AHA Alexa Fluor® 488 Protein Synthesis HCS Assay Kit (Life Technologies, Grand Allen, NY) was used as a method for the detection of nascent protein synthesis utilizing fluorescence microscopy and high-content imaging. Essentially, an amino acid analog of methionine containing an azido moiety, which is similar to 35S-methionine but not radioactive, is fed to cultured cells in 96-well plates. We incorporated this in serum-free, methionine-free medium in the presence of temsirolimus (10µM) and incubated cells overnight for approximately 16 h. The following day, approximately 48 h post-transfection, cells were treated with LPA (10µM) for 30 min or left untreated. Nascent proteins were detected with the green-fluorescent Alexa Fluor® 488 alkyne and imaged using the Cellomics ArrayScan. Data is presented as a bar graph.

Statistics

The statistical differences were analyzed using an analysis of variance (ANOVA) test, followed by Bonferroni's multiple comparison test between groups using GraphPad Prism. When comparing only two groups, the Student's *t-test* was used. Where it is indicated in the figures, * $p < 0.05$ ** $p < 0.01$ and *** $p < 0.001$ indicate the levels of significance. Mean and error bars are \pm SEM.

Results

During our studies to understand the role of RGS10 in ovarian cancer chemoresistance, we sought to determine which specific signaling pathways are altered as a consequence of RGS10 suppression. Elucidating this molecular mechanism would then provide clues into how targeting could be accomplished to aid the reversal of chemoresistance. To commence our investigation, cells were starved of serum overnight and then stimulated with lysophosphatidic acid (LPA) prior to the detection of 4E-BP1 phosphorylation (Kam and Exton). We then treated SKOV-3 ovarian cancer cells with siRNA to knockdown the expression of RGS10 and achieved a reduction >90% (**Figure 3.1A**) prior to measuring the samples for protein phosphorylation. We used a combination approach employing both classical immunoblotting and high-throughput reverse phase protein lysate array (RPPA, **Supplemental Figure 3.1 in Appendix**) to present our results. RPPA detected inconclusive fluctuations in total 4E-BP1 (**Figure 3.1B**), but also consistent and significant increases in 4E-BP1 phosphorylation on Threonine 37/46 (**Figure 3.1C**) and variable phosphorylation of mTOR on Serine 2448 (**Figure 3.1D**) after RGS10 suppression, without LPA treatment. Immunoblotting experiments confirmed that knockdown of RGS10 results in significant 4E-BP1 phosphorylation (**Figure 3.2A and B**) with little change in the total protein (**Figure 3.3A and B**), again without agonist stimulation. Quantification of these results yielded a very substantial difference in the ratio of phosphorylated/total 4E-BP1 between groups in the absence of LPA by siRGS10 at time 0, whereas LPA agonist stimulation alters the effect (**Figure 3.2C**). The phosphorylation of 4E-BP1 (Thr 37/46) after knockdown

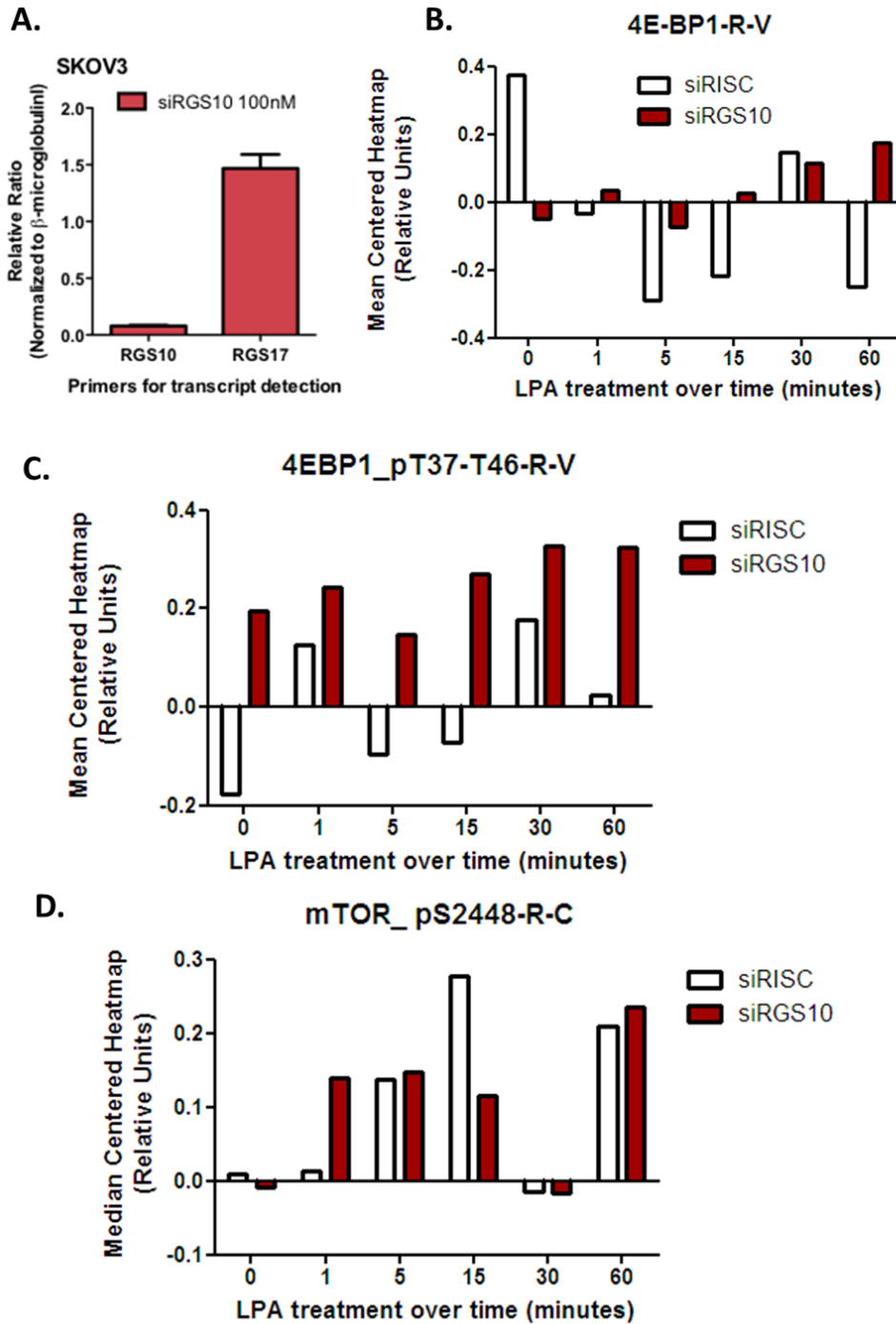


Figure 3.1. Reverse phase protein lysate array (RPPA) in LPA treated SKOV3 cells. SKOV-3 cells were transfected with siRGS10 and analyzed for their reduction in RGS10 or RGS17 mRNA (A). Reverse phase protein lysate array (RPPA) was performed on SKOV-3 cells treated with lysophosphatidic acid (LPA) for the times indicated to determine alterations in protein phosphorylation, compared with siRISC controls (B). The samples are median centered and arranged in order of their submission and demonstrate unpredictable variations in total 4E-BP1 (B), and intriguing differences in phospho-4E-BP1 at Thr37/46 (C) and phospho-mTOR at Ser2448 (D).

of RGS10 was confirmed using another ovarian cancer cell line (**Figure 3.4A and B**). Because ovarian cancer cells may have reduced expression of RGS10 in comparison to cells derived from a normal ovary (Ali et al , Hooks et al), we verified that RGS10 was indeed present among these cell lines and can be suppressed by siRNA transfection (**Figure 3.5 and 3.6**).

Since 4E-BP1 is usually phosphorylated by the mTORC1 complex, we next evaluated mTOR activation to verify the source. Indeed, knockdown of RGS10 in the absence of an inhibitor also elicited phosphorylation of mTOR on Serine 2448 (**Figure 3.7A and B**). Interestingly, LPA stimulation (10 μ M) for 10 and 30 min also induced the phosphorylation of mTOR, even in the presence of temsirolimus (10 μ M), an inhibitor of mTOR kinase activity that binds to the FKBP12-rapamycin binding domain (FRB) (**Figure 3.7C**) (Shor et al). This suggests that the LPA-mediated phosphorylation of mTOR bypasses the inhibition by temsirolimus, possibly stemming from a different signaling circuit (i.e. ERK1/2 phosphorylation). Although temsirolimus reduces the activation of mTOR under these conditions, it does not abolish the downstream phosphorylation of 4E-BP1 (**Figure 3.8.A and B**), it merely reduces the activation.

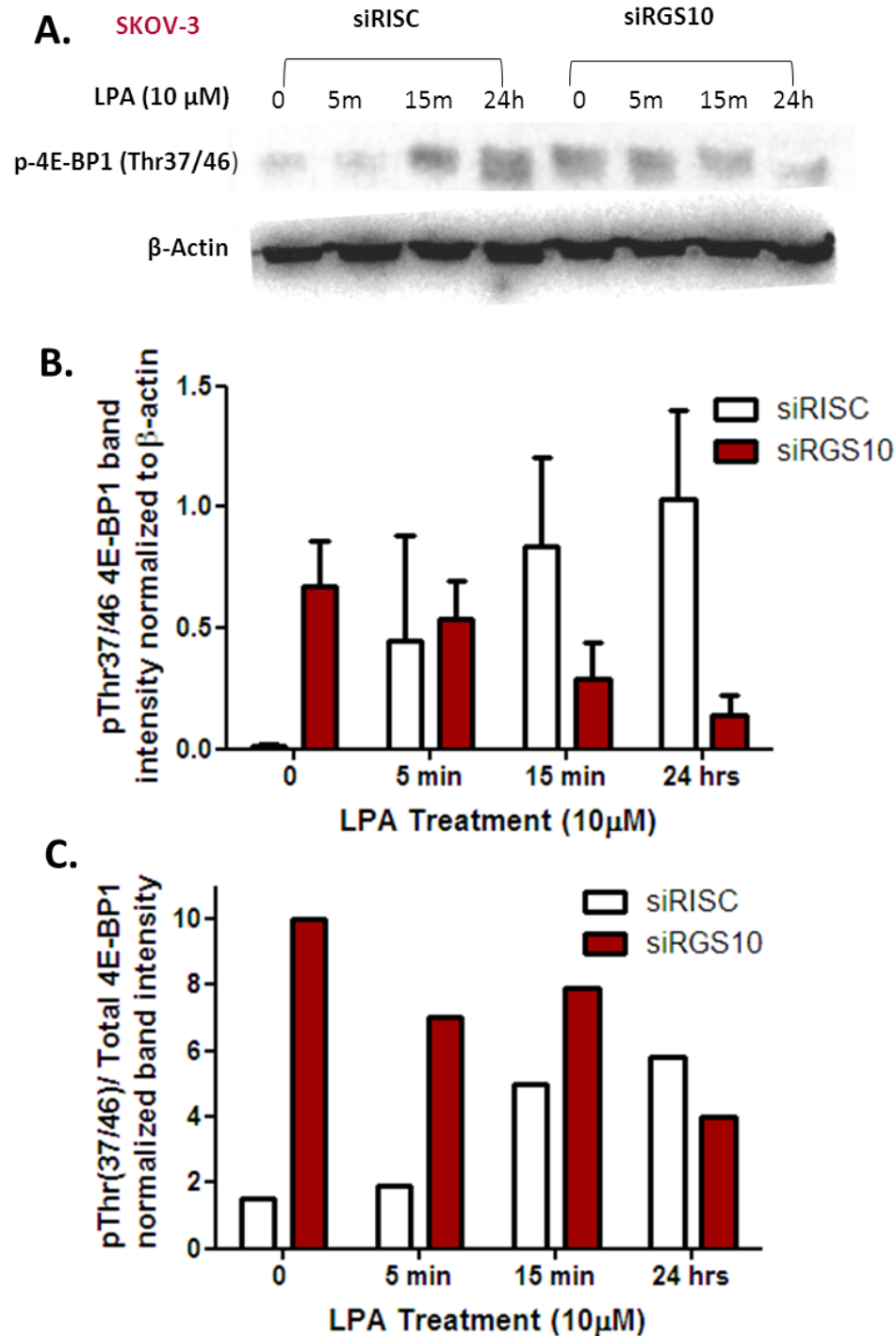


Figure 3.2. Immunoblot analysis confirms RPPA detection of phospho-4E-BP1. (A) Representative western blot at phosphorylated Thr37/46 in SKOV-3 cells. (B) Bands were quantified using Image J, densitometry is shown for N=2 independent experiments, $p > 0.5$, ns. (C) The ratio of immunoblot quantification of bands representing phospho-4E-BP1 over total 4E-BP1 shows a large increase by siRGS10 at time 0, without LPA treatment, LPA agonist stimulation alters the effect.

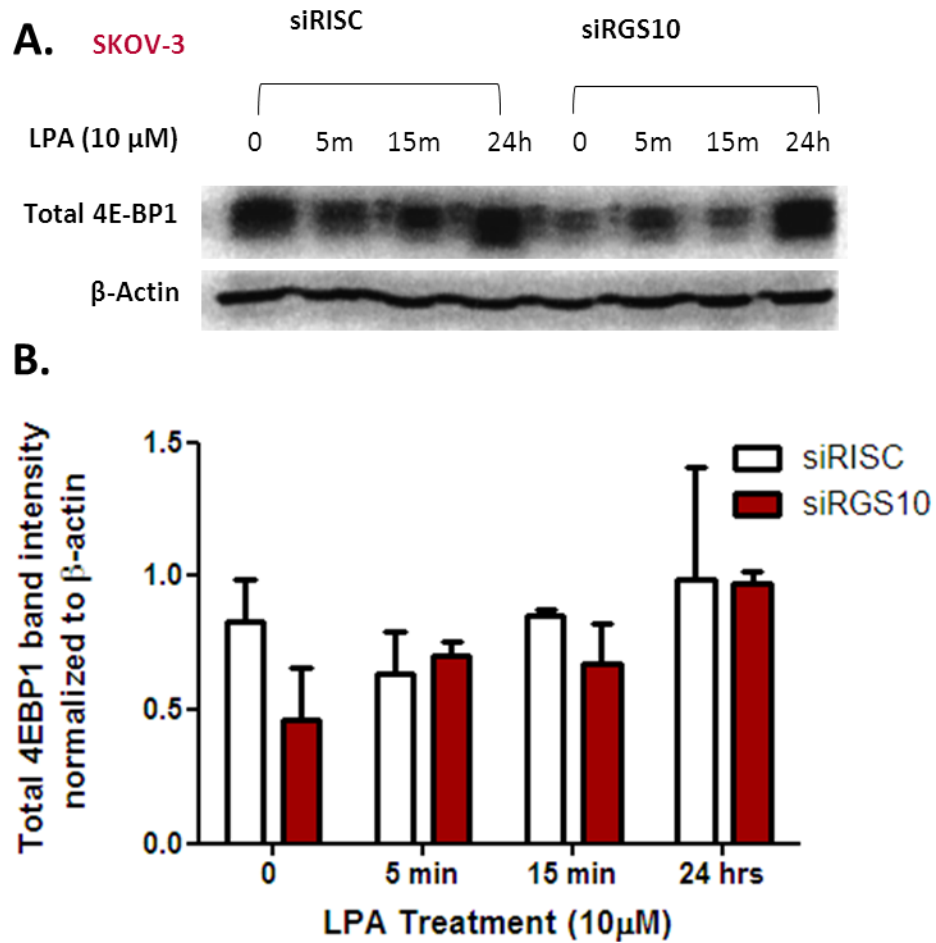


Figure 3.3. Immunoblot analysis confirms RPPA detection of Total 4E-BP.
 (A) Representative western blot probed for total 4E-BP in SKOV-3 cells. (B) Bands were quantified using Image J, densitometry is shown for N=2 independent experiments, $p > 0.5$, ns.

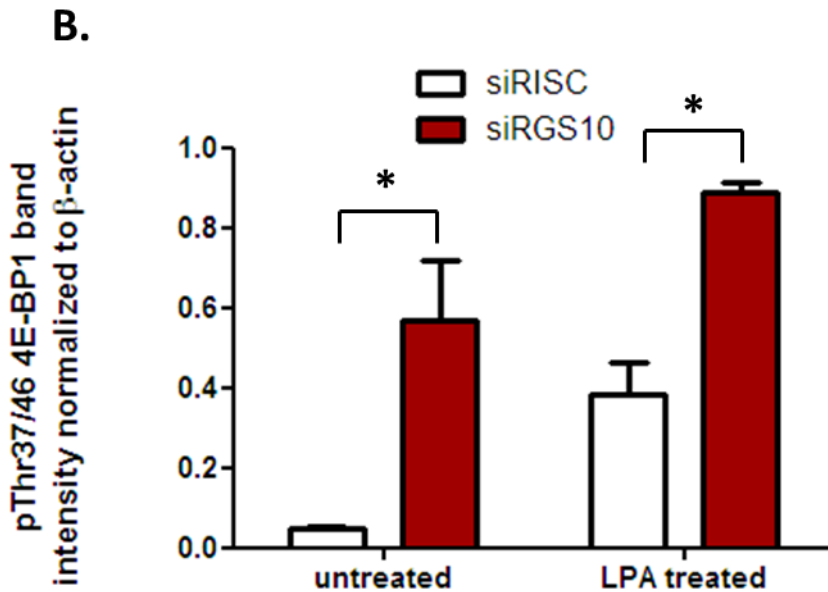
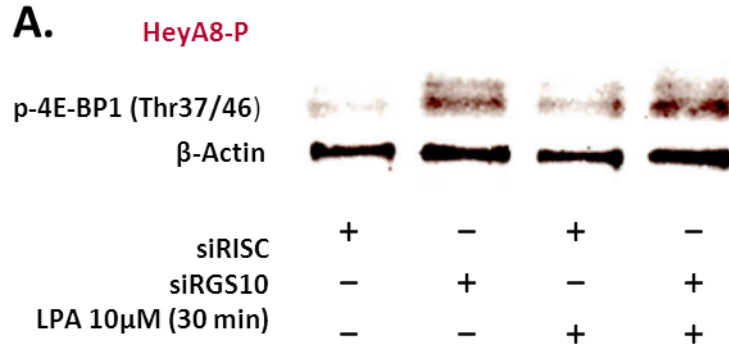


Figure 3.4. Immunoblot experiment results confirm phospho-4E-BP1 in HeyA8 Parental cells. (A) Hey-A8 cells display an increase in phospho-4E-BP1 at Thr37/46 after suppression of RGS10, in comparison to siRISC (negative control) cells, this is augmented by LPA stimulation. (B) Bands were quantified using Image J, densitometry is shown for N=2 independent experiments. *: $p < 0.05$.

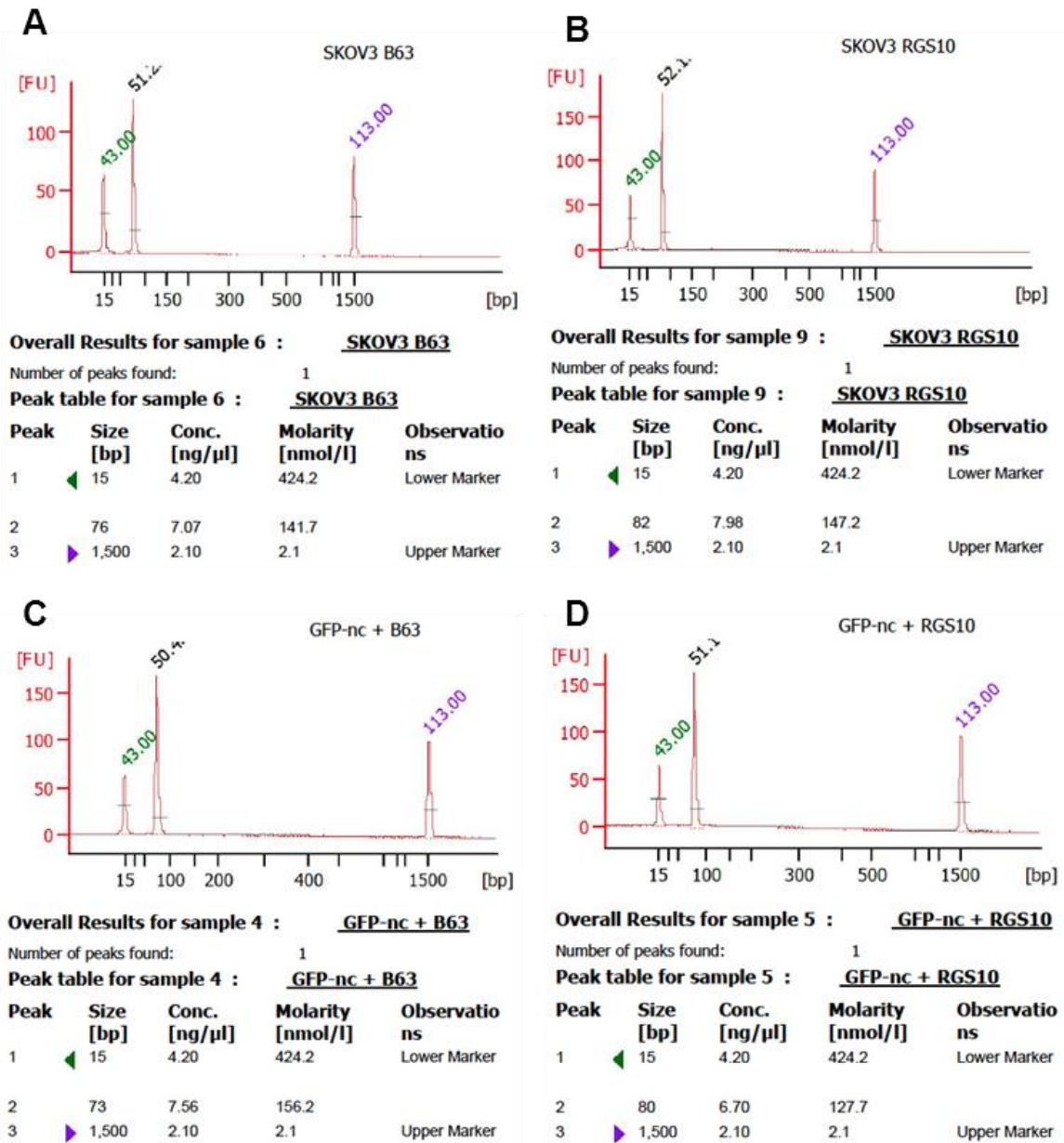


Figure 3.5. Electropherogram mRNA peaks for RGS10 in SKOV-3 and HeyA8 ovarian cancer cells. SKOV3 lysates were collected for mRNA and subsequent cDNA and analyzed with primers for beta-microglobulin (β -63) (A) and RGS10 (B) primers. HeyA8 Parental lysates with stable shGFP expression were collected for mRNA and subsequent cDNA and analyzed with primers for β -63 (C) and RGS10 (D) primers. Lysates were collected 48 h post transfection.

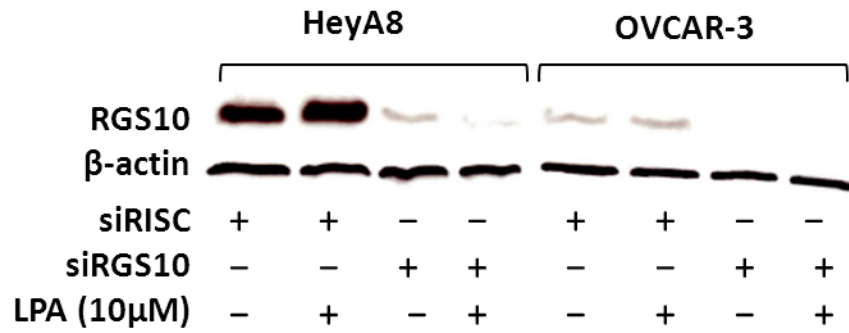


Figure 3.6. Immunoblot analysis of RGS10 expression in HeyA8 and OVCAR-3 cells. Immunoblotting verifies that HeyA8 and OVCAR3 cells transiently transfected with siRNA for RISC-free (negative control) and RGS10 express RGS10 and knockdown is successful in these cell lines. Lysates were collected 48 h post transfection.

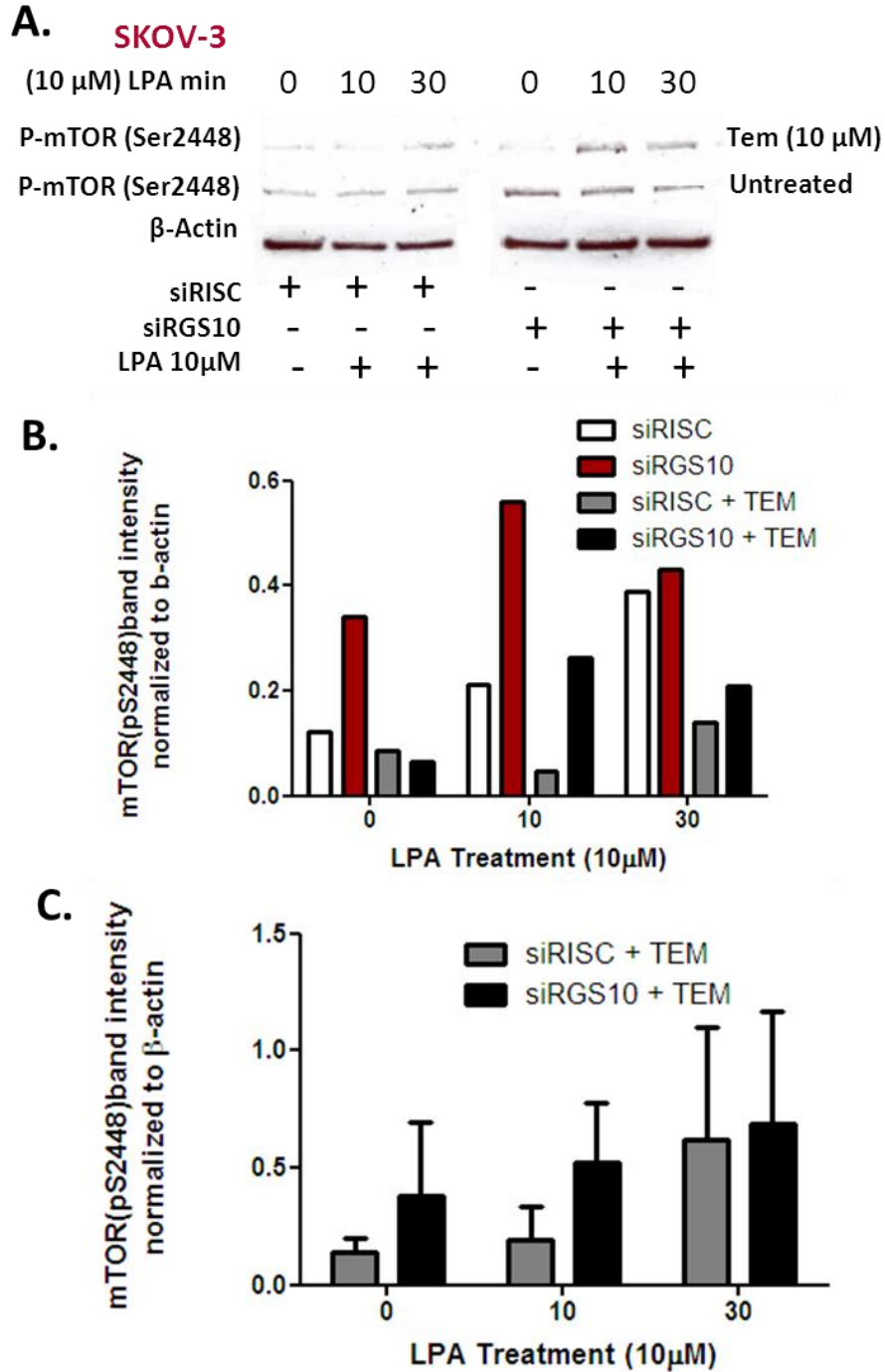


Figure 3.7. Phosphorylation of mTOR is mediated by RGS10 reduction in SKOV-3 cells. (A) SKOV-3 cells were transfected with either siRISC or siRGS10 and treated with or without lysophosphatidic acid (LPA, 10 μ M) for the times indicated either in the presence or absence of temsirolimus (10 μ M) for ~16 h. (B) Lysate was probed for phospho-mTOR at Ser-2448 and densitometry is shown for N=1 experiment. (C) Densitometry for SKOV-3 cell transfected with siRNA and treated with LPA for the times indicated in the presence of temsirolimus, probed for phospho-mTOR at Ser-2448, N=2 independent experiments, $p > 0.05$, ns.

Since this is a known limitation of temsirolimus, we also treated the ovarian cancer cells with INK128, which is an mTOR ATP-competitive inhibitor, thus it also blocks mTORC2 and 4E-BP1 phosphorylation (Guo and Kwiatkowski). Treating ovarian cancer cells with INK128 reduced mTOR (Ser2448) phosphorylation and completely abolished 4E-BP1 (Thr 37/46) phosphorylation in all conditions (**Figure 3.5.A-F**). Of note is that the levels of mTOR (Ser2448) phosphorylation between the control (siRISC) and knockdown of RGS10 (siRGS10) in HeyA8 cells (**Figure 3.5.D**) are equivalent in the presence of INK128 with and without LPA treatment. This is interesting because mTOR (Ser2448) phosphorylation by LPA is usually 1-3 fold higher after suppression of RGS10, but that significant difference is lost in the presence of INK128.

In order to pinpoint how the absence of RGS10 was able to influence the phosphorylation of mTOR and 4E-BP1 independent of agonist stimulation, we assessed direct regulators of mTOR signaling. Interestingly, when RGS10 is suppressed, activated RheB bound to GTP is increased in comparison to control, siRISC conditions (**Figure 3.6A, B**). We therefore needed to confirm whether these proteins were associating and thus performed immunoprecipitation experiments with modulation in RGS10 expression. In the absence of RGS10, RheB is reduced (**Figure 3.6C**) but in the presence of enforced RGS10 expression, the interaction increases (**Figure 3.6D**). This data indicates that RGS10 influences mTOR signaling through its effects on Rheb. Moreover, it also explains how the absence in RGS10 could elicit mTOR phosphorylation.

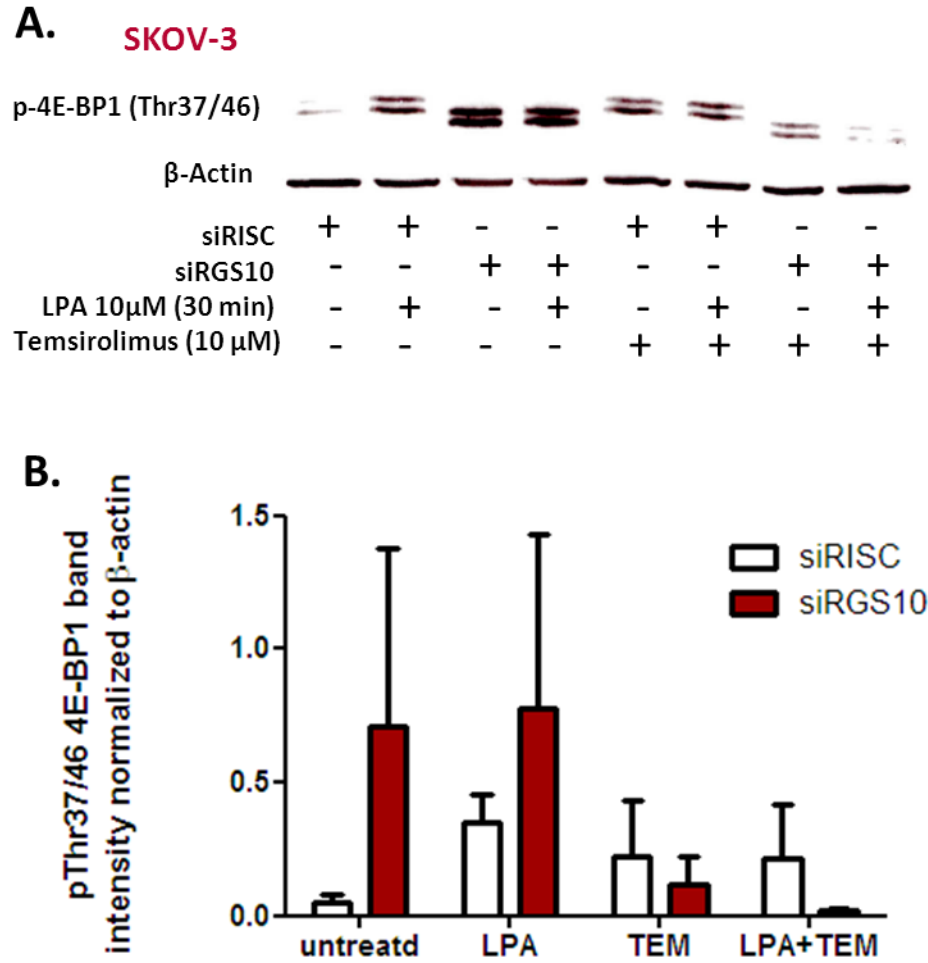
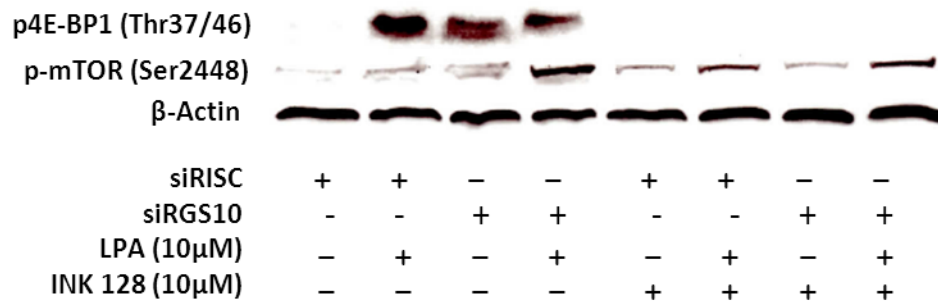
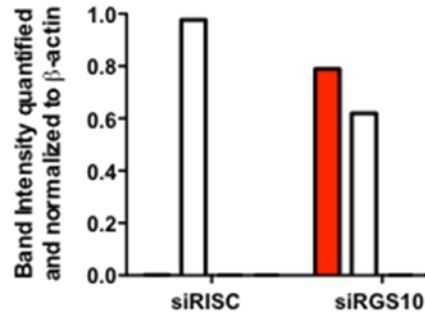


Figure 3.8. Phosphorylation of 4E-BP1 is mediated by RGS10 reduction in SKOV-3 cells. (A) SKOV-3 cells were transfected with either siRISC or siRGS10 and treated with or without lysophosphatidic acid (LPA, 10 μM) for the times indicated in the presence of absence of temsirolimus (10 μM) for ~16 h. Lysate was probed for phospho-4E-BP-1 at Thr37/46 (B) and the bands were quantified using Image J. Representative blot for N=2 independent experiments, $p > 0.05$, ns.

A. HeyA8



B. HeyA8 p-4EBP1



C. HeyA8 p-mTOR

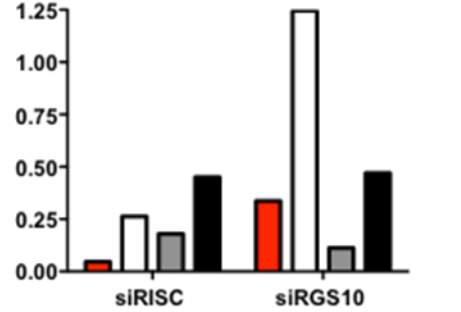


Figure 3.9. INK-128 an mTOR inhibitor impedes phosphorylation in HeyA8 cells.

(A) HeyA8 cells were transfected with either siRISC or siRGS10 and treated with or without LPA (10 μM) for the times indicated in the presence or absence of INK128 (10 μM) for ~18 h prior to the detection of phosphorylated 4E-BP1 and mTOR. Protein bands were quantified using Image J to represent (B) phospho-4E-BP-1 or (C) phospho-mTOR, N=1 experiment.

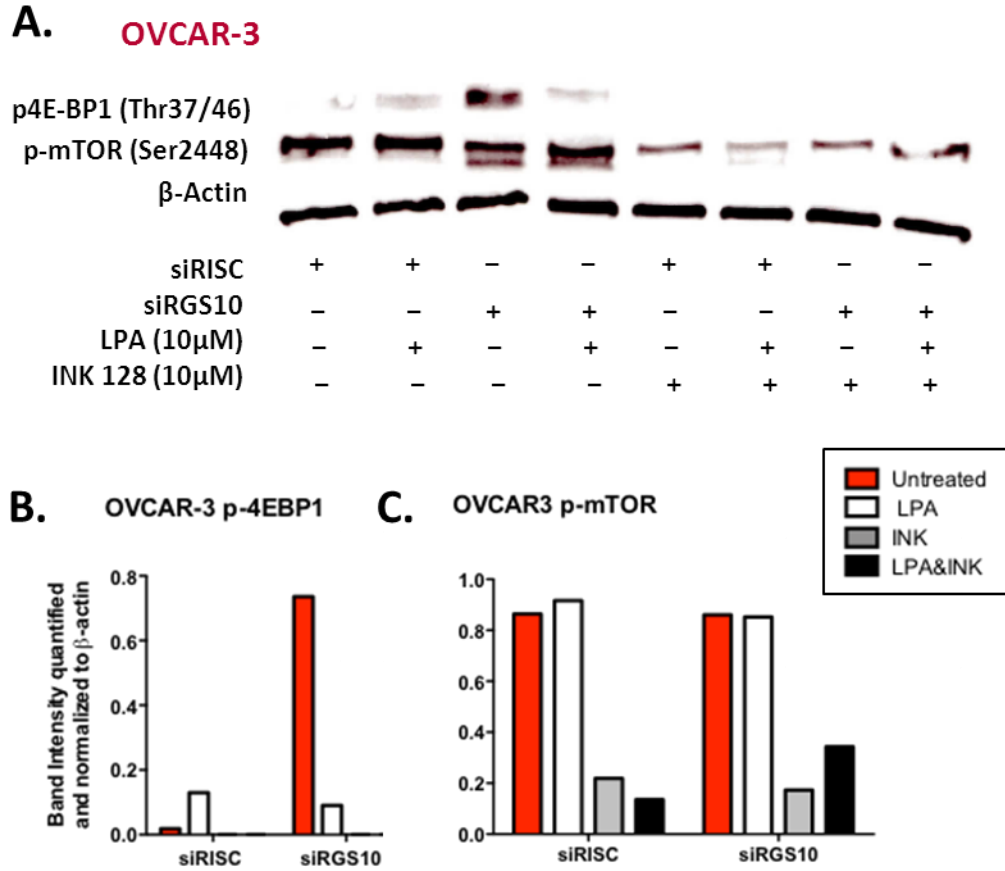


Figure 3.10. INK-128 an mTOR inhibitor impedes phosphorylation in OVCAR-3 cells. (A) OVCAR-3 cells were transfected with either siRISC or siRGS10 and treated with or without LPA (10 μ M) for the times indicated in the presence or absence of INK128 (10 μ M) for \sim 18 h prior to the detection of phosphorylated mTOR and 4E-BP1. Protein bands were quantified using Image J to represent (B) phospho-4E-BP-1 or (C) phospho-mTOR, N=1 experiment.

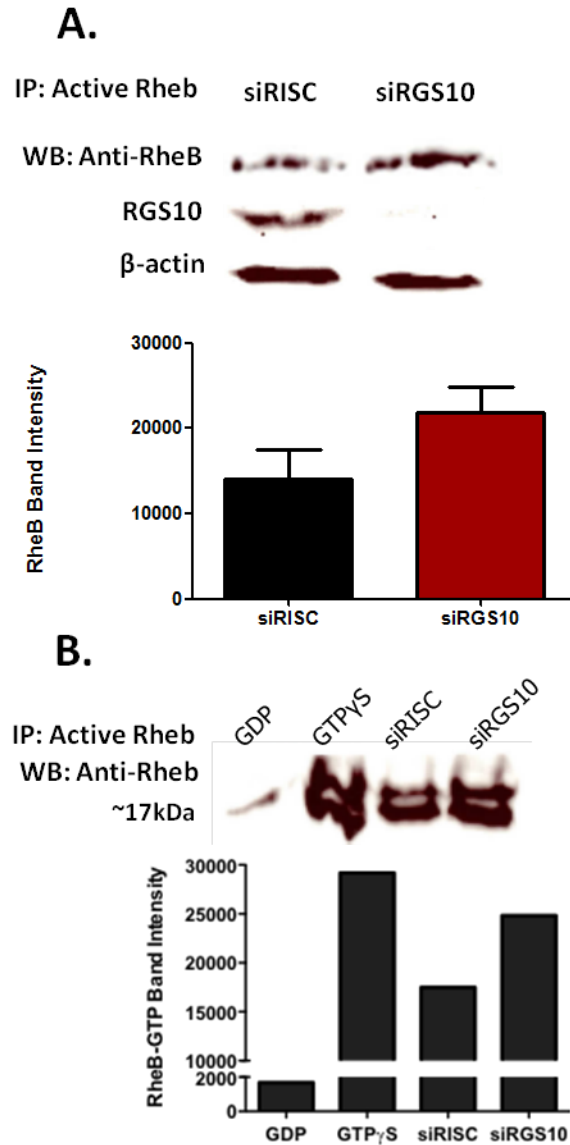


Figure 3.11. Modulating RGS10 affects activated RheB in SKOV-3 cells.

(A) SKOV-3 cells were treated with either siRISC or siRGS10 prior to immunoprecipitation with an anti-active RheB monoclonal antibody and immunoblotting with anti-RheB rabbit polyclonal antibody, anti-RGS10 or Beta-actin. Representative blot is shown for N=2 independent experiments, $p > 0.05$, ns. (B) Cells were treated as above, but GTP γ S and GDP were added to the cell extracts *in vitro* and incubated for 30 minutes prior to the pull-down of active RheB, N=1 experiment.

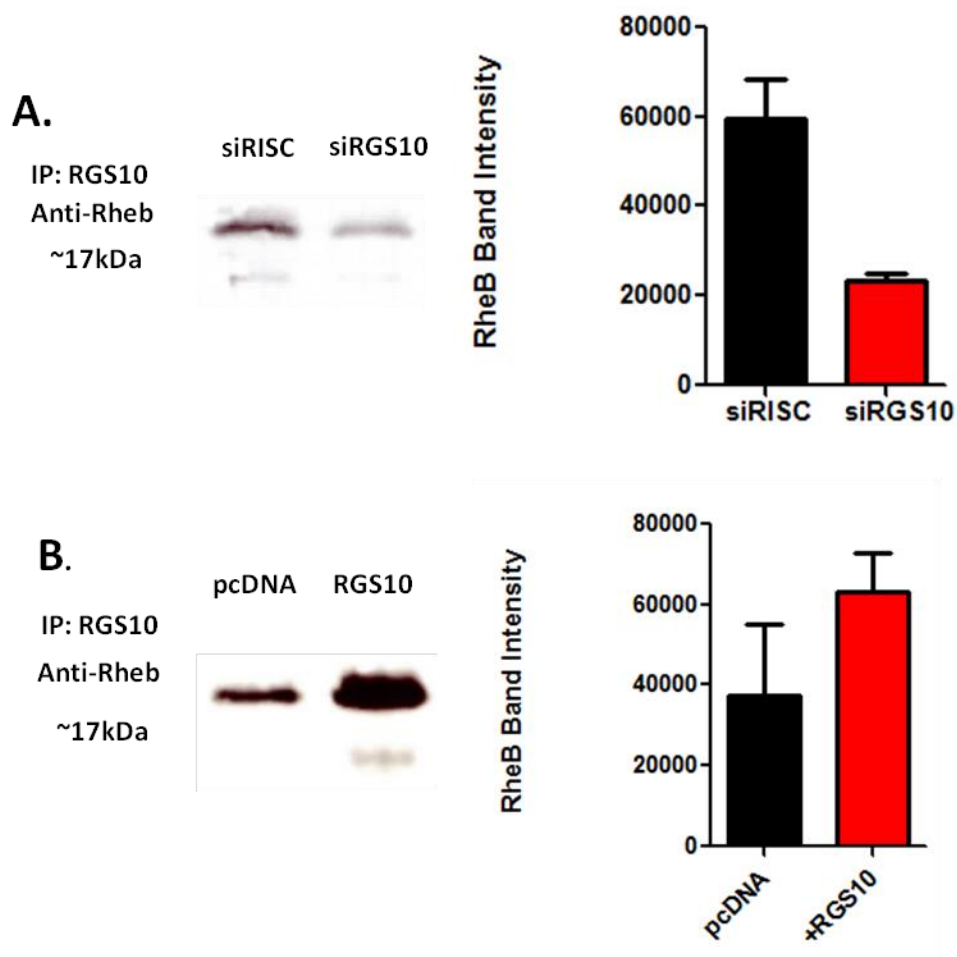


Figure 3.12. Co-immunoprecipitation with RGS10 and Rheb shows co-localization. SKOV-3 cells were transiently transfected with siRISC, siRGS10, pcDNA or RGS10 prior to immunoprecipitation with anti-RGS10 goal polyclonal antibody and blotted with anti-Rheb rabbit polyclonal antibody. (A) SKOV-3 cells were treated with either siRISC or siRGS10, and blotted for anti-Rheb. Representative blot from N=2 independent experiments, densitometry from Image J analysis, $p > 0.05$, ns. (B) SKOV-3 cells were treated with either pcDNA or siRGS10, and blotted for anti-Rheb. Representative blot from N=2 independent experiments, densitometry from Image J analysis, $p > 0.05$, ns.

To assess the functional outcome of RGS10 suppression, we used high-throughput imaging and automated quantification to accurately measure both nascent protein synthesis and cell growth because of the role mTOR plays in regulating these cellular processes. Indeed, RGS10 suppression enlarges SKOV-3 (**Figure 3.13A**) and HeyA8 cells (**Figure 3.14**) and the area is further increased upon stimulation with LPA and decreased upon treatment with temsirolimus. These observations are reflected in the cell morphology whereby visibly swollen cells appear after knockdown of siRGS10 and/or the addition of LPA. In contrast, after treatment with temsirolimus the cells appear longer and thinner, resembling a ‘stretched’ morphology (**Figure 3.13C**).

Nascent protein is significantly increased by LPA stimulation in control cells (siRISC), which are likely to be more ‘receptive’ to a sudden ‘on’ stimulation. Interestingly, this trend is reversed once temsirolimus has been added (**Figure 3.13B**). After temsirolimus addition, only those cells with RGS10 suppression are receptive to nascent protein synthesis. This suggests that RGS10 suppression is capable of bypassing the inhibition of protein synthesis because its effects (i.e. Rheb) are on a different mechanism from temsirolimus inhibition (FKBP12). In other words, it is consistent with our data.

Usually cells will couple growth to proliferation, the former being preparation for the latter event. Even though these processes are not necessarily synchronized in cancer cells, we wanted to determine whether cells were more or less proliferative in response to RGS10 suppression and mTOR inhibition. SKOV-3 cells did not increase their rate of proliferation after RGS10 suppression (**Figure 3.15A and B**), although they became hypersensitive to toxicity induced by INK128 (**Figure 3.15B**), which is an ATP-

competitive mTOR inhibitor. Again, this observation strongly suggests mTOR activation by RGS10 suppression.

The data in SKOV-3 cells was in sharp contrast to HeyA8 cells, which exhibited significantly more proliferation after RGS10 suppression (**Figure 3.16A**). We confirmed that this was active cell proliferation by demonstrating BrdU incorporation into HeyA8 cells with knockdown of RGS10 (**Figure 3.16B**). We constructed a stable HeyA8 cell line expressing either shRGS10 or shGFP and compared the proliferation in response to chemotherapy. Interestingly, shRGS10-expressing cells displayed a significantly greater number of cells in the presence of etoposide and aphidicolin, but not nocodazole or paclitaxel (**Figure 3.16C**), suggesting that the suppression of RGS10 endows HeyA8 cells with a proliferative advantage in the presence of certain chemotherapy. As a consequence, the loss of RGS10 could translate into the acquisition of chemoresistance as we have previously suggested (Hooks et al).

Active proliferation was not observed in SKOV-3 cells (**Figure 3.17A and B**), suggesting that the suppression of RGS10 has cell-type specific effects on proliferation. It also reaffirms that certain ovarian cancer cells have uncoupled the processes of growth from proliferation – these are not necessarily synchronized, in contrast with normal cells. Moreover, it entertains the fascinating possibility that SKOV-3 cells could become chemoresistant with the loss of RGS10 by virtue of their failure to rapidly proliferate; the action of traditional chemotherapy depends on rapidly-dividing cells. Albeit this could be a different mechanism occurring in the SKOV-3 cells versus the HeyA8 cells, however, the outcome of RGS10 suppression on chemoresistance is the same.

Study limitations

A limitation of this current study is that we choose specific proteins/phosphorylation sites based on or RPPA proteomics data. Phosphorylation proteomics data is also subject to the labile nature of phosphorylated-proteins overtime. Additionally, analysis of total mTOR and the 4E-BP1 phosphorylation site (pSer65), would give a more detailed pathway elucidation. Also, our results from the IP assays are in duplicate N=2 experiments. The experiment with siRGS10 IP with RGS10 antibody and blotted with anti-Rheb, $p=0.0571$ and may have reached significance if there were more samples measured. Ideally, one strives to repeat experiments at least in triplicate. Notably, it is very important to the validity of an experiment to have accurate controls (i.e. loading control, positive, as well as negative controls). In our studies, we are currently lacking pull-down IP experiments that show the effects of a non-specific RGS protein (i.e. RGS20 siRNA). For example, RGS20 is not thought to be involved in the development of chemoresistance in ovarian cancer. With the immunoprecipitation (IP) of RGS10, we were limited by lack of knowledge about our RGS10 antibody's suitability for IP. There are a few studies that have successfully used the same RGS10 antibody for IP, but the methods are lacking full details of the experiment (Rivero et al 2010). Thus, we optimized the RGS10 antibody for co-IP in ovarian cancer cells in our laboratory.

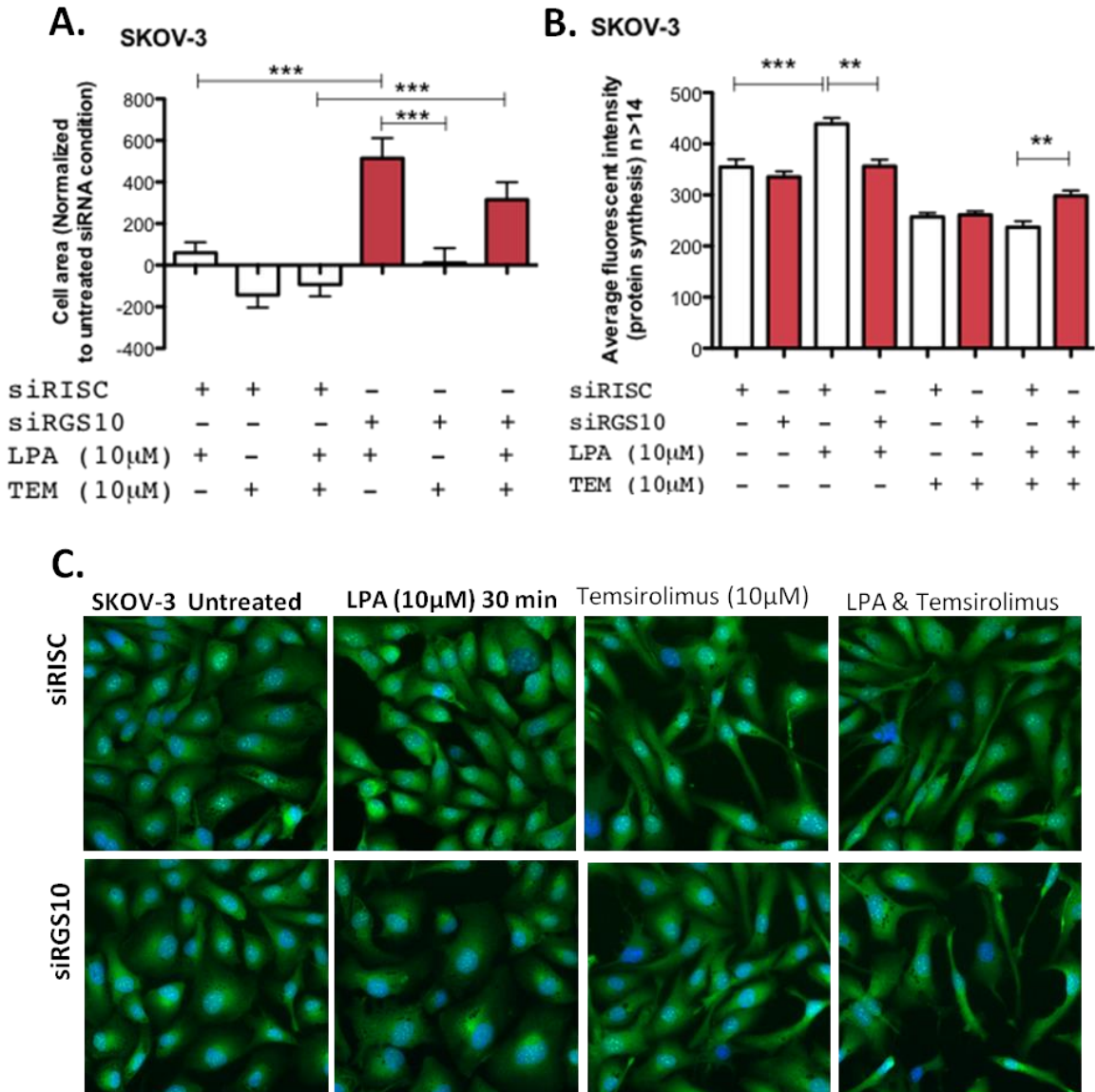


Figure 3.13. Reducing the expression of RGS10 enlarges ovarian cancer cells via the mTOR pathway. SKOV-3 cells were transfected with either siRISC or siRGS10, treated with or without lysophosphatidic acid (LPA, 30 min, 10 µM) in the presence or absence of temsirolimus (10 µM, ~16 h) where indicated. Cells were prepared for immunofluorescence and scanned using high-throughput automation to calculate cell size. (A) Data shows the average from 62-146 different fields per condition from a series of N=2 independent experiments and is normalized to each untreated condition (i.e. siRISC-white bars or siRGS10-shaded bars). (B) The average fluorescent intensity of nascent protein synthesis among SKOV-3 cells was automatically measured. Bar graph results show a representative experiment with n>14 fields measured. ***p<0.001, **p<0.01 in the comparisons as indicated. (C) Representative images of SKOV-3 cells under the indicated conditions show the variations in cell morphology.

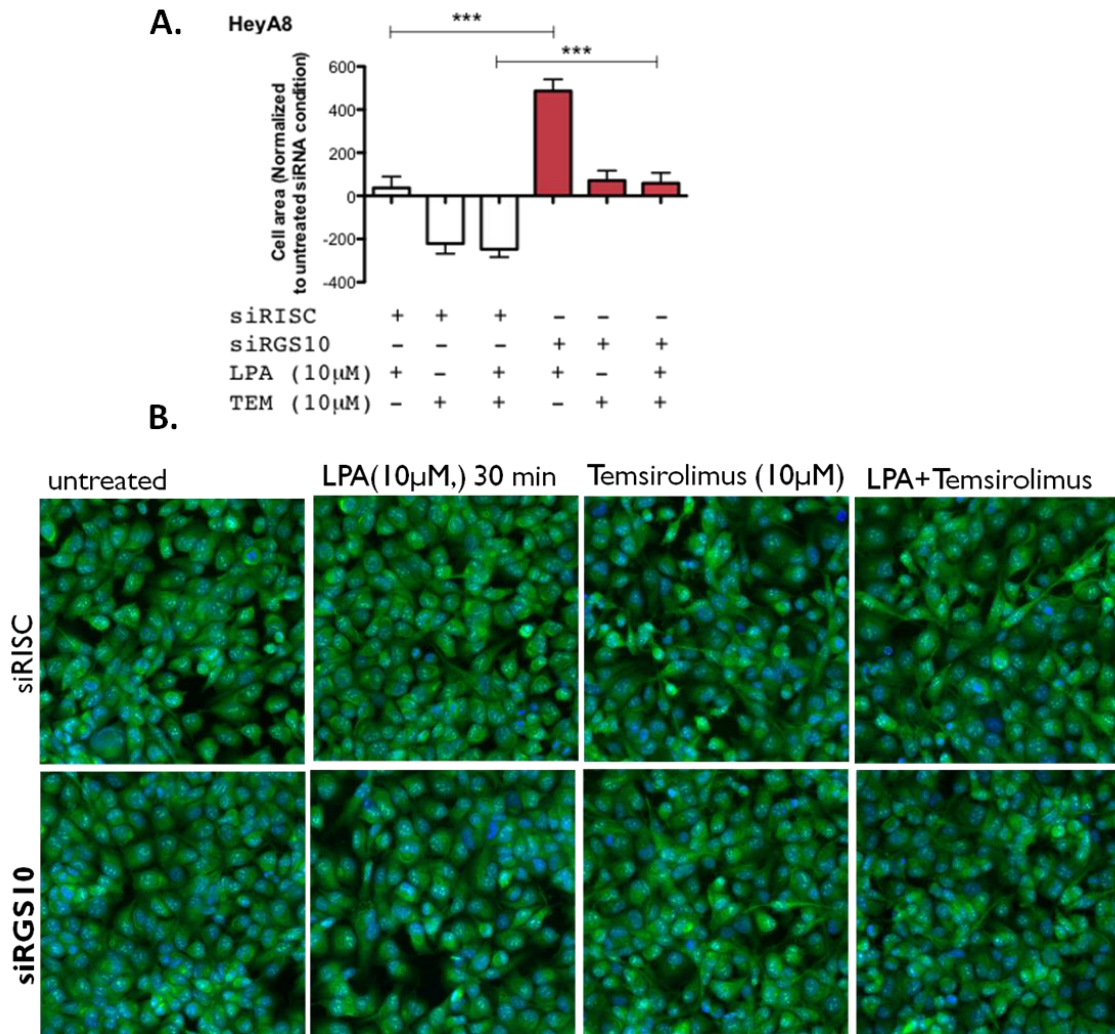


Figure 3.14. Reducing the expression of RGS10 has marginal effects on cell size in HeyA8 parental cells. HeyA8 cells were transfected with either siRISC or siRGS10, treated with lysophosphatidic acid (LPA, 30 min, 10 μ M) or temsirolimus (10 μ M, ~16 h) where indicated. Cells were prepared for immunofluorescence and scanned using high-throughput automation to calculate cell size. (A) Data shows the average from 62-146 different fields per condition from a series of N=2 independent experiments and is normalized to each untreated condition (i.e. siRISC-white bars or siRGS10-shaded bars). (B) Representative images of HeyA8 parental cells under the indicated conditions show dense cells.

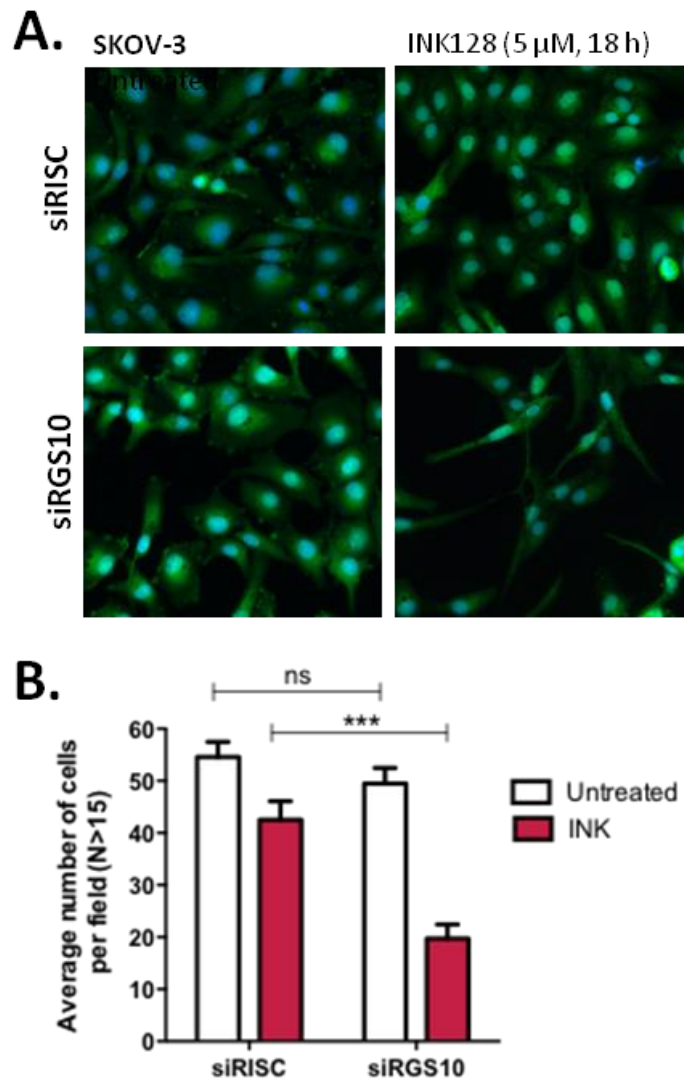


Figure 13.15. The effects of RGS10 reduction is modulated by the selective mTOR inhibitor INK-128 in SKOV-3 cells. (A) SKOV-3 cells were transfected with either siRISC or siRGS10 and treated with INK128 (5 μ M, ~18 h) prior to preparation for immunofluorescence. Representative images are shown. (B) Cells were automatically counted by the high-throughput imager and results were quantified and the average number of cells per field ($n > 15$) is displayed as a bar graph for $N = 2$ independent experiments.

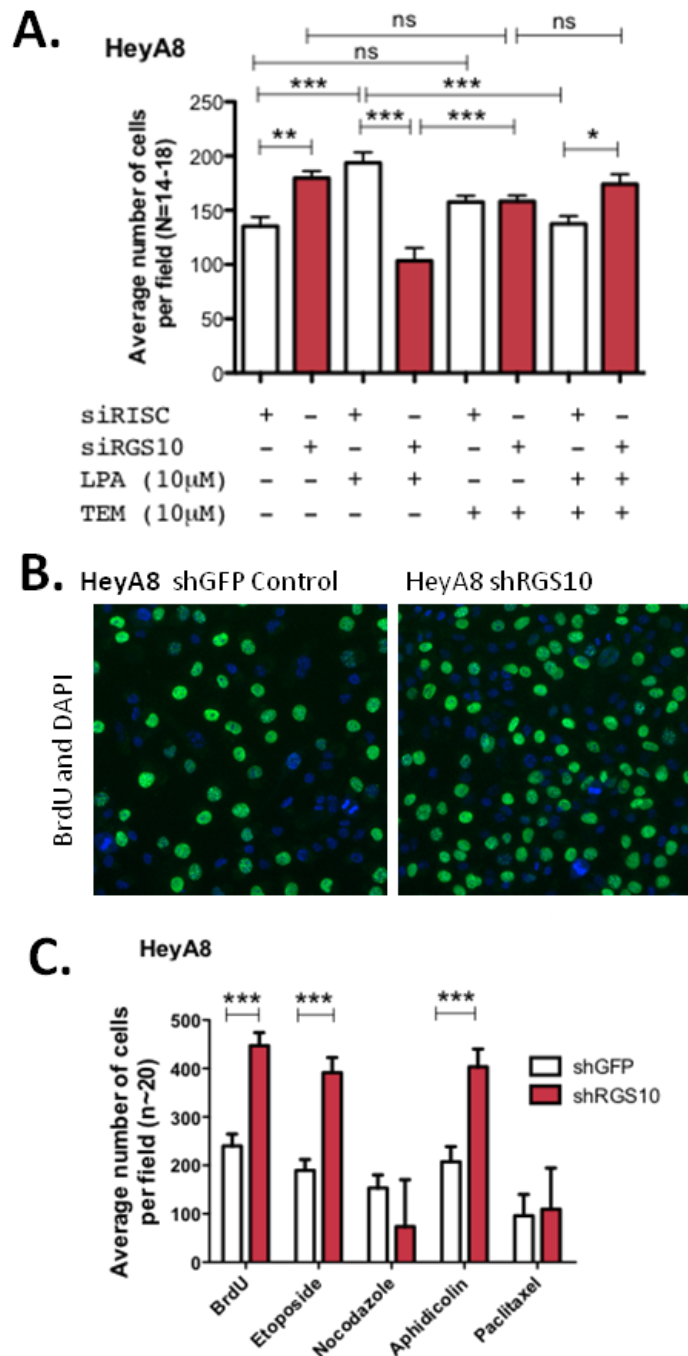


Figure 13.16. Reducing the expression of RGS10 affects proliferation in HeyA8 parental cells. (A) HeyA8 cells with either siRISC or siRGS10 and treated with TEM, 10 µM ~16 h or LPA, 10 µM, 30 min prior to processing for high-throughput imaging. N=2 independent experiments (n=14-18 number of fields). (B) HeyA8 cells were pulse-treated for one hour with a BrdU analog. Cells were fixed and then stained with DAPI and an anti-BrdU antibody prior to imaging. Fluorescent images of HeyA8 cells visualize the difference between active proliferation among control cells and suppression of RGS10. (C) In other experiments, shGFP or shRGS10 stably-expressing HeyA8 cells were treated with different drugs or a BrdU analog prior to fixation, immunofluorescence staining and automatic cell counting.

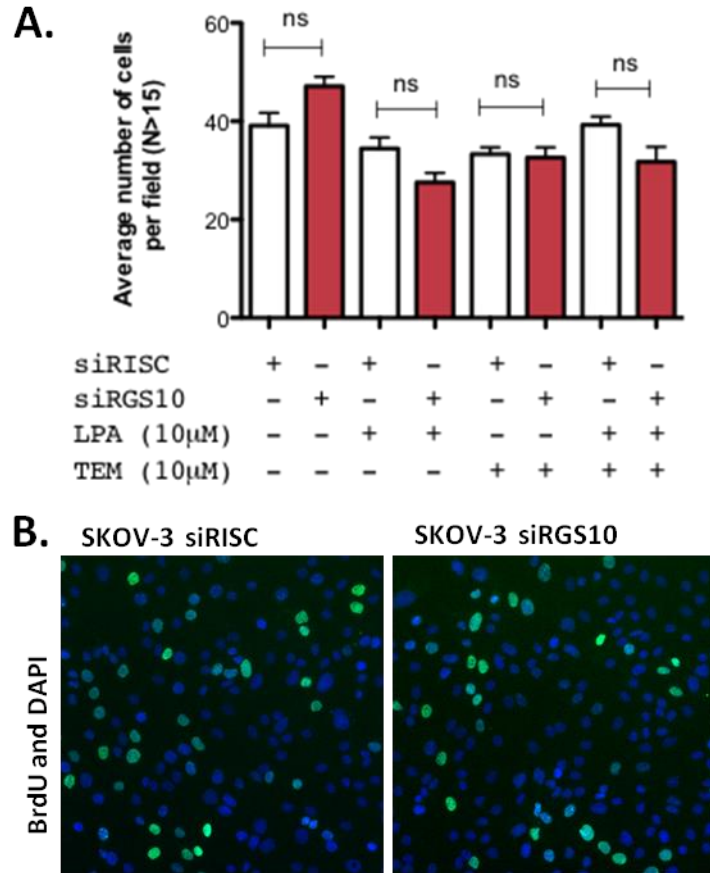


Figure 3.17. Reducing the expression of RGS10 doesn't affect proliferation in SKOV-3 cells. (A) SKOV-3 cells were transfected with either siRISC or siRGS10 and treated with TEM or LPA where indicated. No significant changes were detected after automated cell counts using high-throughput imaging. (B) SKOV-3 cells were pulse-treated for one hour with a BrdU analog. Cells were fixed and then stained with DAPI and an anti-BrdU antibody prior to high-throughput imaging.

Discussion

Herein we show that reducing RGS10 in ovarian cancer cells results in mTOR signaling activation. More specifically, the suppression of RGS10 leads to an increase in activated RheB bound to GTP, which causes phosphorylation of mTOR. Indeed, we show that RGS10 knockdown increases the phosphorylation of 4E-BP1 and mTOR. As a functional consequence of RGS10 suppression, ovarian cancer cells increase in size and this effect is inhibited in the presence of chemical inhibitors of mTOR. Nascent protein synthesis is modestly affected and cell proliferation appears to be cell-type dependent. Our results are highly novel and significant; no reports in the literature to date have proposed that RGS10 is an effector antagonist of the mTOR signaling pathway. Nor has any report characterized the functional outcomes in cancer cells resultant from RGS10 suppression (e.g. cell enlargement, nascent protein synthesis, etc.). Thus, our study fills a major gap in our understanding of how mTOR signaling is regulated and the role of RGS10.

This knowledge is important because the mTOR signaling pathway remains a crucial and often functionally dysregulated among cancer cells, especially since it is linked to PI3K signaling. The PI3K/mTOR pathway is critical because it regulates the cell's decision to grow, survive and proliferate, which are all at the heart of establishing the difference between a normal and a cancerous cell. Our prior studies are the only other reports found in the literature that describe the role of RGS10 in ovarian cancer cells (Ali et al , Hooks et al). In this regard, we previously found that the suppression of RGS10 is acquired through epigenetic changes (Ali et al) as chemoresistance develops,

which allows ovarian cancer cells to survive significantly higher doses of chemotherapy than usual (Hooks et al).

Herein we have uncovered the specific molecular mechanism that explains these prior observations. However, there has not been any focus on RGS10 modulation in cancer because its role was previously completely unknown. Its structure is so basic that it yields no clues to its function, which we now understand is related to Rheb activation as depicted in **Figure 3.18**. Because the PI3K/mTOR pathway is frequently dysregulated in cancer, it represents an enormous focus of targeted inhibition. Currently there are several FDA-approved therapeutics, everolimus and temsirolimus, which inhibit mTOR and are used in the clinical management of cancer patients, particularly for renal cell carcinoma. These agents owe their existence to the soil bacteria living on Easter Island where their parent compound, rapamycin or sirolimus, was discovered (Vezina et al). Other similar agents are under development, although there have been issues with safety and a lack of overall survival advantage, which are major concerns preventing further development and FDA approval.

The obvious connection between our current study and our previous work is the idea of using mTOR inhibition as a mechanism to alleviate chemoresistance in ovarian cancer. Indeed, other studies have already shown that mTOR inhibition represents a strategy to overcome chemoresistance in a variety of different types of cancers (Beeram et al , Grunwald et al , Lu et al , Schewe and Aguirre-Ghiso , Tsurutani et al), especially with combination therapy, which is the mainstay of treating almost every cancer type. This also insinuates that our results could be adaptable to other subtypes of cancer,

beyond our focus herein on ovarian cancer cells. Among ovarian tumors, serous epithelial ovarian adenocarcinoma

frequently displays enhanced mTOR phosphorylation; additionally, this occurs particularly among cisplatin-resistant ovarian cancer cells, in comparison to their matched parental cisplatin-sensitive control cells, which also translates to a greater sensitivity to mTOR inhibition (Mabuchi et al). This study, although not focused on RGS10, is nevertheless directly aligned with our findings and interpretation of results and observations.

In order to *directly* test this theory *in vivo*, a tumor model with controlled suppression of RGS10 is necessary. Our repeated attempts to maintain such a model long-term were thwarted by the inability to continuously passage cells with suppressed RGS10. We observed that cells quickly regain RGS10 expression, time after time, even though we can successfully manipulate the expression of other RGS proteins ((Altman et al) and data not shown). However, since we hypothesize that the net effect of this model would be the continual activation of Rheb, similar work has already been produced (Jiang and Vogt). In this study, Jiang and Vogt describe a constitutively active Rheb that phosphorylates 4E-BP1, produces larger cells with more protein and generally induces oncogenic transformation.

It is fascinating that no agonist is needed by ovarian cancer cells to achieve phosphorylated mTOR and 4E-BP1 if they allow the suppression of one small GAP protein – RGS10. The implication of our findings with tumor biology is that the loss of RGS10 would have drastically negative consequences on a cell, particularly one without a properly functioning TSC1/TSC2 complex. Molecularly, there would be a loss in the

ability to regulate Rheb activity. Future studies will need to test this hypothesis and determine whether additional regulator molecules and/or effector antagonists are also present and compensate for aberrant signaling. The answers to these questions are currently unknown.

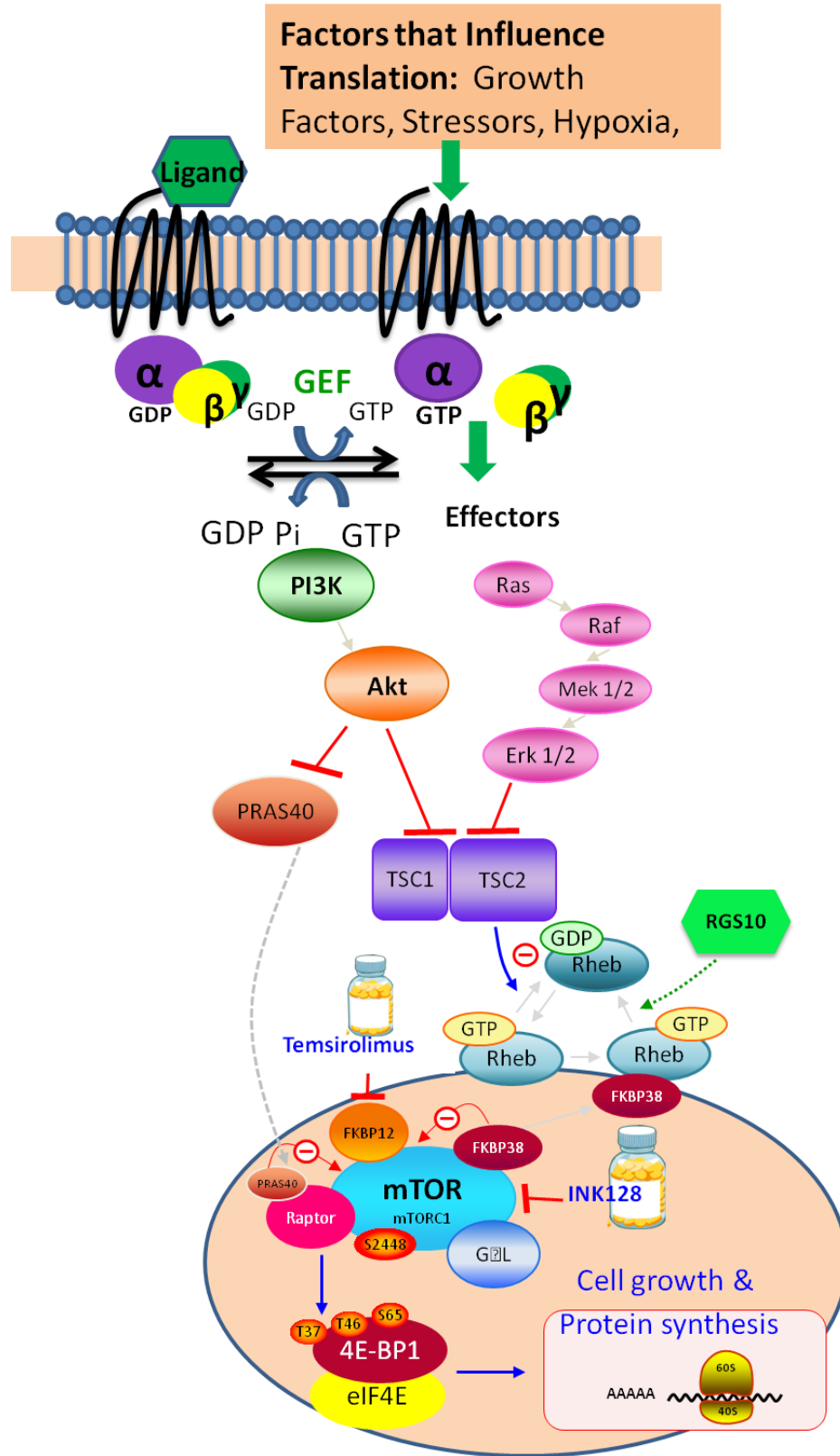


Figure 3.18. Our model for RGS10 involvement with Rheb and mTOR pathway activation.

CHAPTER 4

REGULATOR OF G-PROTEIN SIGNALING 5 REDUCES HEYA8 OVARIAN CANCER CELL PROLIFERATION AND EXTENDS SURVIVAL IN A MURINE TUMOR MODEL¹

¹ Altman, MK., Nguyen, DT., Patel, SB., Fambrough, JM., Beedle, AM., Hardman, WJ., and Murph, MM. 2012, *Biochemistry Research International*, 2012: 518437.
Reprinted here with permission of the publisher.

Abstract

The regulator of G-protein signaling 5 (RGS5) belongs to a family of GTPase activators that terminate signaling cascades initiated by extracellular mediators and G protein-coupled receptors. RGS5 has an interesting dual biological role. One functional RGS5 role is as a pericyte biomarker influencing the switch to angiogenesis during malignant progression. Its other functional role is to promote apoptosis in hypoxic environments. We set out to clarify the extent to which RGS5 expression regulates tumor progression – whether it plays a pathogenic or protective role in ovarian tumor biology. We thus constructed an inducible gene expression system to achieve RGS5 expression in HeyA8-MDR ovarian cancer cells. Through this we observed that inducible RGS5 expression significantly reduces *in vitro* BrdU-positive HeyA8-MDR cells, although this did not correlate with a reduction in tumor volume observed using an *in vivo* mouse model of ovarian cancer. Interestingly, mice bearing RGS5-expressing tumors demonstrated an increase in survival compared with controls, which might be attributed to the vast regions of necrosis observed by pathological examination. Additionally, mice bearing RGS5-expressing tumors were less likely to have ulcerated tumors. Taken together, this data supports the idea that temporal expression and stabilization of RGS5 could be a valuable tactic within the context of a multi-component approach for modulating tumor progression.

Introduction

The regulator of G-protein signaling 5 (RGS5) belongs to a family of GTPase activators and signal transduction molecules that negatively regulate the function of G proteins. In other words, RGS proteins terminate cellular signaling cascades initiated by extracellular mediators that bind to and activate G protein-coupled receptors. More specifically, RGS5 binds to G alpha (i), (q) and (o) subunits within heterotrimeric G-proteins to terminate signaling and is located along the plasma membrane and within the cytosol (Zhou et al). RGS5 was isolated in 1997 from mouse pituitary, although its preferential expression is in the heart (particularly aorta), skeletal muscle, lung, small intestine and thyroid (Chen et al , Seki et al). *Rgs5* is located at 1q23.1, a region on chromosome 1 of interest for lipid metabolism (Xiao et al), hypertension (Chang et al , Faruque et al), blood pressure regulation (Cho et al), severity of schizophrenia symptoms (Campbell et al) and association with SNPs that have specific effects dependent upon genetic background (Smith et al).

Using a platelet-derived growth factor knockout mouse model and comparing it to the gene expression of wild-type mice, Bondjers et al. was the first to identify RGS5 as a biomarker of pericytes (Bondjers et al), cells that wrap around the walls of capillaries. Pericytes are thus involved in the regulation of blood flow and the transformation of new blood vessels. Berger et al. verified that RGS5 is an angiogenic pericyte marker and a component involved in the switch to angiogenesis during malignant progression (Berger et al), with context-specific expression (i.e. during wound healing). Mitchell et al. confirmed that the expression of RGS5 is temporally upregulated during pathological

angiogenesis, at approximately 5-6 days after corneal scraping, a period when the nascent vessel sprouts acquire their pericyte covering (Mitchell et al).

Looking more broadly at the gene expression of RGS5 in malignant tumors produces mixed results. Nearly an equivalent number of microarray expression experiments archived in the European Bioinformatics Institute Atlas report that the gene is over-expressed or under-expressed. The interpretation of these mixed results portrays a complex association within intratumor heterogeneity, where gene expression is highly dependent on location (Gerlinger et al) and in the specific example of RGS5, also on several other factors, including hypoxia and vascular remodeling.

However, other reports offer more clearly defined explanations. For example, a study by Silini et al. showed a low level (<1%) of RGS5 fluorescence covered the normal ovary whereas RGS5 increased to 7.3% coverage in ovarian carcinoma specimens from patient biopsies. Furthermore, the staining pattern of RGS5 coincided with vessel-like structures, which is suggestive of a biomarker for cancer vasculature and consistent with RGS5 expression predominantly resulting from the vascular endothelium of carcinoma. (Silini et al) Therefore, RGS5 levels could be expected to vary according to the extent and stage of tumor vascularization, perhaps explaining the gene expression variability for RGS5 among single biopsies specimens.

Not surprisingly given its association with the vasculature, RGS5 is also significantly affected by hypoxia, which is a response initiated by cells in low-oxygen environments that would otherwise succumb to toxic anoxia and cell death. Cancer cells in solid tumors are notorious for adapting to hypoxic environments by downregulating mitochondrial function (Papandreou et al 2006) and shifting to aerobic glycolysis

(Warburg 1956). Interestingly, Jin et al. showed that endothelial cells exposed to a hypoxic environment (<1% oxygen) display an increase in both mRNA and protein expression of RGS5 beginning at 30 min after exposure and tapering off around 24 hours. Furthermore, they identified RGS5 as a hypoxia-inducible gene that stimulates apoptosis and is regulated by the alpha subunit hypoxia-inducible factor-1 (HIF-1 α) (Jin et al). The HIF-1 heterodimeric transcription factor is an important regulator of angiogenesis because it causes the expression of numerous target genes (VEGF, PDGF, TGF- α , PDK1, COX4I2 etc.) which are involved in neovascularization, erythropoiesis, glucose transport and energy metabolism (Weinberg). Over-expression of VEGF and HIF-1 α has been associated with a poor prognosis in ovarian cancer and breast cancer patients (Weis and Cheresh 2005).

Further studies using an *RGS5*-deficient RIP1-Tag5 transgenic mouse model demonstrated an increased rate of tumorigenesis and reduction in the overall survival of mice through the development of a normalized network of blood vessels, decreased hypoxia and reduced vessel permeability (Hamzah et al , Manzur et al , Manzur et al). Interestingly, Hamzah, et al. also reported that RGS5 is “a master gene responsible for the abnormal tumor vascular morphology in mice” (Hamzah et al). We thus questioned whether the inducible expression of RGS5 in a tumor model of ovarian cancer might counter the effects observed in knockout mice and support a longer period of survival *in vivo*. Since the role of angiogenesis inhibitors are somewhat controversial (see discussion for more details), such a study may also clarify the extent to which RGS5 expression regulates tumor progression, perhaps via altered vascularization. Herein we observed an increase in the survival time in mice bearing tumors with RGS5 expression coupled with

increased areas of necrosis and a reduction in tumor ulceration. The control animals with tumors expressing the vector alone displayed more malignant cells within tumors and more had ulcerated tumors. Although all animals eventually succumb to disease, these studies are suggestive that RGS5 expression reduces malignancy in tumors, thus increasing survival time, and this is independent of its role in vascular normalization and remodeling.

Experimental Methods

Materials

HeyA8-MDR taxane-resistant line of cells were previously described (Hooks et al) and are maintained in RPMI 1640 medium (Mediatech, Inc., Manassas, VA.) supplemented with 300 ng/mL paclitaxel (Sigma-Aldrich, St. Louis, MO) with 15% fetal bovine serum (PAA Laboratories, Inc., Etobicoke Ontario, Canada). Approved fetal bovine serum (Clontech Inc., Mountain View, CA) was used in the medium for the pTet Dual RGS5-modified HeyA8-MDR cells. Doxycycline Hyclate for suppressed gene expression in the Tet-Off system (Sigma-Aldrich, St. Louis, MO). The compounds nocodazole, BrdU, etoposide, and aphidicolin were purchased Assay Kit from Millipore (Billerica, MA).

Construction of an inducible RGS5 cell line

The Tet-Off® Advanced Inducible gene expression system (Clontech) was used to create the RGS5-inducible HeyA8-MDR cell line. The pTRE-Tight dual RGS5-expressing DNA plasmid was constructed by standard restriction enzyme cloning to

insert an HA-tagged RGS5 coding sequence cassette (Missouri S&T cDNA Resource Center, Rolla, MO) into the pTRE-Tight Dual vector using the restriction enzymes XbaI and NheI. The constructs were verified by DNA sequencing using specific primers that were designed to recognize the N⁷-terminus of our Advanced Vector promoter. In order to create the doxycycline inducible cell line, 2.5×10^5 HeyA8-MDR cells were plated in a 6-well dish and transfected at a 1:5 ratio (plasmid DNA:Lipofectamine 2000, Life Technologies, Grand Island, NY) with pTet Advanced inducible vector plasmid DNA. Positive clones were selected using G418 (Geneticin[®], Life Technologies). These stable cells were then co-transfected with pTRE-Tight, Dual HA-RGS5 containing plasmid DNA and the linear hygromycin marker to enable selection with hygromycin. Positive clones were maintained in paclitaxel, G418, doxycycline and hygromycin.

Gene expression was verified in HeyA8-MDR pTet dual HA-tagged RGS5-inducible cells by seeding the cells in a multiple 6-well plates in medium with tetracycline-free fetal bovine serum without doxycycline for 24, 48 and 72 hours. Cells were harvested at the indicated time points, the RNA was isolated and processed for qRT-PCR using primers to detect RGS5 expression (amplicon size: 153 bp) resulting from the Tet-Off Advanced inducible system. The following primers were selected from PrimerBank (pga.mgh.harvard.edu/primerbank/), to confirm gene expression using qRT-PCR (RGS5 Fwd: 5'-ATTCAAACGGAGGCTCCTAAAG-3' and RGS5 Rev: 5'-CACAAAGCGAGGCAGAGAATC-3').

BrdU proliferation analysis

HeyA8-MDR cells were plated in a 96-well plate at a density of 3,000 cells per well. Half of the plate was grown in medium containing regular fetal bovine serum with doxycycline and the other half doxycycline-free with medium containing tetracycline-free fetal bovine serum. Cells were then incubated at 37°C for 72 hours to allow for RGS5-inducible gene expression. Prior to fixation, HeyA8-MDR cells were pulse-treated for 1 hour with BrdU and then treated for 4 hours with the indicated cell cycle arrest compounds. Cells were then fixed and stained for proliferation and nuclear morphology according to standard procedures from the manufacturer's protocol (BrdU Assay Kit, Millipore). Representative images taken using the Cellomics ArrayScan VTI HCS Reader (Thermo Fisher Scientific, Waltham, MA) as previously described (Jia et al) and are shown here. High content scanning analysis software was used to determine the average number of cells per field. The data was retrieved from the manufacturer's software and results were plotted with GraphPad Prism (La Jolla, CA).

Animal model of ovarian cancer with gene modulation

Six-week-old female athymic nude mice 6 weeks of age acclimated to the animal facility for 1 week prior to the commencement of the study. Animals were injected intraperitoneally with Extracel[®] containing approximately 5 million cells of either HeyA8-MDR pTet Advanced Vector (N=10) or HeyA8-MDR pTet Dual RGS5 expressing cells (N=10) per 0.2µl injection. Injected mice were monitored for tumor formation, weight and stomach circumference. After one week, 100% of mice displayed tumor formation. The animals were monitored over a course of 2 months and euthanized according to the

animal use protocol approved by the University of Georgia IACUC committee. The tumor volume (mm³) was calculated using the equation tumor volume = (width)² x length/2, and then graphed using Prism. The time of survival for each group and overall significance was plotted on a Kaplan-Meier survival curve also using GraphPad Prism.

Measurement of vascular endothelial growth factor

At necropsy, blood from all animals was collected in BD microtainer tubes with serum separator (Becton Dickinson Co., Franklin Lakes, NJ). The serum-containing fraction was isolated using centrifugation, placed into glass vials and frozen immediately. After thawing on ice, the mouse serum was measured for the presence and concentration of vascular endothelial growth factor a mouse VEGF ELISA kit following the manufacturer's protocol (RayBiotech, Inc., Norcross, GA).

Tissue collection, histology, and immunofluorescence

Mice were euthanized according to standard protocols. Visible tumors were dissected from the abdomen, measured for size, and flash frozen with cryomatrix (Thermo Fisher Scientific) in 2-methylbutane (Sigma) cooled to -140 C. Cryopreserved tumors were cut in 10 µm sections using a Thermo Fisher Scientific cryostat and mounted on microscope slides. Hematoxylin and eosin staining was performed according to standard protocols and imaged using a Leica microscope for pathological evaluation.

For immunofluorescence, tissues were blocked for 30 minutes in 5% normal donkey serum (Jackson ImmunoResearch Laboratories, Inc., West Grove, PA) in phosphate-buffered saline (PBS) for 30 minutes at room temperature. The tumor sections

were incubated in the primary antibody CD31 (1:500, BD Pharmingen, San Diego, CA) at 4°C overnight in a humidity chamber, washed with PBS, and detected with the secondary antibody Cy3-anti-rat IgG. DAPI nuclear stain (final 1:10,000) was included in the secondary antibody incubation. After thorough washing with PBS, slides were coverslipped with permount (Thermofisher Scientific). Immunofluorescence was imaged using an X71 inverted microscope (Olympus, Center Valley, PA) at 20x magnification. Images were resized and adjusted identically using Photoshop (Adobe, San Jose, CA). Overlapping pictures were aligned in Microsoft PowerPoint to generate an image of an entire tumor cryosection. Each compiled tumor section was imported into Image Pro Express (Media Cybernetics, Bethesda, MD) for analysis. Tumor vascularization was determined by analyzing the number of pixels and fluorescence units above background to indicate CD31 positive cells, normalized to tumor area.

Statistics

The statistical differences were analyzed using the Student's *t-test* to compare only two groups on Graph Pad Prism. Where it is indicated in the figures, * $p < 0.05$ and ** $p < 0.01$ indicate the levels of significance. Error bars are standard error of the mean (SEM). For comparison of the survival curves the Log-rank (Mantel-Cox) test was used to determine if the curves were significantly different in Graph Pad Prism. Where it is indicated in the figure, * $p < 0.05$ is significant.

Results

Expression of RGS5 reduces in vitro proliferation of HeyA8-MDR ovarian cancer cells

Although RGS5 is a biomarker for tumor vasculature, we sought to understand whether RGS5 itself plays a pathogenic or protective role in ovarian tumor biology. To address this question, we constructed RGS5 in an inducible gene expression system to induce high levels of RGS5 protein when cells were cultured in the absence of the antibiotic doxycycline. The Tet-Off[®] inducible system was necessary because RGS proteins regulate G protein-coupled receptor signaling cascades, which are required for cancer cells survival and are often critical to cells with oncogenic addictions to survival pathways. When cells were grown in the absence of doxycycline and medium containing FBS free of tetracycline, the expression of RGS5 protein reached ~7-fold after 48 hours and ~4.5-fold after 72 hours (**Figure 4.1A**).

When we compared the vector control cells (+ doxycycline) versus RGS5-expressing HeyA8-MDR cells (– doxycycline), we observed a significant reduction in the number of proliferating cells among the latter group with induced expression of RGS5 (**Figure 4.1B**). Representative images are shown from high-throughput scanning (see methods). We next analyzed cancer cell proliferation using automated quantification of cells detected per field after a pulse with bromodeoxyuridine (BrdU), a nucleoside analogue and marker for proliferating cells. Cells engineered to inducibly express RGS5 showed a significant reduction in the number of BrdU-positive proliferating cells (***) $p < 0.001$, comparing +dox with –dox). Treating the cells with either anti-neoplastic reagents etoposide, a topoisomerase II inhibitor, or nocodazole, an inhibitor of microtubule polymerization, further reduced the average number of cells measured per

field (**Figure 4.1B and C**; *** $p < 0.001$), although the ratio was similar between the non-treated and treated conditions. As a control, we measured no net change in the mean difference of “target” BrdU fluorescence intensity among the specific cell cycle compounds, suggesting no net bias effect of the fluorescence. Taken together, these data suggest that RGS5 expression reduces the proliferative capacity of HeyA8-MDR ovarian cancer cells.

Since RGS5 has been shown to be a hypoxia-inducible gene regulated by HIF-1 α (Jin et al), we measured vascular endothelial growth factor (VEGF) in serum. Solid tumors will develop hypoxic regions, which would then up-regulate RGS5 and possibly interfere with our results. We chose VEGF because HIF-1 regulates VEGF expression as

Table 4.1. Histological examination of tumor sections by a pathologist.

Table I. Histological examination of tumor sections by a pathologist.

Vector Controls	Tissue Type	Tumor %	Necrosis	Mitoses mm ²	Karyorrhexis
1	mesentery	70	Not identified	<1	yes
2	skin	95	Ulcer/focal	<1	yes
3	mesentery	>90	Not identified	<1	yes
RGS5-expressing					
1	mesentery	>90	Broad area	1	yes
2	mesentery	>90	Broad area(s)	1	yes
3	mesentery	60	Scattered	1	yes

well as RGS5. If we detected significantly altered levels of VEGF between the groups, then this could indicate a problem with the data. However, there was no significant difference between the serum levels of VEGF between the groups (**Figure 4.2C**), suggesting that endogenous RGS5 regulation was unchanged.

Histological studies suggest large areas of necrosis in RGS5-expressing tumors

We randomly selected tumors from each group for sectioning and histological analysis. Interestingly, the hematoxylin and eosin stained tumor sections showed several important differences between control and RGS5-expressing tumors. In the control group of mice with tumors containing the empty vector, diffuse sheets of malignant cells comprised 70-95% of the sampled tissue, demonstrating extensive involvement of the tumor (**Table 4.1**).

Expression of RGS5 in an ovarian tumor model increases survival

Previous studies have examined the absence of RGS5 expression *in vivo* using knockout mice (Manzur et al). In contrast with these studies, we created an *in vivo* model of tumorigenesis with inducible expression of RGS5 to measure whether there was an effect on tumor regression. Athymic nude female mice were injected intraperitoneally with tumors containing either the vector alone or RGS5-expressing tumors. We routinely measured tumor volume, but were unable to detect any differences between these groups (**Figure 4.2A**). In contrast, control animals with empty vector tumors displayed lower

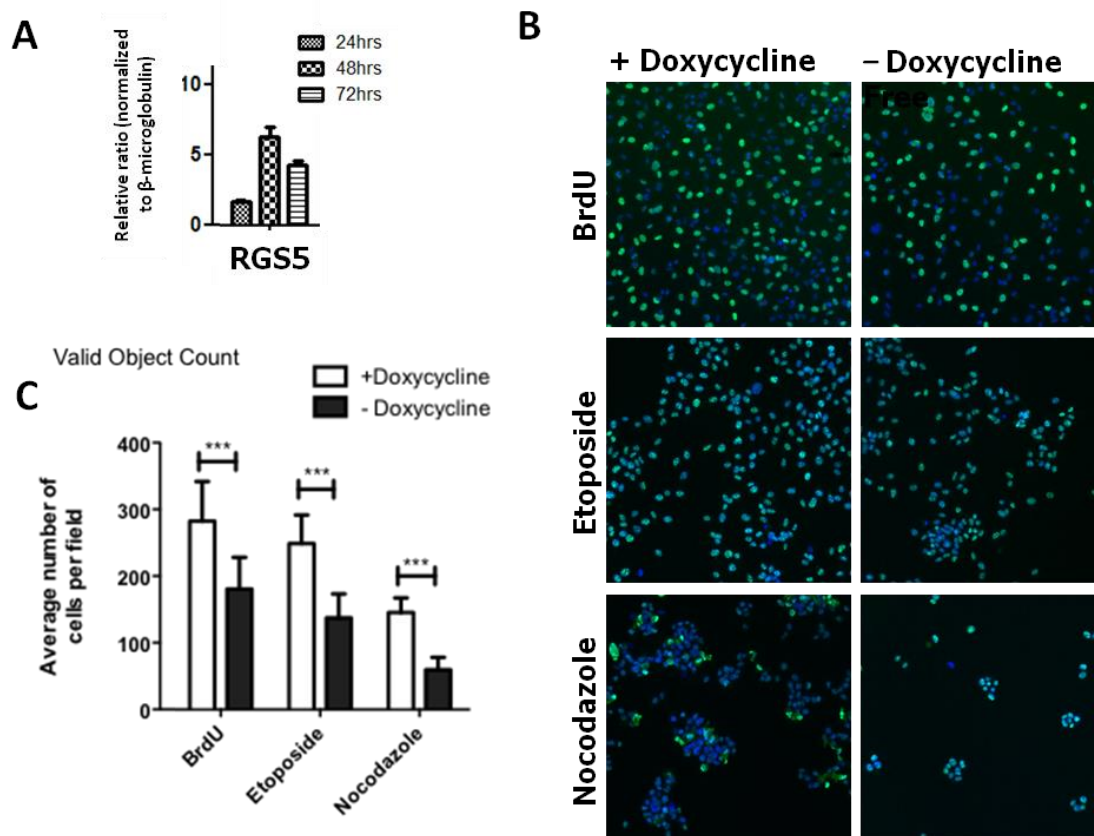


Figure 4.1. RGS5 inducible expression in HeyA8-MDR cells reduces proliferation. (A) HeyA8-MDR pTet dual RGS5 inducible cells were seeded in a multiple 6-wells and cultured in medium with tetracycline-free fetal bovine serum without doxycycline for 24, 48 and 72 hours. Cells were harvested; the RNA was isolated and processed for qRT-PCR using primers to detect RGS5 expression resulting from the Tet-Off Advanced inducible system. Without the presence of doxycycline or other members of the tetracycline antibiotics, RGS5 expression was observed. (B) HeyA8-MDR cells were plated in a 96-well plate at a density of 3,000 cells per well. Half of the plate was grown in medium containing regular FBS with doxycycline and the other half containing doxycycline-free media. Cells were then incubated at 37°C for 72 hours to allow for RGS5-inducible gene expression. Prior to fixation, HeyA8 MDR cells were pulse-treated for 1 hour with BrdU and then treated for 4 hours with the indicated cell cycle arrest compounds. Cells were then fixed and stained for proliferation and nuclear morphology. Representative images taken using the Cellomics ArrayScan VTI HCS Reader and are shown here. (C) High content scanning analysis software was used to determine the average number of cells per field.

body conditioning scores than mice bearing RGS5 tumors and therefore had to be monitored more frequently. Mice bearing RGS5 tumors displayed more active behavior and appeared healthier over a longer period of time with higher body conditioning scores in comparison (data not shown).

We also measured the difference in survival times between the two groups. The control mice with empty vector tumors began to die (or were euthanized because they reached humane endpoints) at 22 days and all succumbed to disease by 47 days (**Figure 4.2B**). In comparison, the first mouse from the group bearing RGS5 tumors died at 28 days and the last two in the group died after 55 days. The results suggest a significant increase in survival time ($p=0.0143$) with RGS5 expression, although there were no animals that ultimately survived the disease.

In contrast, mice bearing tumors expressing RGS5 had regions of necrosis that varied from scattered necrotic areas to broad and large areas of central necrosis. RGS5-expressing tissue was also composed of ~60-90% tumor. In the necrotic areas of RGS5-expressing tumors, pyknotic nuclei and dark eosinophil cytoplasm were observed in the malignant cells along the peripheral areas of the necrotic regions. Finally, the histological tumor samples of the control mice showed areas of skin ulceration, whereas the RGS5-expressing sections did not. This is in agreement with the overall observations where we observed a reduced presence of tumor ulceration in mice bearing RGS5-expressing tumors (**Figure 4.3**).

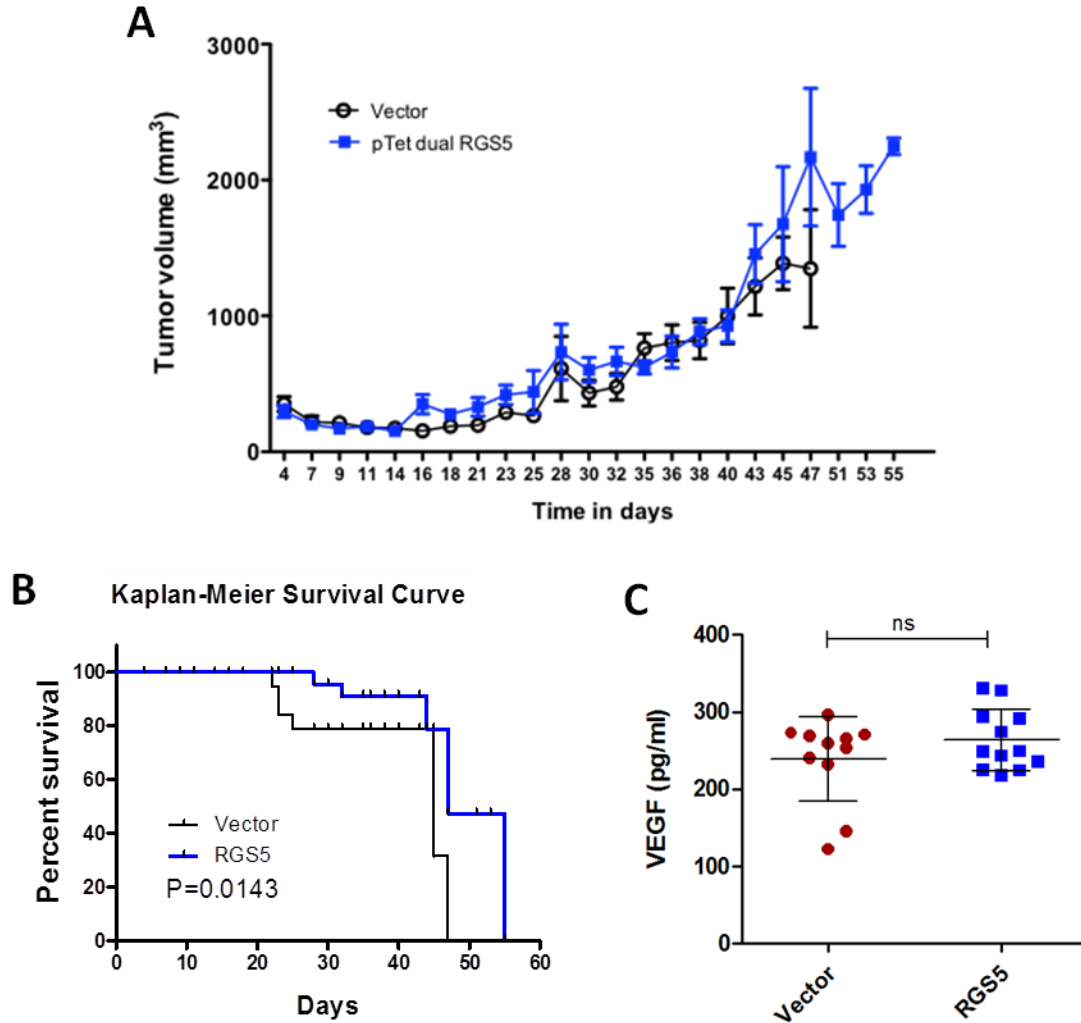


Figure 4.2. Expression of RGS5 in ovarian tumors did not significantly reduce the rate of growth, but did increase the overall survival time of mice bearing such tumors. (A) Female athymic nude mice were given intra-peritoneal injections of Extracel[®] containing approximately 5 million cells of either HeyA8 MDR pTet Advanced Vector (N=10) or HeyA8-MDR pTet Dual RGS5 expressing cells (N=10) per 0.2 μ l injection. All mice were monitored for tumor formation and measurements of weight and stomach circumference were routinely taken. The graph plots tumor volume (mm³). (B) Mice bearing HeyA8-MDR pTet Dual RGS5-expressing tumors had a significant increase in survival time (in days, *p=0.0143, compared to their pTet Advanced Vector alone counterparts). (C) Blood was collected from mice at necropsy. The serum-containing fraction was isolated and measured for vascular endothelial growth factor. Results are non-significant (ns) between the groups.

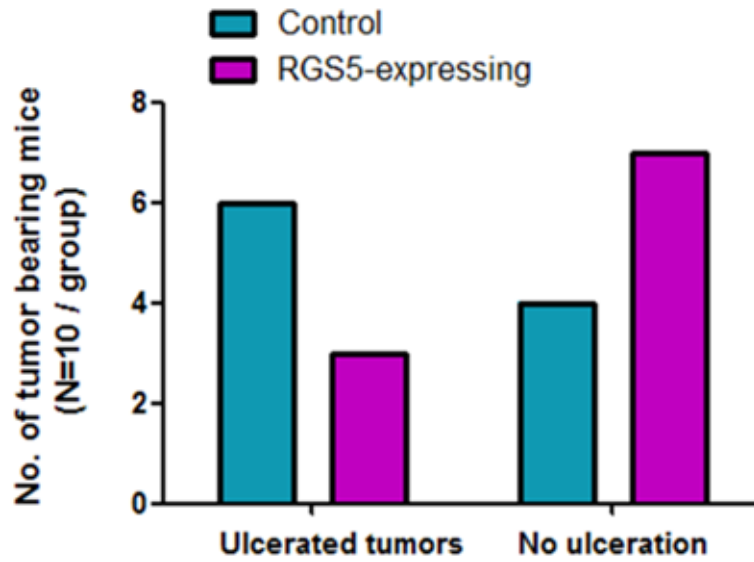


Figure 4.3. Mice bearing RGS5-expressing ovarian tumors displayed less frequent tumor ulceration. The number of mice with ulcerated tumors observed at necropsy was recorded (N=10 per group). Tumor sizes were relatively similar between the two groups.

Tumor angiogenesis

To clarify the functional contribution of RGS5 expression in tumor angiogenesis, we randomly selected tumors from each group for sectioning and analysis of positively-stained structures of the cluster of differentiation 31 (CD31) or platelet/endothelial cell adhesion molecule 1 (PECAM-1), which is glycoprotein biomarker expressed on vascular endothelial cells used to assess the degree of angiogenesis. We observed CD31-positive structures in tumor specimens from both groups of animals (**Figure 4.4A**). The RGS5-expressing tumors displayed a greater frequency of CD31-positive vessel-like structures, compared with the vector-expressing tumors (**Figure 4.4B**, ** $p < 0.01$). This is consistent with the role of RGS5 as a pericyte biomarker that is temporally upregulated during the switch to angiogenesis in malignancy. The data is suggestive that introducing RGS5 into the solid tumor likely influenced the balance of this switch in favor of angiogenesis.

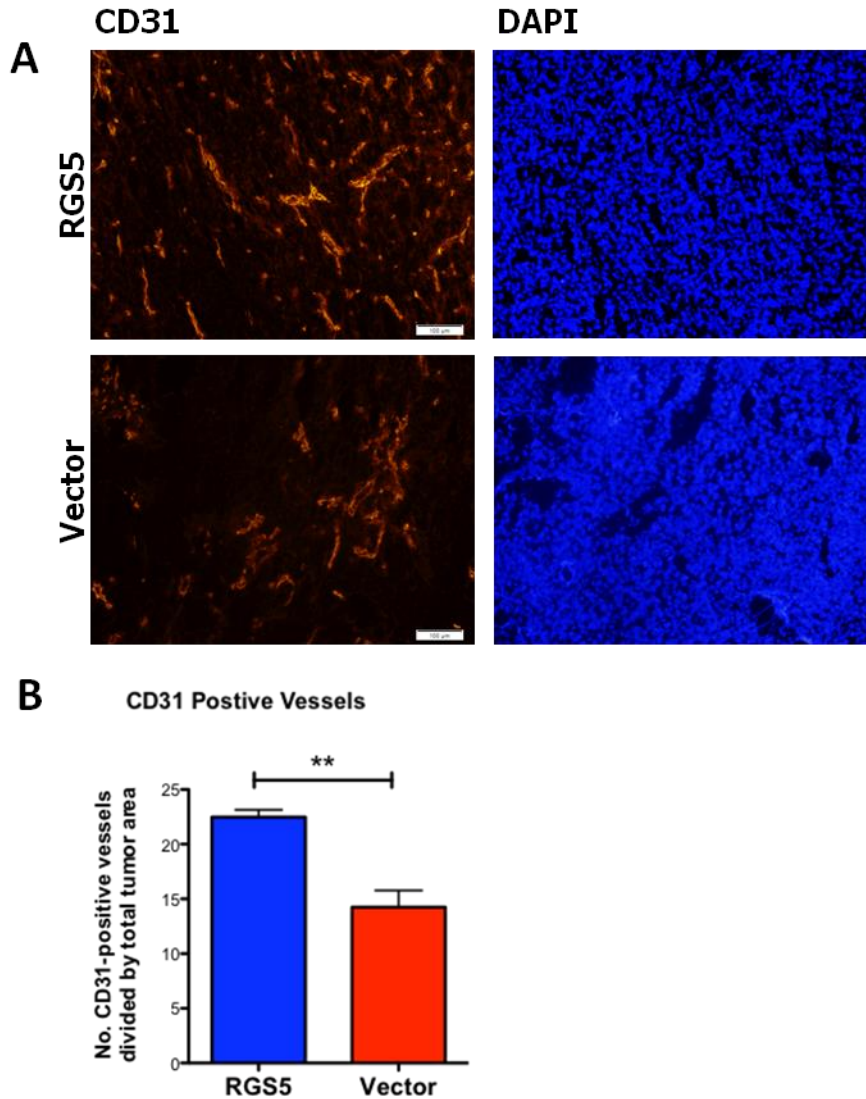


Figure 4.4. RGS5-expressing ovarian tumors increase the number of CD31-positive vessel-like structures. Tumor specimens were sectioned and prepared on slides for immunofluorescence. (A) Tumor sections were probed with CD31 overnight prior to visualization using secondary antibodies (shown) and DAPI (not shown). Images presented are representative and the bar graph (B) displays quantified data (N=4), which was generated using CellSens and GraphPad Prism software. **p<0.01, comparing vector vs. RGS5.

Discussion

In this study, we used Tet-off inducible expression to study the role of RGS5, *in vitro* and *in vivo*, in tumor proliferation and pathology. We found that mice bearing RGS5-expressing tumors survived longer than controls and displayed large regions of necrosis within their tumors. They were also less likely to have ulcerated tumors in comparison to control mice. Our study is consistent with previous work that produced RGS5-deficient mice and suggested that RGS5 loss accelerated tumor development, enhanced tumor growth (in the later tumor stages), reduced survival, decreased hypoxia and decreased vessel permeability (Hamzah et al , Manzur et al , Manzur et al).

Hamzah et al. created an RGS5 knockout mouse model using a mix of normal 129 and C57BL/6 mice crossed with the C3H background, which then allowed the assessment of immune function. Although not statistically significant, the RGS5 knockout mouse model resulted in the opening of solid tumors to spontaneous immune effector T-cell infiltration into the tumor parenchyma. In addition, this model showed prolonged survival among tumor-bearing mice *with* the transfer of activated and specific T cells. (Hamzah et al) Our study used athymic immunodeficient nude mice, which manifest an inhibition of the immune system and thus will not mount an immune response to xenograft injection. It is interesting that we observed vast regions of necrosis in the solid tumors without the immune system modulating this response in RGS5-expressing tumors. This necrosis is likely due to two factors: hypoxia resulting from aberrant tumor vasculature and RGS5 induction of apoptosis (Jin et al 2009).

Although we observed an increase in the survival time in mice bearing RGS5-expressing tumors, the overall increase in time was modest. Too many chemotherapies

and biological agents also achieve mediocre increases in overall survival, leading the industry to focus instead on quality-of-life parameters for measuring drug ‘successes’. The results of our study dampen enthusiasm for pursuing RGS5 as a *single* target for therapeutics in tumorigenesis. However, our study does provide support for including RGS5 as *one* important component of a multi-component approach to help modulate tumor progression. As the treatment of cancer is a multifaceted discipline, and cytotoxic chemotherapy is combinatorial, momentum for combinatorial biological therapies is also gaining, even among “magic bullet” therapeutics (i.e. imatinib and vemurafenib). The shift is being driven by chemoresistance to therapy, which is relevant in this setting because RGS proteins are involved in chemoresistance (Hooks et al) as well as hypoxia – a driver of chemoresistance (Sorensen et al).

Our study also demonstrates that RGS5 effects active cellular proliferation in HeyA8-MDR cells *in vitro* using the BrdU assay. This result is in contrast with other studies suggesting that the overexpression of RGS5 reduces the rate of growth without affecting cell proliferation (Jin et al). The differences between the two studies are likely the model system. Whereas we are using rapidly-proliferating ovarian cancer cells resistant to paclitaxel, the previous study used human umbilical vein endothelial cells. Thus, our model system is highly aggressive, tumorigenic and drug resistant with or without RGS5 expression.

The addition of chemotherapeutic agents (etoposide or nocodazole) to the culture of RGS5-inducible HeyA8-MDR cells further reduced the average number of cells present and proliferating. Although very exciting, the fact that RGS5 has a dual role tumor biology (i.e. vascularization vs. tumor growth) makes it unclear how modulation of

RGS expression would affect therapy. For example, RGS5 modulation could significantly complicate drug delivery into solid tumor parenchyma. On one hand, RGS5 loss results in normalization of the vasculature *in vivo*, which would allow penetration of T cells and chemotherapy, but otherwise RGS5 loss enhances tumor growth (Hamzah et al). On the other hand, RGS5 is overexpressed in aberrant tumor vascular (Berger et al), but its expression induces endothelial apoptosis (Jin et al), reduces cell proliferation and increases overall survival. Indeed, in our study the mice bearing RGS5-expressing tumors that showed large areas of central necrosis were not treated with cytotoxic chemotherapy; however, if we had treated these mice with intravenous cisplatin or carboplatin, it is unclear whether these drugs could have reached the tumor parenchyma without a robust vasculature and what the effect on overall survival would have been.

In addition, whether or not angiogenesis is an optimal target for therapy against solid tumors is another growing controversy. Recent studies in glioblastoma hypothesize that vascular normalization improves survival through tumor perfusion (Sorensen et al). Furthermore, another study of bevacizumab (Avastin™)-treated rats bearing human glioblastoma multiforme tumors demonstrated, “a strong and highly significant increase in the number of tumor cells invading the normal brain” (Keunen et al), suggesting a negative effect on tumor biology in that setting.

In 2011, the Food and Drug Administration revoked its approval of bevacizumab for therapy in metastatic breast cancer because it lacked efficacy and increased the risk for lethal side effects. Some speculated this review by the FDA was also necessary due to bevacizumab’s extraordinarily high yearly cost without the possibility of achieving monotherapeutic cure. For example, bevacizumab is indicated for use as *combination*

therapy in metastatic colorectal cancer, non-squamous non-small cell lung cancer and metastatic renal cell carcinoma and as a single agent for glioblastoma patients based on objective response rate, not survival (Genentech). Thus, combination regimens with angiogenesis inhibitors have substantially increased the expense of cancer treatment through drug costs and the costs associated with hospitalization for adverse drug responses (Jackson and Sood). A better understanding of the tumor vasculature and its impact on the biology of solid tumors and therapy is needed to address this controversial approach.

Future studies might explore the roles of combinations of RGS5 with other RGS proteins in ovarian cancer. For example, on chromosome 1q23.3-1q31 there are 5 genes encoding RGS family members (RGS2, RGS4, RGS5, RGS8 and RGS16) and these have overlapping cellular functions (Campbell et al). It is unclear whether combinations of these RGS proteins would further modulate the aggressiveness of ovarian cancer cells or tumors in mice. Since RGS proteins turn off signaling cascades from growth factors, future studies could also assess the modulation of these with other proteins affecting G protein-coupled receptors and receptor inhibitors. Much is left to learn about RGS proteins and their role in tumorigenesis and therapy.

CHAPTER 5

TARGETING MELANOMA GROWTH AND VIABILITY REVEALS DUALISTIC FUNCTIONALITY OF THE PHOSPHONOTHIONATE ANALOGUE OF CARBA CYCLIC PHOSPHATIDIC ACID¹

¹ Altman, MK., Gopal, V., Jia, W., Yu, S., Hall, H., Mills, GB., McGinnis, AC., Bartlett, MG., Jiang, G., Madan, D., Prestwich, GD., Xu, Y., Davies, MA., and Murph, MM.. 2010, *Molecular Cancer*, 9:140. Reprinted here with permission of the publisher.

Abstract

Background: Although the incidence of melanoma in the U.S. is rising faster than any other cancer, the FDA-approved chemotherapies lack efficacy for advanced disease, which results in poor overall survival. Lysophosphatidic acid (LPA), autotaxin (ATX), the enzyme that produces LPA, and the LPA receptors represent an emerging group of therapeutic targets in cancer, although it is not known which of these is most effective.

Results: Herein we demonstrate that thio-ccPA 18:1, a stabilized phosphonothionate analogue of carba cyclic phosphatidic acid, ATX inhibitor and LPA1/3 receptor antagonist, induced a marked reduction in the viability of B16F10 metastatic melanoma cells compared with PBS-treated control by 80-100%. Exogenous LPA 18:1 or D-sn-1-O-oleoyl-2-O-methylglyceryl-3-phosphothioate did not reverse the effect of thio-ccPA 18:1. The reduction in viability mediated by thio-ccPA 18:1 was also observed in A375 and MeWo melanoma cell lines, suggesting that the effects are generalizable. Interestingly, siRNA to LPA3 (siLPA3) but not other LPA receptors recapitulated the effects of thio-ccPA 18:1 on viability, suggesting that inhibition of the LPA3 receptor is an important dualistic function of the compound. In addition, siLPA3 reduced proliferation, plasma membrane integrity and altered morphology of A375 cells. Another experimental compound designed to antagonize the LPA1/3 receptors significantly reduced viability in MeWo cells, which predominantly express the LPA3 receptor.

Conclusions: Thus the ability of thio-ccPA 18:1 to inhibit the LPA3 receptor and ATX are key to its molecular mechanism, particularly in melanoma cells that predominantly express the LPA3.

Introduction

The incidence of melanoma, the most aggressive form of skin cancer, is rising faster than any other cancer in the U.S. with a 619% increase from 1950 to 2000 (Tsao et al 2004). While mortality from many cancers is in decline, melanoma of the skin is among only three types, including liver and esophageal, with increasing mortality among males in the U.S. (Jemal et al 2008). Although remarkable strides in research, prevention and treatment continue to reduce cancer-related mortality overall, the mortality from melanoma is expected to rise due to the combination of increasing incidence and lack of effective therapies. Factors that increase melanoma susceptibility include accumulating genomic mutations from environmental sun exposure, a decrease in keratinocyte stem cell proliferation capacity, a decline in the regeneration ability of the skin and evolving changes in cellular signaling (Weinberg 2007b).

Advanced metastatic melanoma has an alarming average survival of only 6 to 10 months with less than 5% of patients living 5 years after diagnosis (Jemal et al 2002). Unfortunately FDA-approved chemotherapy and immunotherapy used against advanced metastatic melanoma such as dacarbazine (DTIC), interferon (IFN) and interleukin-2 (IL-2) do not significantly improve patient outcomes in the majority (>80%) of patients (Hocker and Tsao 2007). Thus, more basic research is desperately needed to develop new, more effective therapeutic strategies for this disease.

The potential involvement of the lysophosphatidic acid (LPA) signaling pathway in melanoma was hypothesized when autotaxin (ATX, ENPP2) was demonstrated to be identical to a motility-stimulating factor secreted by melanoma cells (Stracke et al 1992). ATX is the enzyme that generates the main extracellular pool of LPA (Umezu-Goto et al

2002). LPA is a normal lipid constituent of biological fluids with a wide range of molecular signaling and resultant cellular outcomes (Mills and Moolenaar 2003, Murph et al 2006) LPA has been proposed to activate at least eight known G protein coupled receptors (LPA1 (Hecht et al 1996), LPA2(An et al 1998), LPA3 (Bandoh et al 1999) LPA4/GPR23 (Noguchi et al 2003), LPA5/GPR92/93 (Kotarsky et al 2006, Lee et al 2006a), GPR87 (Tabata et al 2007), P2Y5 (Pasternack et al 2008) and P2Y10 (putative dual LPA and S1P receptor) (Murakami et al 2008). LPA has also been demonstrated to activate PPAR γ (McIntyre et al 2003) and participates in cross communication with tyrosine kinase receptors through as yet unclear mechanisms (Oyesanya et al 2010, Shah et al 2005) The role of LPA production, LPA receptor activation and LPA receptor expression in mela- noma progression, and as potential therapeutic targets, remains poorly understood.

Cyclic phosphatidic acid (1-acyl-sn-glycerol-2,3-cyclic phosphate; cPA) is a naturally-occurring compound that was originally isolated from the lipid fraction of slime mold. cPA was initially demonstrated to have strong inhibitory activity on eukaryotic DNA polymerase α , but not β or γ (Murakami-Murofushi et al 1992) However, cPA exhibits multiple other actions in mammalian cells. For example, cPA prevents tumor cell migration through its ability to down-regulate active RhoA and thus the downstream autophosphorylation of focal adhesion kinase (Mukai et al 2003). Previously we demonstrated that carba analogues of cyclic phosphatidic acid (ccPA) potently inhibit ATX activity, LPA synthesis and metastatic melanoma progression in vivo (Baker et al 2006). Interestingly, ccPA compounds demonstrate anti-metastatic effects accompanied by inhibition of RhoA activation. This effect is not due to inhibition of LPA receptor

activation (Uchiyama et al 2007) suggesting that inhibition of ATX and subsequent LPA production represents a critical target.

We have developed the next generation of ccPA compound, the stabilized analogue thio-ccPA 18:1, as a mechanistic probe and potential therapeutic modality. Thio- ccPA 18:1 is a phosphonothioate analogue of ccPA with an enhanced ability to inhibit ATX activity (89% at 10 μ M) (Xu et al 2006). Thio-ccPA 18:1 is also unique due to its action as a selective inhibitor of LPA receptors, blocking LPA1 and LPA3, with no effect on LPA2 (Hasegawa et al 2008, Prestwich et al 2008) Thio-ccPA 18:1 has not demonstrated any detectable agonist-related activation of the LPA receptors examined, including LPA1, LPA2 or LPA3 (Xu et al 2006).

Herein we tested the potential of thio-ccPA 18:1 as a melanoma therapeutic in vitro and as a probe of relative efficacy of inhibition of ATX, LPA1 and LPA3. We observed that thio-ccPA 18:1 reduces viability in the highly aggressive B16F10 model for metastatic disease progression. Our data demonstrates that thio-ccPA 18:1 directly inhibits the growth and viability of B16F10 melanoma cells, as well as two commonly used human melanoma cell lines, A375 and MeWo. Although ATX inhibition contributes greatly to therapeutic efficacy against melanoma (Baker et al 2006), the effect of thio-ccPA 18:1 on viability is not only related ATX inhibition since neither LPA nor a stabilized LPA analog, R-OMPT (Hasegawa et al 2003) that would bypass the inhibition of ATX, were able to override the inhibitory effects of thio-ccPA 18:1. In addition, we demonstrated that inhibition of LPA3 by siRNA also results in a decrease in cell viability in melanoma cells. These studies are the first to implicate LPA3 as a critical mediator of melanoma growth and survival, and provide evidence that LPA3 mediated receptor

signaling may represent an important therapeutic target in melanoma, providing an enhanced benefit of the phosphonothionate analogue.

Experimental Methods

Reagents and Materials

LPA (18:1, 1-oleoyl-2-hydroxy-sn-glycero-3-phosphate and 14:0, 1-myristoyl-2-Hydroxy-sn-Glycero-3-Phosphate) and (S)-phosphoric acid mono-{2-octadec-9-enoylamino-3-4-(pyridin-2-ylmethoxy)-phenyl-propyl} ester was purchased from Avanti Polar Lipids Inc (Alabaster, AL). D-sn-1-O-oleoyl-2-O-methylglyceryl-3-phosphothionate (R-OMPT) was purchased from Echelon Biosciences, Inc. (Salt Lake City, UT). A375 epithelial malignant melanoma, MeWo fibroblast malignant melanoma cells and OVCAR-3, A549 and MDA-MB-231 cells were acquired from ATCC (Manassas, VA) and maintained in Cellgro RPMI (Mediatech, Inc., Manassas, VA) supplemented with 5% (MeWo and A375) or 10% (OVCAR-3, A549 and MDA-MB-231) FBS (Sigma, St Louis, MO). B16-F10 murine melanoma were the kind gift of Dr. Isaiah J. Fidler at The University of Texas MD Anderson Cancer Center, Department of Cancer Biology and maintained in DMEM (Mediatech, Inc.) supplemented with 10% FBS (Sigma). The phosphonothionate ccPA 18:1 analogue (thio-ccPA 18:1) was synthesized as previously described (24). The solid lyophilized sodium salt of thio-ccPA 18:1 was reconstituted in PBS prior to use.

Mouse xenograft model

All animal studies were conducted in compliance with the policies and regulations of the University of Texas M.D. Anderson Cancer Center Institutional Animal Care and Use Committee (IACUC). To analyze the consequence of treating metastatic melanoma tumors with thio-ccPA in vivo, thirty C57/B16 mice (male, 4-6 weeks old) were injected intravenously with 5×10^4 B16F10 cells into the tail vein. Three days post injection, ten mice were randomly selected for treatment with thio-ccPA 18:1. Of this group, mice were given the indicated doses of thio-ccPA by intraperitoneal injection. Thio-ccPA 18:1 injections were repeated seven days post tumor cell injection. After 21 days all surviving mice were euthanized, gross necropsy was performed and lungs were removed for further examination for the presence of metastatic lesions. Surviving mice were N = 17 for the control and N = 10 for thio-ccPA 18:1. One murine lung was processed for pathological examination and immunohistochemistry. The other lung was examined for lesions using a dissecting microscope and imaged using a Nikon Coolpix camera (Southern Microscope, Inc., Haw River, NC). Two independent observers assessed the number of nodules present on the lungs and results were averaged. Results are means \pm SE of experiments, **p < 0.01 treatment groups vs. control by Tukey's test and analysis of variance.

Cell viability

B16F10, A375 or MeWo cells were examined for viability by seeding the indicated number of cells (1×10^3 - 25×10^3) in 96-well plates in quadruplicates. Cells were allowed to attach to the plate for 4-8 h in 1% FCS containing medium (or 10% FCS containing medium where indicated) prior to stimulation with PBS, 10-250 μ M thio-

ccPA 18:1, FBS or 0.1-10 μ M 18:1 LPA where indicated. In some experiments, cells were transfected with the indicated ON-TARGETplus SMARTpool siRNA reagent (Dharmacon, Lafayette, CO) and DharmaFECT (Dharmacon) for 48 h (see below for details). CellTiter™ Blue reagent (Promega, Madison, WI) was added to plates and cells were incubated at 37°C to assess viability as previously described (Hasegawa et al 2008). Images of individual wells of 96-well plates were acquired using a 12 megapixel Nikon Coolpix camera (Southern Microscope, Inc., Haw River, NC). All images show representative photos corresponding to quadruplicate conditions.

Cell proliferation assay

A375 cells were seeded in quadruplicates in 96-well plates (2,000 cells/well) and allowed to attach for 8-16 h. Cells were then placed in 1% serum-containing medium and Transfected with the indicated indicated ON-TARGETplus SMARTpool siRNA reagent (Dharmacon) for 48 h. Proliferation was assessed as previously described using crystal violet (Hasegawa et al 2008). Experimental groups were compared with siRNA negative control (Applied Biosystems, Foster City, CA) and mock transfected controls. Results are means \pm SE of experiments. * $p < 0.05$ treatment groups vs. control by Bonferroni's test and analysis of variance.

Small interfering RNA (siRNA) transfection

We down-regulated individual LPA receptor expression by using sequence-specific siRNA purchased from ON- TARGETplus SMARTpool siRNA reagents (Dharmacon). The cells were transfected according to the manufacturer's protocol using

either reagents DharmaFECT (Dharmacon) or the X-tremeGENE siRNA transfection reagent (Roche, Palo Alto, CA). Negative control siRNA (control) was purchased from Applied Biosystems (Foster City, CA). Expression levels of gene knockdown were optimized as previously described (Hasegawa et al 2008, Yu et al 2008).

Assessment of siRNA transfection

Cells were transfected with SMARTpool siRNA reagents (Dharmacon), which contain four different siRNA, each consisting of 21 base pairs. The siRNA was extracted separately from the media and cells and analyzed by ion chromatography using UV detection. Samples of the cell medium and RNA isolated from transfected cells were collected after 0, 6, 10 and 24 h. Along with ion chromatography showing siRNA inside the cell, RNA and visual observations of cells also corroborated successful transfection targeting this receptor.

Trypan blue exclusion

The A375 and Mewo cells were seeded in 6-well dishes at a density of 10^5 cells/well and allowed to attach overnight. The cells were transfected with 20 nM of the indicated siRNAs using the X-tremeGENE transfection reagent (Roche, Palo Alto, CA). After 72 h of incubation, the cells from separate wells were trypsinized, cell samples were mixed with an equal volume of a solution of 0.4% Trypan Blue dye (Sigma, St. Louis, MO) just before the counting of cells. The cells from each replicate sample were immediately transferred into both grids of a Neubauer hemocytometer and the viable (dye excluding) fraction of cells in all ten squares of both grids were counted under a

microscope. Cell numbers from all squares were averaged and the total number of cells for each replicate sample was determined.

Real-time PCR

mRNA of MeWo and A375 cells was extracted with Gen-Elute Direct mRNA kit (Sigma Aldrich, St. Louis, MO) and reverse transcribed into cDNA using Superscript III kit (Invitrogen, Carlsbad, CA) following the manufacturer's protocol. Total human skin RNA was purchased from Agilent Technologies (Palo Alto, CA). Real-time PCR was performed using the primers for LPA1, LPA2, LPA3, LPA4 and LPA5 as previously described (Valentine et al 2008) and other primers for p2y5: forward 5'- TTGTATGGGTG- CATG TTCAGC-3' and reverse 5'- GCCAATTCCGTGT- TGTGAAGT -3'; p2y10: forward 5'- GTTTCCT GACGTGCATCAGTC -3' and reverse 5' - AGTCCCCACAACGATCCAGAT -3' based on algorithm generated sequences from Primer Bank <http://pga.mgh.harvard.edu/primerbank/> (Wang and Seed 2003). Other primers used included GPR87: forward 5'- GAGCAAGTTGTTCCAGTAGTCG-3' and reverse 5' - CTTTGAAACTAAGGTCGGCAGG-3'; ATX: forward 5'- CTCGTTCCAGTCGTGTCAGA -3' and reverse 5' - CAAGATCCGGAGATGTTGGT - 3'. PCR products were visualized by loading 1 µl of product onto the Agilent DNA 1000 chip in gel-dye matrix and running the chip for 35 min in the Bioanalyzer 2100 (Agilent Technologies) following the manufacturer's protocol.

Cell morphology

B16F10 or A375 cells were seeded in quadruplicates in 96-well plates and treated with 50 μ M thio-ccPA 18:1 or transfected with the indicated siRNA for 48 h prior to the examination of cell morphology. Cells were visualized using an Axiovert 40 inverted microscope (Carl Zeiss MicroImaging Inc., Thornwood, NY) and photomicrographs were captured using a Nikon Coolpix camera (Southern Microscope, Inc.).

Gene expression analysis

For examination of variations in biomarker expression among patient datasets, a publicly available melanoma gene expression dataset (GSE7553, N = 87) (Riker et al 2008) was downloaded from the NCBI Entrez Gene Expression Omnibus (GEO) DataSets website <http://www.ncbi.nlm.nih.gov/sites/entrez?db=gds> and analyzed as previously described (Murph et al 2009). Box plots using the normalized gene expression were created with GraphPad Prism (GraphPad Software, Inc., La Jolla, CA).

Results

Previous observations that carba analogues of ccPA- treated animals have reduced lesions in the lungs are striking (Baker et al 2006) and warrant further investigation. Thus, the next generation compound was synthesized based on enhanced metabolic stability of the carbacylic structure (**Figure 5.1A**) and improved receptor binding properties. We thus hypothesized that the phosphonothionate analogue of carba cyclic phosphatidic acid, thio-ccPA 18:1 (**Figure 5.1B**), would have interesting biological properties related to receptor binding and could be used to explore approaches against melanoma progression.

In order to assess the most fundamental question, whether thio-ccPA 18:1 had an effect on melanoma cell viability, we examined the viability of metastatic melanoma B16F10 cells in vitro in the presence or absence of thio-ccPA 18:1. No significant reduction in viability was observed at 10 or 25 μM thio-ccPA 18:1 after 48 h; however, concentrations of 50 μM and above induced a dramatic reduction in viability, approximately 49% at 50 μM and 85% at 100 μM (**P = 0.01 vs. PBS control **Figure 5.1C**). Thio-ccPA 18:1 (50 μM) treated B16F10 appeared small and rounded compared with untreated controls that were flattened and exhibited lamellipodia protrusions (**Figure 5.1D**). Visual examination of individual wells treated with 100 μM detected few attached cells after 48 h (data not shown).

Thio-ccPA 18:1 targets several components of the LPA signaling pathway. It is an effective inhibitor of ATX, similar to other cyclic phosphatidic acid analogues, but it also is a direct antagonist of the LPA1 and LPA3 receptors (Prestwich et al 2008). If ATX activity is the only important target of thio- ccPA 18:1 (Stracke et al 1992) then

exogenous LPA should override the effects of thio-ccPA 18:1 (Baker et al 2006). In order to test this hypothesis, we pre-treated the melanoma cells with LPA 18:1 (10 μ M) or the metabolically stabilized LPA analogue D-sn-1-O-oleoyl-2-O-methylglyceryl-3-phosphothionate (R- OMPT) (1 μ M) (Hasegawa et al 2008) prior to treatment with thio-ccPA 18:1 (50 μ M). Pre-treatment of LPA or R-OMPT was unable to bypass the reduction in cell viability induced by thio-ccPA 18:1 (**Figure 5.1E**). This suggests that additional targets, complementary to ATX inhibition, contribute to the ability of thio-ccPA 18:1 to reduce melanoma cell viability.

We next tested whether thio-ccPA 18:1 inhibits the viability of human melanoma cells. This was done in order to better represent translational applications of the phosphonothionate analogue to humans, to broadly examine multiple melanoma cell lines and their responses to thio-ccPA 18:1 and because B16F10 cells are hypersensitive to fluctuations in the concentration of serum contained in medium which could reflect an oncogenic addiction to growth factors or bias in our in vitro data (Weinberg 2007b).

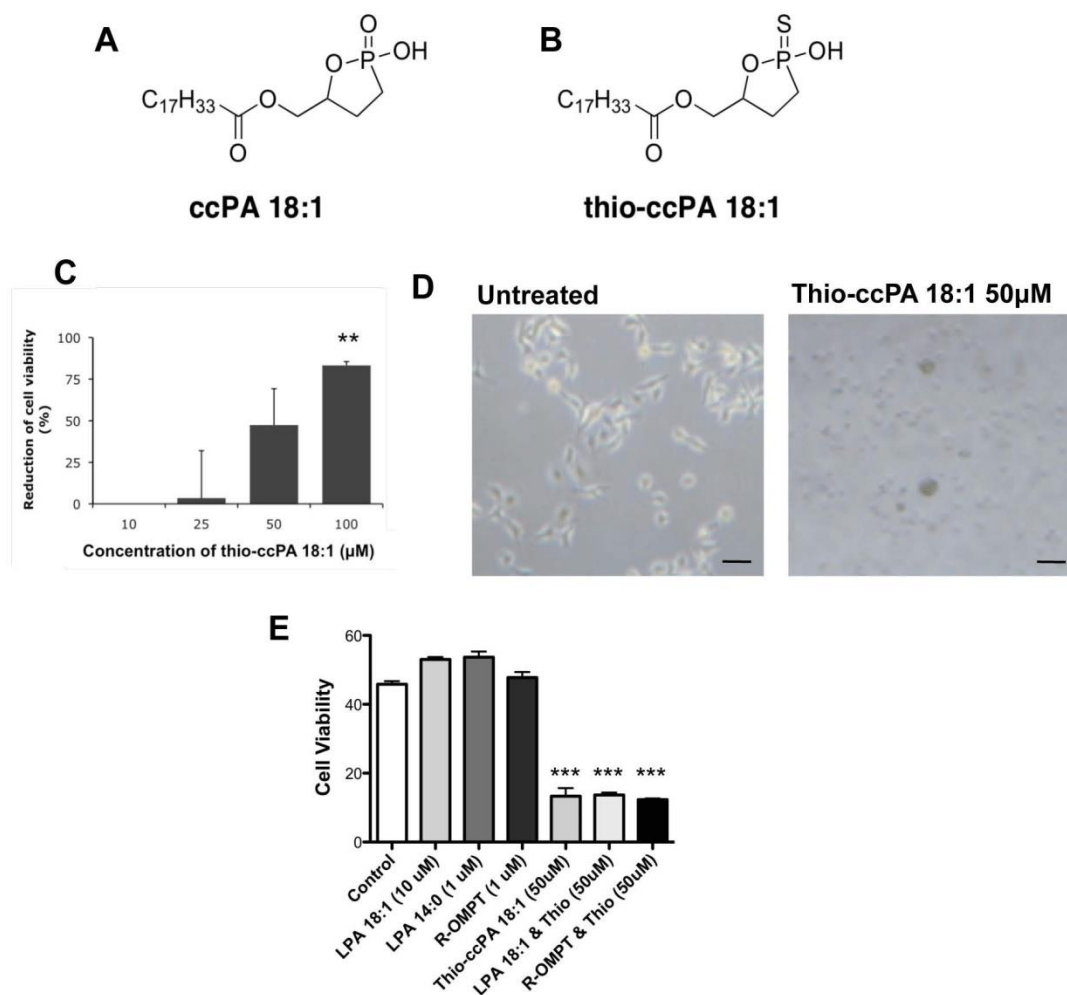


Figure 5.1. Thio-ccPA 18:1 reduces the viability of B16F10 cells in vitro. (A) Chemical structure of ccPA 18:1 and (B) thio-ccPA 18:1. (C) B16F10 cells were treated with increasing concentrations (10-100 μM) of thio-ccPA 18:1 and analyzed for cell viability after 48 h. The graph presents the data as the percentage of reduction in cell viability (% of PBS control). $**p < 0.01$ vs. control by Bonferroni's t-test and analysis of variance. (D) B16F10 cells were either untreated (control) or treated with thio-ccPA 18:1 (50 μM). Images demonstrate the difference in B16F10 cell morphology after 48 h treatments with 50 μM thio-ccPA 18:1. (E) B16F10 cells were either untreated (control) or treated with LPA 18:1 (10 μM), LPA 14:0 (1 μM), R-OMPT (1 μM), thio-ccPA 18:1 (50 μM) or a combination of these as shown. Cell viability was assessed after 48 h. $***p < 0.001$ vs. control by Bonferroni's t-test and analysis of variance.

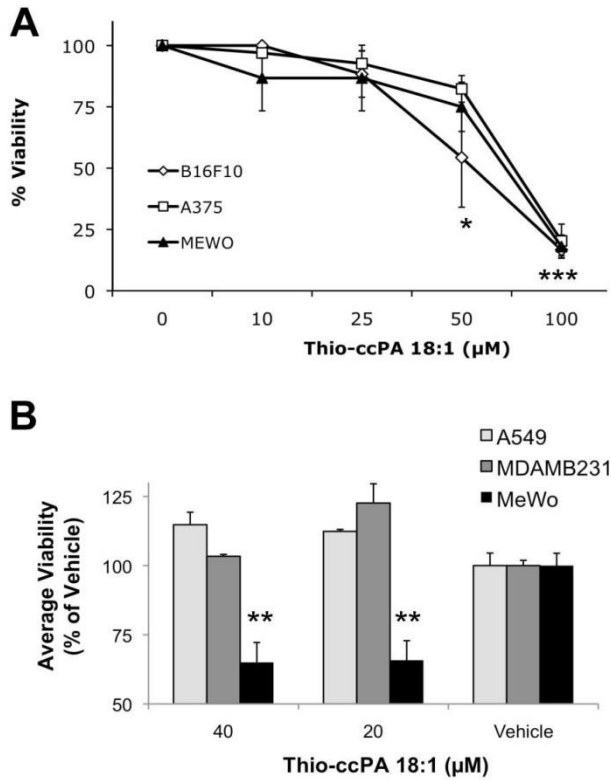


Figure 5.2. Cell line comparison of viability reduction by thio-ccPA 18:1. (A) B16F10, A375 and MeWo melanoma cells were treated with increasing concentrations (0-100 µM) of thio-ccPA 18:1 for 48 h and examined for viability. * $p < 0.05$ and *** $p < 0.001$ vs. control by Bonferroni's t-test and analysis of variance. (B) A549, MDA-MB-231 and MeWo melanoma cells were treated with either 40 µM or 20 µM of thio-ccPA 18:1 and examined for viability. Results show the percent of viability compared to vehicle (dH₂O). ** $p < 0.01$ vs. vehicle by Bonferroni's t-test and analysis of variance.

Although the three melanoma cell lines represent distinct and common genetic abnormalities observed in melanoma, B16F10 (RAS), A375 (activating B-RAF, constitutively active MAPK) and MeWo (no BRAF or NRAS), they exhibited similar decreases in cell viability in the presence of increasing concentrations of thio-ccPA 18:1 (**Figure 5.2A**). This suggests the existence of a "common" mechanism exploited by thio-ccPA 18:1 on the LPA signaling pathway in these melanoma cells. Furthermore, this mechanism is not shared by all tumor cell types since A549, a lung cancer cell line, and MDA-MB-231, a breast cancer cell line, are insensitive to the effects of thio-ccPA 18:1 (**Figure 5.2B**). A549 cells express LPA1 > LPA4 > LPA2 receptors and the MDA-MB-231 cells express LPA1 >> LPA2 receptors. Both cell lines express low levels of ATX and no LPA3 receptors (Kishi et al 2006).

In addition to its inhibition of ATX, thio-ccPA 18:1 is an LPA1/3 receptor antagonist (Prestwich et al 2008). We wanted to determine the importance of the receptor antagonism to the efficacy of the analogue, especially considering that the drug is insensitive in cells that lack the LPA3 receptor. We therefore assessed whether sequential inhibition of individual LPA receptors affected melanoma cell viability. Specific inhibitors targeting all LPA receptors individually do not exist (Murph and Mills 2007); thus, we used siRNA to target individual LPA receptors. With siRNA we can consistently reduce the amount of LPA receptor expression approximately 60% or greater (Hasegawa et al 2008) without activating compensatory receptor expression mechanisms. We have previously established that LPA receptor knock-down reduces LPA-mediated functions of LPA receptors in vitro and in vivo (Hasegawa et al 2008, Yu et al 2008). Herein, we also assessed the ability of siRNA to enter the cell from the

transfected medium using ion chromatography using UV detection. Strikingly, we detected siRNA inside MeWo cells 6 h after transfection and this was detected in subsequent time points of 10 h and 24 h.

We next transfected A375 cells with siRNA for the LPA receptors and detected a significant reduction in cell viability when the LPA3 receptor expression was reduced (**Figure 5.3A**). The expression of verified LPA receptors in A375 cells is LPA1, LPA2, LPA3, p2y5 >> LPA4, LPA5 (**Figure 5.3B**), demonstrating that the LPA3 receptor is present in A375 cells. Similar results were achieved using siRNA in MeWo cells (**Figure 5.3C**). The expression pattern of LPA receptors was very different in MeWo cells, LPA3, LPA4 >> LPA2 (**Figure 5.3D**) compared to A375 cells. The commonalities between the two cell lines are expression of the LPA2, LPA3 and LPA4 receptors. This pattern is not commonly observed among cancer cell lines (Kishi et al 2006). This also led us to examine LPA receptor expression in normal skin where we detected expression of p2y5 and LPA1 receptors and little (LPA2, LPA3) to no (LPA4, LPA5) expression of other receptors (**Figure 5.3E**).

To further investigate the effects of thio-ccPA 18:1 on melanoma cells and determine whether targeting the LPA3 receptor has a complementary role to ATX inhibition, we examined LPA receptor-mediated cell viability using A375 melanoma cells. Cells were treated for 48 h in serum-free medium with LPA 18:1 (0.1 - 10 μ M) and assessed for cell viability. Indeed, the addition of LPA alone enhanced the overall number of A375 cells (**Figure 5.4A**). We next assessed cell death by measuring the integrity of the cell membrane using trypan blue exclusion and A375 cells transfected with increasing concentrations and combinations of siRNA for the LPA1, LPA2 or LPA3

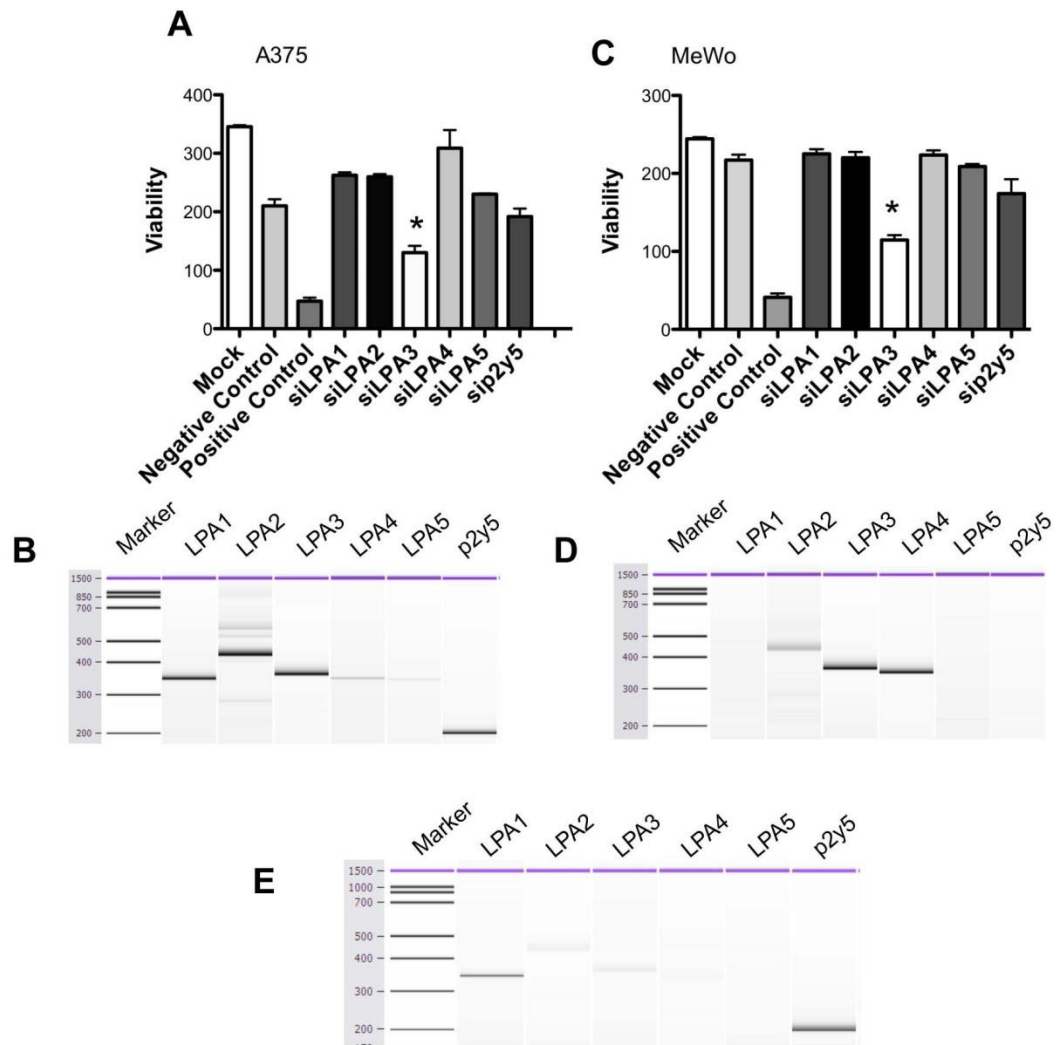


Figure 5.3. The LPA3 receptor mediates viability in A375 and MeWo melanoma cells. Individual LPA receptors were targeted with siRNA to sequentially inhibit receptor expression. (A) A375 cells were transfected for 48 h with the indicated siRNA and examined for viability. * $P < 0.05$, vs. Mock in A375 by Bonferroni's t-test and analysis of variance. (B) RT-PCR showing LPA receptor expression in A375 cells visualized using the Bioanalyzer 2100. (C) MeWo cells were transfected for 48 h with the indicated siRNA and examined for viability. * $P < 0.05$, vs. Negative Control (RISC-free) in MeWo. (D) RT-PCR showing LPA receptor expression in MeWo cells visualized using the Bioanalyzer 2100. (E) RT-PCR showing LPA receptor expression in normal human skin visualized using the Bioanalyzer 2100.

receptors. Only cells transfected with siLPA3 (20 nM, 60 nM or combination) produced conditions that significantly affected the number of live cells (**Figure 5.4B**). A375 cells transfected with 20 nM or 60 nM siLPA3 contained 45% and 30%, respectively, of live cells compared with Mock control. Cell number was further assessed using crystal violet (proliferation) staining and (20 nM) siLPA3. We measured a decrease of 70% and 50% in the number of cells transfected with siLPA3 compared with untreated (Control) and Mock control, respectively (**Figure 5.4C**). A375 cells transfected with siLPA3 have rounded cell morphology that is distinct from normal control cells (**Figure 5.4D**) but reminiscent of thio-ccPA 18:1 treated cells shown in (**Figure 5.1E**).

To assess whether ATX was a major contributor to viability in A375 cells, we measured the amount of expression using RT-PCR. We were barely able to distinguish a marginal level of ATX in A375 cells, although fetal skin and MeWo cells did express detectable levels of ATX (**Figure 5.4E**). Taken together, this suggests that inhibition of the LPA3 receptor signaling reduces the viability of A375 melanoma cells and may be complimentary to ATX inhibition as a dualistic mechanism of action of thio-ccPA 18:1. The expression pattern observed in MeWo cells (ATX and the LPA3 receptor) makes this the quintessential line for confirming the efficacy of thio-ccPA 18:1. Inhibiting the abundance of these two transcripts and then assessing cell viability demonstrated that either siLPA3 or siATX was capable of reducing viability (**Figure 5.5A**). Combining siLPA3 and siATX further reduced viability over each individually and was comparable to siPLK1, a positive control for siRNA transfection that results in termination of cells.

We next asked whether the LPA3 receptor plays a large role in mediating LPA-induced cell viability in MeWo cells. A selective LPA receptor agonist induced an

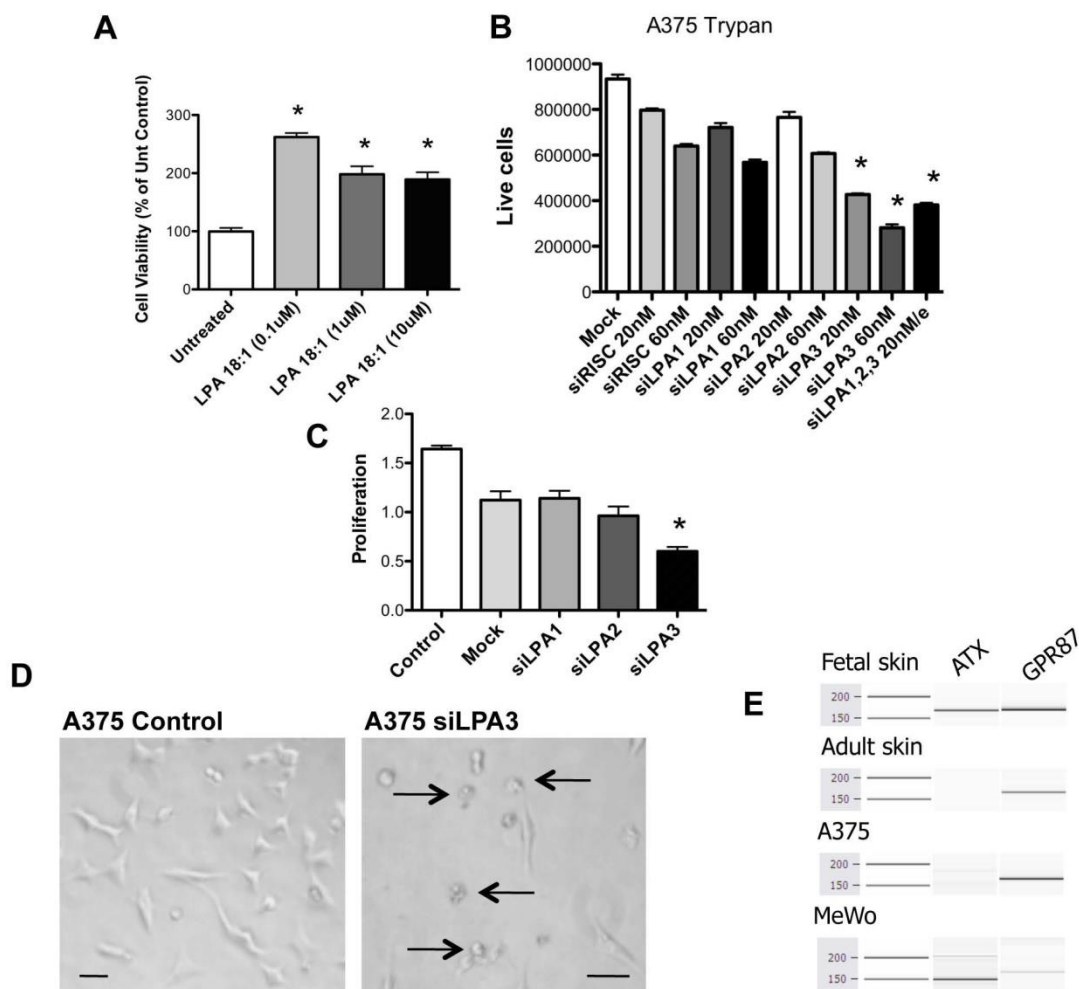


Figure 5.4. Knockdown of the LPA3 receptor induces cell death in A375 melanoma cells. (A) LPA 18:1 treatment (0.1-10 μ M) of A375 cells in serum free medium for 48 h enhances viability. * $p < 0.001$ vs. untreated control. (B) A375 cells were transfected for 48 h with the indicated siRNAs and assessed for membrane integrity and cell death using trypan blue exclusion assay. Cell numbers reflect the cells with intact membranes. * $P < 0.001$, comparing siRISC 60 nM vs. treatment conditions. (C) Transfection of siRNA targeting the LPA receptors in A375 cells for 48 h demonstrates that reducing the expression of the LPA3 receptor decreases the number of live cells assessed by crystal violet staining. * $p < 0.05$ vs. control. (D) Photomicrograph images demonstrating changes in cell morphology after 48 h of siLPA3 transfection. (E) RT-PCR demonstrating the level of expression of ATX and GPR87 in fetal skin, normal human skin, A375 and MeWo cells.

enhancement in viability by 21% under control conditions in MeWo cells, 37% under control conditions in OVCAR-3 cells but only 9% after MeWo cells were transiently transfected with siRNA against the LPA3 receptor and after overnight treatment with the agonist (**Figure 5.5B**). We further inhibited the LPA3 receptor using a selective antagonist for LPA1/3, VPC32183, in MeWo cells (which do not express the LPA1 receptor). We treated the MeWo cells for 48 h and measured approximately 75% decrease in cell viability (**Figure 5.5C**). The marked reduction in viability was blunted after transiently transfecting MeWo cells with siRNA against the LPA3 receptor or by using the OVCAR-3 cell line, which expresses multiple LPA receptors. This suggests that LPA3 expression, but likely lack of LPA2 expression, is required for response to the antagonist VPC32183. The effect on blunting the cellular response to the compound was not observed after transiently transfecting MeWo cells with siRNA against the LPA3 receptor and treating with thio-ccPA 18:1 (**Figure 5.5D**). In the presence of LPA3 receptor knock-down, thio-ccPA 18:1 further reduced cell viability, suggesting multiple targets induce the effects of thio-ccPA 18:1. We also noted the response of VPC32183 was reduced by the presence of serum (**Figure 5.5E**). Our data suggests the unique pattern of expression in MeWo cells (ATX and the LPA3 receptor, without the LPA1 or LPA2 receptors) provides a quintessential model for achieving a response to thio-ccPA 18:1 and represents a type of tumor that is susceptible to the actions of thio-ccPA 18:1.

In order to determine whether thio-ccPA 18:1 would influence metastatic melanoma tumors in vivo, we tested its efficacy using the B16F10 metastatic melanoma mouse model (Jiang et al 2007). We injected B16F10 metastatic melanoma cells into the tail vein of C57/Bl6 mice. Animals were intraperitoneally injected on days 3 and 7 after

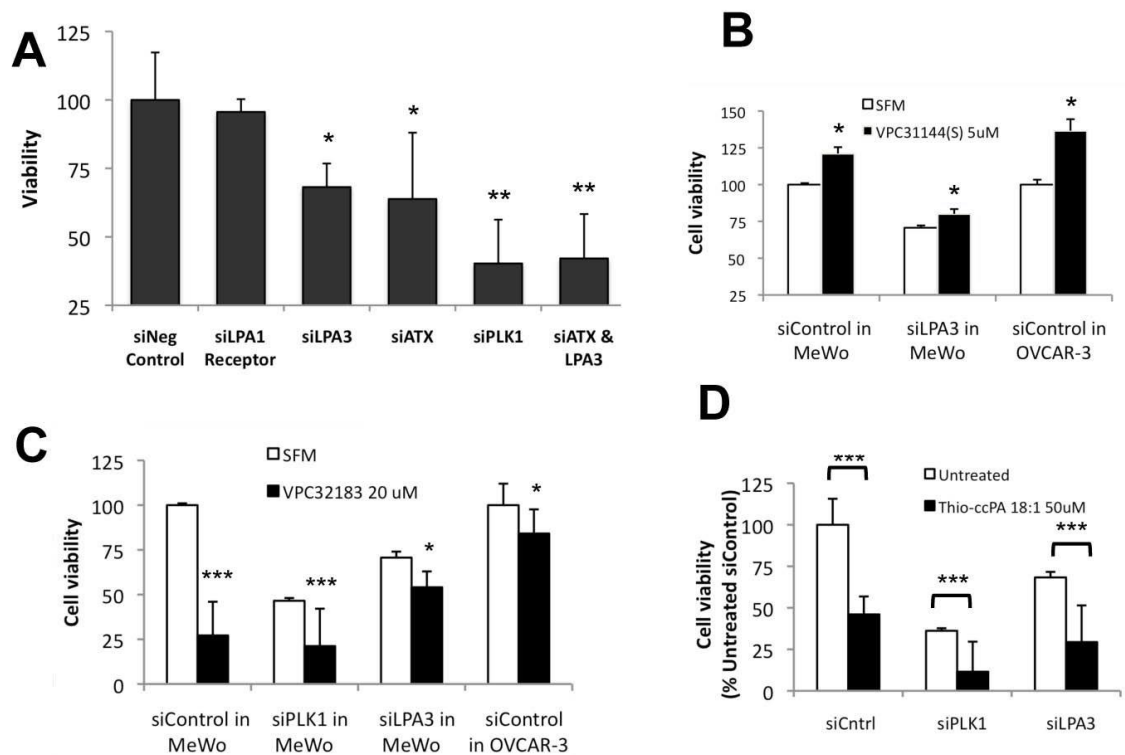


Figure 5.5. Inhibition of the LPA3 receptor using siRNA knockdown or LPA3 antagonists reduces viability of MeWo melanoma cells. (A) MeWo cells were plated in 96-wells and transfected with the indicated siRNAs for 24 h prior to the assessment of viability. The control, siNegative (non-targeting siRNA), was normalized to 100%. * $p < 0.05$ and ** $p < 0.01$ vs. siNegative control. (B) The agonist, VPC31144(S) for LPA1/3, 5 μM was added to either MeWo cells or OVCAR-3 cells in 96-well plates in serum-free medium and compared to control, serum-free medium alone. * $p < 0.05$ comparing agonist to untreated in each group. (C) MeWo or OVCAR-3 cells were plated in 96-wells prior to transfection with the indicated siRNA conditions. The LPA1/3 antagonist, VPC32183 (20 μM) was added to the cells and viability was assessed. * $p < 0.05$, *** $p < 0.001$ comparing treated vs. untreated in each transfection condition. (D) MeWo cells were plated in 96-wells prior to transfection with the indicated siRNAs for 24 h and treatment with Thio-ccPA 18:1 (50 μM) in serum-containing medium. Cell viability was assessed and the siNegative control was normalized to 100%. *** $p < 0.001$ comparing treated vs. untreated in each transfection condition.

intravenous cell injection with 200 µg (10 mg/kg per dose) concentrations of thio-ccPA 18:1 or PBS (Control). Mice were then sacrificed 21 days after the initial injection of B16F10 cells, and tissues were fixed and analyzed for the number of metastases. Treatment with thio-ccPA 18:1 significantly reduced the number of pulmonary metastases in mice as compared to the control treatment ($p < 0.01$, **Figure 5.6A, B and C**). In addition to the effect on pulmonary metastasis, all control animals ($N = 17$) had metastatic lesions to organs outside of the lungs, whereas only twenty percent ($N = 2/10$) of thio-ccPA 18:1 treated animals had detectable non-pulmonary metastases (**Figure 5.6D**).

If expression patterns reflect biomarker signatures that confer susceptibility to thio-ccPA 18:1, we were curious how prevalent high levels of ATX and the LPA3 receptor expression are in melanoma. For this we profiled gene expression microarray data downloaded from the NCBI Gene Expression Omnibus. Among patient specimen datasets (GSE7553, $N = 87$) (Riker et al 2008), gene expression analyses reveals significant variation of LPA3 receptor expression in metastatic melanoma (**Figure 5.7A**), suggesting that not all types of advanced melanoma might be strongly susceptible to thio-ccPA 18:1. This is consistent with the variation in LPA3 receptor expression we observed among melanoma cell lines. We also detected a significantly increased level of ATX among metastatic melanoma specimens ($N= 40$) compared with basal cell

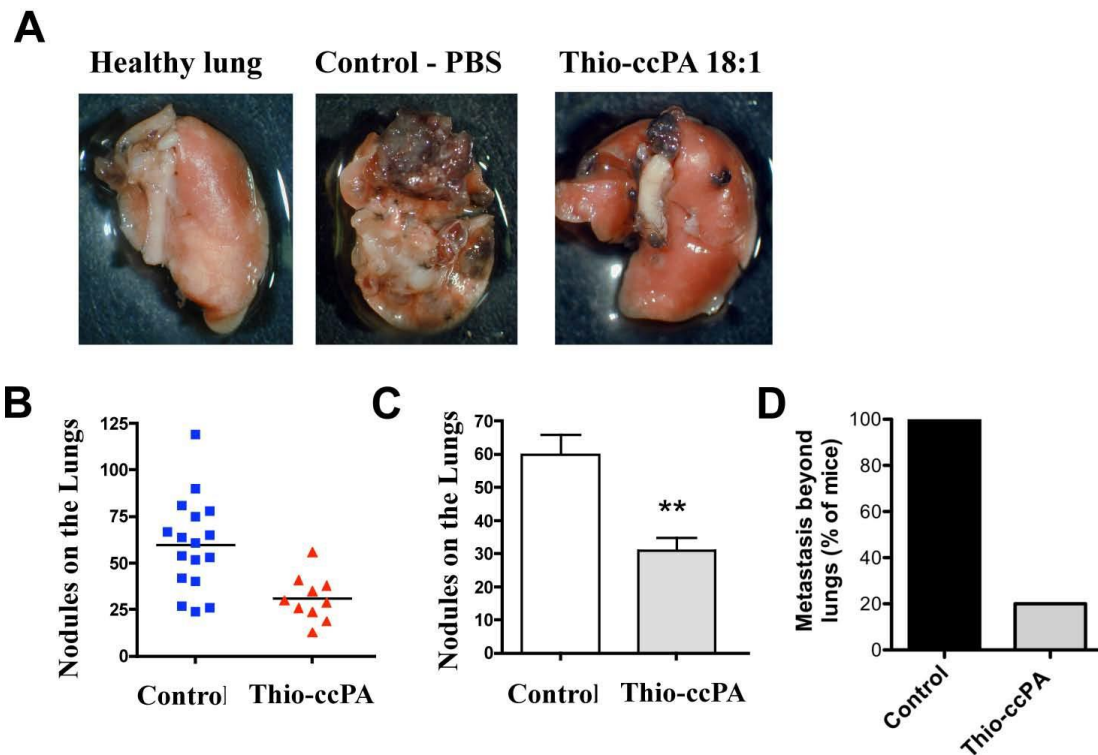


Figure 5.6. Thio-ccPA 18:1 reduces metastatic melanoma lesions in murine lungs. C57/BL6 mice (N = 27) were injected with 5×10^4 B16F10 cells into the tail vein. Thio-ccPA 18:1 was administered on days 3 and 7 during the 21-day study. (A) Necropsy images of left lung lobes demonstrate the presence of tumor. Quantification of tumor revealed a reduction in nodules on the lungs shown as both scatter (B) and bar (C) graphs. ** $p < 0.01$ comparing control (PBS) with thio-ccPA 18:1 treated groups. (D) Quantification of additional lesions detected on organs outside the lungs (kidney, liver, pancreas and intestines) and presented as a percentage of mice in each group (Control N = 17, 100%; thio-ccPA 18:1 N = 2 of 10, 20%; thio-ccPA 18:1).

carcinoma (N = 15), normal skin (N = 5) and squamous cell carcinoma of the skin (N = 11) (**Figure 5.7B** and **5.7C**). ATX expression in primary melanoma (N = 14) is also increased in comparison to melanoma in situ, basal and squamous cell carcinoma. Taken together, the data suggests that a portion of metastatic melanomas, estimated at approximately 20%, express high levels of ATX and/or the LPA3 receptor and this population represents the most appealing pool for therapeutic intervention.

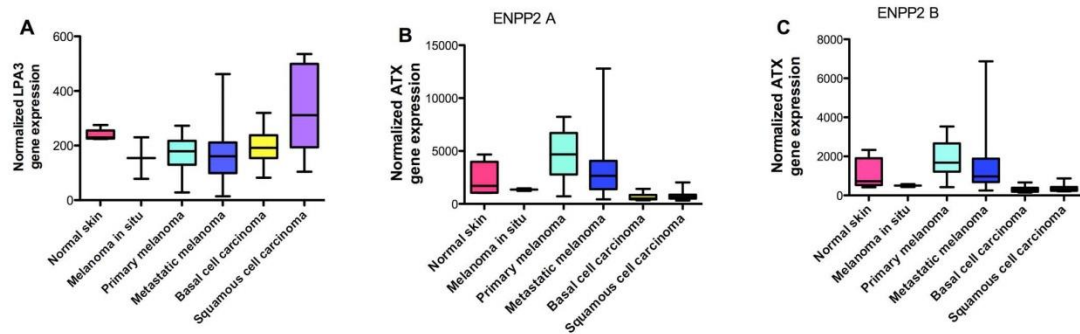


Figure 5.7. A subset of melanomas express high levels of the LPA3 receptor and ATX. Gene expression microarray data was downloaded from the NCBI Gene Expression Omnibus containing patient specimen datasets (GSE7553, N = 87). The genes (A) LPA3 and (B and C) ATX (ENPP2 A and B) were selected and the data was converted into box plot graphs to demonstrate the range of expression levels among these genes.

Discussion

Thio-ccPA 18:1 is a unique compound with multiple targets. Biological testing of thio-ccPA 18:1 demonstrated it is an antagonist of the LPA1 and LPA3 receptors along with its activity as an effective inhibitor of ATX (Prestwich et al 2008). Thus, the compound is described as having a "one-two- punch" (Jiang et al 2007) because it inhibits the generation of LPA and the initiation of LPA-mediated signaling through LPA1 and LPA3 receptors. In this study, we demonstrate the in vitro and in vivo efficacy of thio-ccPA 18:1 and describe its dualistic mechanism of action, responsible for decreasing in vitro viability in melanoma cells. Either addition of thio-ccPA 18:1 or siRNA for the LPA3 receptor significantly reduces A375, MeWo and B16F10 melanoma cell viability in vitro suggesting that the effects may be generalizable to melanoma cells. In addition, siLPA3 reduces the membrane integrity and proliferation of A375 cells and alters cell morphology. Neither thio-ccPA 18:1 nor siLPA3 induced nuclear fragmentation (unpublished observations), suggestive of a non-apoptotic mechanism of reduced cell viability. We also show that in vivo treatment with thio-ccPA 18:1 inhibits B16F10 cell metastatic lesions that develop in the lungs and prevents the spread of metastases to distant organs.

Previous studies have examined carba analogues of cyclic phosphatidic acid that inhibit ATX activity. Our collaborative study suggested that ATX is a major mediator of melanoma metastasis in vivo and cancer cell invasion in vitro and that these analogues work effectively by inhibiting ATX activity, without receptor antagonism (Baker et al 2006). Indeed, studies demonstrating the anti-metastatic capability of ccPA compounds suggested this effect did not require inhibition of LPA receptor activation (Uchiyama et

al 2007). However, these observations did not address whether coupling ATX inhibition with receptor blockade would be more effective than targeting ATX alone or whether different populations of melanoma cells have specific LPA receptor targeting susceptibilities.

Other studies have confirmed that ATX inhibitors reduce melanoma cell migration and invasion (Saunders et al 2008). ATX continues to be an important therapeutic target for cancer because it may be involved in protecting cells from apoptosis-induced chemotherapy (Samadi et al 2009). Besides melanoma, ATX may also play a role in the motility of glioblastoma cells, which may be critical due to the high expression of ATX among the CNS and glioblastoma multiforme (Kishi et al 2006). We have also shown that carba analogues of cyclic phosphatidic acid inhibit the LPA-stimulated motility of prostate cancer cells (Hasegawa et al 2008). In other diseases, ATX may provide a useful serum biomarker for follicular lymphoma (Masuda et al 2008) and chronic hepatitis C (Watanabe et al 2007).

Unlike ATX, there are few studies devoted to the investigation of the efficacy of targeting the LPA3 receptor. Our current study enhances the biological understanding of LPA3 receptor function and these findings are a major novelty of this study. Our previous study suggested the increased presence of any of the LPA1, LPA2 or LPA3 receptors enhances tumorigenicity and aggressiveness of ovarian cancer (Yu et al 2008). Thus far, the only known independent function of the LPA3 receptor occurs in reproductive biology where it regulates embryo implantation and spacing (Ye et al 2005). Another study suggests women with endometriosis have decreased expression of the

LPA3 receptor in the endometrium, suggesting a hypothesis for their observed subfertility (Wei et al 2009).

The study presented herein is the first to suggest that the LPA3 receptor plays a crucial role in melanoma cell viability *in vitro*. This is the first study to characterize this unappreciated mechanism of action of the novel compound, thio-ccPA 18:1. It fills a gap in our knowledge about novel ccPA compounds designed to inhibit LPA signaling because it highlights a role for receptor antagonism, in addition to blocking ATX activity. The fact that compounds which inhibit ATX are potent agents against tumor progression is intriguing but leads to an obvious mechanistic question - why does inhibiting the production of LPA have potent biological effects? Based on our data, we hypothesize that the lack of LPA production resultant from ATX inhibition leads to a critical reduction of LPA receptor-mediated survival signaling required for viability among specific populations of melanoma cells.

One limitation of our study surrounds the intrinsic properties of siRNA and their utility. We used gene silencing to target individual LPA receptors to verify the receptor antagonist properties of thio-ccPA 18:1; however, off-target activity of siRNAs can lead to complex interpretations of observed phenotypes. Studies using microarray gene expression profiling previously supported the notion that induction of siRNA would specifically silence the intended target but it is now acknowledged that off-target activity can occur and is not ameliorated by decreasing the siRNA concentration (Jackson and Linsley 2010). In our study we cannot rule out the possibility that siRNA of the LPA3 receptor (or siRNA for ATX or any other LPA receptor) may have off-target effects through microRNA-like down regulation; however, we are using pooled siRNA reagents

which reduces the overall number of off-targets through competition among siRNAs. In addition, we observe a similar reduction in cell viability using either thio-ccPA 18:1 or VPC32183. This suggests both the receptor antagonism of the compounds and siRNA are all targeting the same receptor and the phenotype is identical. Therefore, this limitation is not a major concern since specific antagonists targeting the LPA3 receptor significantly reduced cell viability in MeWo cells. Finally, we used a novel approach of ion chromatography and UV detection to demonstrate that the siRNA was incorporated into the cells. This technique showed that each of the four siRNAs contained in the SMARTpool entered the cells.

The findings of our study have several future therapeutic and translational potentials. The data suggests targeting the LPA signaling pathway has efficacy against tumor progression, in particular against metastatic melanoma. It compliments previous studies (Baker et al 2006, Uchiyama et al 2007) and strengthens a need for further research using melanoma models that we are currently undertaking. The pattern of LPA receptor expression in melanoma cells may be important to understanding how the elimination of one receptor, which is presumably part of a redundant signaling family, results in a marked decrease in viability. For example, Lee et al. suggested that it is not merely the expression of the LPA1 receptor which controls LPA-mediated cell motility as previously suggested (Hama et al 2004), but the lack of LPA4 receptor expression that affects motility as it would otherwise regulate function of the LPA1 receptor (Lee et al 2006a). A similar dualistic mechanism could account for LPA-mediated cell viability and that expression of this yet unknown counter-regulating protein or receptor is absent in these melanoma cells. Finally, it is important to clarify the molecular mechanism of

action of pharmaceutical compounds to improve lead compound design and predict potential side effects that may appear during clinical and preclinical trials so they can be monitored and managed appropriately.

CHAPTER 6

THE *IN VITRO* CHARACTERIZATION OF A NOVEL INHIBITOR OF AUTOTAXIN¹

¹ Molly K. Altman, Mandi M. Murph, Glen Prestwich. To be submitted to *ACS Medicinal Chemistry*.

Abstract

Autotaxin is an enzyme discovered in conditioned medium of cultured melanoma cells and identified as a protein that strongly stimulates motility. This unique ectonucleotide pyrophosphatase and phosphodiesterase facilitates the removal of a choline headgroup from lysophosphatidylcholine to yield lysophosphatidic acid, which is a potent lipid stimulator of tumorigenesis. Thus, autotaxin has received renewed attention because it has a prominent role in malignant progression and represents a promising area of research with significant translational potential. Since autotaxin inhibitors may have broad implications for therapy, we sought to create a novel series of inhibitors for use against cancer, especially melanoma. A set of vinyl sulfone analogs of lysophosphatidylcholine were synthesized by our collaborator that function as inhibitors of autotoxin and inactivate the enzyme. We commenced with biological testing of the compound autotaxinab *in vivo* (*in vitro* data not shown). Most importantly, the vinyl sulfone significantly inhibited melanoma progression in an *in vivo* tumor model by preventing angiogenesis. Taken together, this suggests that the vinyl sulfone is a potent irreversible autotaxin inhibitor with significant biological activity.

Introduction

The ectonucleotide pyrophosphatase/phosphodiesterase 2 or its more common designation autotaxin, is an enzyme with lysophospholipase D activity that converts lysophosphatidylcholine to lysophosphatidic acid (Umezū-Goto et al) by hydrolyzing the choline headgroup from lysophosphatidylcholine. After its isolation from conditioned medium of melanoma cells (Stracke et al 1992), it was discovered to play a major role in the development of both the vascular (Albers et al 2010, Tanaka et al 2006) and nervous systems as well as malignancy (Liu et al 2009a) (Liu et al , Liu et al). In particular, autotaxin functions negatively in many cancers to increase growth factor signaling, cell survival, proliferation and migration, including pancreatic cancer (Nakai et al), cutaneous and uveal melanoma (Altman et al , Baker et al , Singh et al), breast cancer (Liu et al), follicular lymphoma (Masuda et al), glioblastoma multiforme (Kishi et al) and gynecologic malignancies (Tokumura et al). In addition, autotaxin also protects cancer cells from chemotherapy-induced apoptosis (Samadi et al), which would significantly complicate treatment and result in worsened outcomes when autotaxin is present in the tumor microenvironment.

Another occurrence affecting cancer treatment is angiogenesis. This is the process whereby tumors develop blood vessels to access nutrients and oxygen from circulation and is necessary for tumor growth beyond 1 mm, at which point necrosis occurs in otherwise hypoxic tissues. To state succinctly – angiogenesis is required for cancer progression. Without angiogenesis, the growing tumor will not thrive and will remain small. Because of this dependency, anticancer therapeutics targeting angiogenesis exploit tumors by inhibiting growth factors required for the formation of new blood vessels, such

as the vascular endothelial growth factor (VEGF). This and other growth factors are secreted by the tumor when it exceeds a certain distance from its primary blood supply and senses hypoxia. On the other hand, since the circulatory system is exploited by intravenous anticancer therapeutics to reach the insides of tumors, timing is critical to properly treat patients with angiogenesis inhibitors.

Interestingly, autotaxin is a direct and indirect angiogenic factor that stimulates human endothelial cells to form tubules and tumors to become more hyperemic (Nam et al , Ptaszynska et al). It is thus not surprising that the effect of knocking out autotaxin on vasculogenesis results in embryonic lethal mutations in mice embryos which display aberrant blood vessel formation upon death (Tanaka et al , van Meeteren et al). Mechanistically, an increase in VEGF increases autotaxin expression and/or secretion among (at least) ovarian cancer cells, which results in more lysophosphatidic acid and also drives cells to produce more of the receptors LPA3, LPA4 and VEGFR2 (Ptaszynska et al). This represents a positive feedback loop between autotaxin and growth factors involved in angiogenesis, especially since lysophosphatidic acid also stimulates VEGF production.

Because of the critical role autotaxin has in angiogenesis and various malignancies, extensive research is devoted to the design, synthesis and evaluation of novel inhibitors of autotaxin (Albers et al , Albers and Ovaa , Altman et al , Baker et al , Clair et al , Durgam et al , East et al , Ferry et al , Gierse et al , Gupte et al , Hoeglund et al , Prestwich et al , St-Coeur et al , Xu et al , Zhang et al) as well as the evaluation of natural substances with inhibitory activity (Ueda et al 2010). Interestingly, autotaxin is also product-inhibited by both sphingosine 1-phosphate and lysophosphatidic acid (van

Meeteren et al), suggesting that these bioactive lipids are capable of regulating their synthesis and abundance in the tumor microenvironment. Some of the recently designed chemical inhibitors such as HA130 have not possessed the necessary characteristics to proceed into clinical development due to a lack of bioavailability or large millimolar concentrations required for activity.

Other studies have elucidated the crystal structure of autotaxin (Nishimasu et al) and further described how the enzyme discriminates substrates (Hausmann et al) and resulted in novel ideas for the design of additional autotaxin inhibitors. Although adverse events are also of concern with autotaxin inhibitors, most chemotherapy produces harsh side effects for patients, but is tolerated because of favorable therapeutic indexes and the potential for treating a life-threatening illness. Even new targeted biologics possess severe unwanted side effects, some even serving as a measure of therapeutic activity, yet certain patients are unable to continue using these supposedly “milder” forms of therapy.

Indeed, we observed the ability of the vinyl sulfone autotaxinab to reduce *in vitro* cell viability, cell motility, wound closure (data not shown) and melanoma growth *in vivo*. Our collaborators previously synthesized autotaxin inhibitors and our lab examined their biological activity against melanoma (Altman et al , Baker et al , Nguyen et al) and other malignancies (Xu et al , Xu and Prestwich , Zhang et al). Since the *in vitro* activity observed by autotaxin inhibitors on melanoma cells is striking, we hypothesized that the mechanism of action is a directly-targeted, cellular consequence. However, we did not observe a direct effect against proliferation of melanoma models *in vivo*. Instead, the animal tumors treated with the highest compound concentration displayed significantly smaller tumors than controls and a commercial inhibitor HA130, which resulted from an

inhibition of angiogenesis, not mitogenesis. The commercial inhibitor HA130 is a reversible inhibitor of lysophospholipase D activity in ATX and thereby is able to reduce circulating LPA levels when injected into mice so it was a good comparison for our experimental compound autotaxinab (Albers et al 2010). Herein we report the *in vivo* characterization of the novel vinyl sulfone autotaxinab and its action against the progression of melanoma via angiogenesis inhibition.

Experimental Methods

Cell Culture

Cell lines were acquired from the American Type Culture Collection or ATCC (Manassas, VA). The human cancer cell line MeWo fibroblast malignant melanoma cells were cultured in supplemented 5% FBS in RPMI (Mediatech).

Materials and Reagents

Oleoyl lysophosphatidic acid was purchased from Avanti Polar Lipids (Alabaster, AL) and reconstituted in chloroform and methanol. Prior to cell incubation, organic solutions were removed and lysophosphatidic acid was added in 0.1% charcoal-stripped BSA. Dimethylformamide (DMF) (Sigma-Aldrich) <1% in ultrapure water was used to reconstitute the HA130 compound (Echelon Biosciences, Salt Lake City, UT).

Animal model of melanoma

Six-week old female athymic nude mice acclimated to the animal facility for one week prior to the study commencement. Animals were anesthetized before tumor cell injection into their right flank with Glycosan Extracel[®] (BioTime, Inc, Alameda, CA)

containing approximately 1×10^6 MeWo cells per 0.15 mL injection. Extracel[®] was used in this study over traditional Matrigel to eliminate potential interference of exogenous mouse growth factors which could have affected our in vivo study. In addition, Glycosan Extracel[®] allows us to conserve resources through the achievement of a 100% tumor efficiency rate, whereby this rate is typically unachievable otherwise. Injected mice were measured for tumor formation, tumor volume, body weight and body conditioning scores.

After three weeks, 100% of mice displayed tumor formation at which time they were randomized into treatment groups; control, autotaxinab at 20 mg/kg or 50 mg/kg dose per 0.1 mL injection. Mice in each treatment group were anesthetized (2-4% isoflurane) before i.p. treatment injections three times a week over the course of the 65-day study. The animals were euthanized according to the animal use protocol approved by the University of Georgia IACUC committee. The tumor volume (mm^3) was calculated using the equation: tumor volume = $(\text{width})^2 \times \text{length}/2$, and then graphed using GraphPad Prism (La Jolla, CA). The tumor volume for each group and overall significance was plotted.

Tumor specimen sectioning and fluorescence

Melanoma tumors were dissected from the right flank of athymic nude mice and flash-frozen with cryomatrix (Thermo Fisher Scientific Inc, Waltham, MA) in 2-methylbutane (Sigma) and cooled to -140°C . Cryopreserved tumors were cut in $9 \mu\text{m}$ sections using a cryostat (Thermo Fisher Scientific) and then mounted on microscope slides. Hematoxylin and eosin staining was performed according to standard protocols and processed for pathological evaluation.

For tissues stained with antibodies specific for immunofluorescence, tissue sections first were blocked for 30 min in 5% donkey serum (Jackson ImmunoResearch Laboratories Inc, West Grove, PA, USA) diluted in phosphate-buffered saline (PBS) for 30 min at room temperature. The tumor sections were then incubated in primary antibodies at 4°C overnight using a humidity chamber. The following day slides were washed with PBS and the primary antibody was detected using a fluorescent secondary antibody. After washing the slides again with PBS, they were mounted with Permount (Thermo Fisher Scientific) and imaged using an X71 inverted microscope (Olympus, Center Valley, PA) at 20x magnification. Overlapping pictures were aligned to generate an image of an entire tumor cryosection. Ki-67 positive staining intensity was determined by tracing the area of interest for each specimen. The Image-Pro Precision Software (Media Cybernetics, Bethesda, MD) was used to calculate the staining intensity within the area of interest for each tumor specimen. Tumor area was calculated automatically using the polygon tool in Image-Pro Precision software. Once the area was defined in the program, the pixel staining intensity of Ki-67 was determined by Image-Pro Precision software. The average pixel staining intensity per area measurement was plotted.

Quantitative real time PCR analysis

Gene expression was measured in xenograft tumors of athymic nude mice. Cryopreserved tumors were cut in sections using a Thermo Fisher Scientific cryostat and razor blade. Cut specimens were weighed and 1.0 mL of TRIzol reagent (Life Technologies, Grand Allen, NY, USA.) was added per approximately 0.1 g of specimen. The samples were homogenized in TRIzol reagent using a Sonic Dismembrator (Fisher

Scientific) prior to RNA isolation and preparation for qRT-PCR. The RNA from the tumor samples was converted to cDNA using an iScript cDNA Synthesis kit (Bio-Rad, Life Science, CA, USA). The following specific primers were selected from PrimerBank (pga.mgh.harvard.edu/primerbank/), to measure human gene expression in xenograft tumor specimens: ATX (5'-CTTTCGGCCCTGAGGAGAGTA-3' and 5'-AGCAACTGGTCTTTCCTGTCT-3'); CXCR2 (5'CCTGTCTTACTTTTCCGAAGGAC-3' and 5'-TTGCTGTATTGTTGCCCATGT-3'); VEGFR1 (5'-TTTGCCTGAAATGGTGAGTAAGG-3' and 5'-TGGTTTGCTTGAGCTGTGTTC-3'); VEGFR2 (5'-GGCCCAATAATCAGAGTCGCA-3' and 5'-CCGGTGTCAATTCGATCACTTT-3').

Cytokine analysis

Whole blood was collected from animals at necropsy in BD Blood Serum Collection Tubes and placed on ice until processed for serum collection. Serum was collected using sterile Gel BD Blood Serum Collection tubes. The gel tubes form a physical barrier between the serum and plasma and blood cells during centrifugation. Tubes contain the blood were allowed to clot at room temperature for 20 minutes. The tubes were then inverted 5 times before they were centrifuged for 10 min at 2000 RCF at room temperature. An approximate volume of 200µL serum was collected from the tubes and transferred to small glass vials for storage at -80°C. The serum was analyzed for cytokines, chemokines, growth factors and interleukins using the mouse Bio-Plex, 23-

Plex panel (Bio-Rad, Hercules, CA) and following the instructions provided by the manufacturer. The assay plates were measured using the Bio-Plex Multiplex Suspension Array system (Bio-Rad). Serum samples were measured via comparison to an 8-point standard dilution series included as an integral component of the high-throughput assay.

Statistics

The statistical differences were analyzed using an analysis of variance (ANOVA) test, followed by Bonferroni's multiple comparison test between groups using GraphPad Prism. When comparing only two groups, the Student's *t-test* was used. Where it is indicated in the figures, * $p < 0.05$ ** $p < 0.01$ and *** $p < 0.001$ indicate the levels of significance. Error bars are standard error of the mean.

Results

Biological Activity

In order to determine whether autotaxinab possessed *in vitro* biological activity, studies were conducted in our lab to explore the functional potency of autotaxinab against cell viability (data not shown). For the *in vitro* studies, multiple cancer cell lines were used to represent a wide range of subtypes including HT-29 (colon), PC-3 (prostate), MDA-MB-231 (breast), MeWo (melanoma), SB-2 (melanoma), OVCAR-3 (ovarian) and SKOV-3 (ovarian) (data not shown). In all cell lines, autotaxinab reduced cell viability and migration to some extent. Interestingly, autotaxinab had strong activity against MDA-MB-231 cells but was effective against all cell lines tested (data not shown).

In light of the fact that this data suggested autotaxinab had significant biological activity *in vitro*, we wanted to next assess whether it also had *in vivo* activity. Since there is a dearth of clinical therapeutics to treat melanomas lacking BRAF mutations, we examined autotaxinab in an animal model of melanoma. After establishing small pigmented melanoma tumors using MeWo cells injected with Glycosan Extracel[®], the mice were randomized into groups and then treated every-other-day with either diluent (control), autotaxinab at 20 mg/kg or autotaxinab at 50 mg/kg, which began 21 days post tumor cell injection. Prior to day 45, the tumor sizes in all groups appeared identical, but then began to diverge with the control groups displaying a linear rate of growth (**Figure 6.1A**). The group of mice treated with 20 mg/kg of autotaxinab also showed linear growth around day 50. On day 57, the tumor sizes between groups achieved statistical significance (**Figure 6.1A**, * $p < 0.05$, 50-40 mg/kg autotaxinab vs. control; day 65 - *** $p < 0.001$, 50-40 mg/kg autotaxinab vs. control) and this trend continued through the conclusion of the study, whereby control groups reached maximum allowable tumor volume. In comparison, the mice that were treated with

Of note is that on the 46th day of the study, the group of mice treated with 50 mg/kg of autotaxinab looked severely dehydrated and required medical intervention. Unfortunately, one mouse in the 50 mg/kg group (with an infinitesimally small tumor and no signs of ascites) rapidly declined in health and then died the following day, even after veterinarians helped treat the mouse for this condition. Thus, on the 48th day, we reduced the concentration of autotaxinab to 40 mg/kg (marked with an arrow) so that the experiment could continue safely without any other treated mice succumbing to the unspecified side effects of autotaxinab. Subsequently, all of the mice in this group were

then fed a special diet to curb dehydration, in addition to their regular chew pellets and no others were lost before the date of necropsy.

Upon necropsy, we collected tissues and serum from all mice remaining in the study. We then measured the mouse serum for 25 different secreted factors, including cytokines, chemokines, interleukins, etc. Understanding that many interleukins would only be expressed by animals with immune-intact systems, we also coupled this study to another whereby we treated C57/Bl6 animals with autotaxinab and measured their serum (data not shown). Interestingly, the most significant decrease in chemokines among treated animal serum from the present study was the keratinocyte chemoattractant (KC, also referred to as Chemokine C-X-C Motif Ligand 1 (CXCL1) or the Melanoma Growth Stimulating Activity Alpha protein) (**Figure 6.2C**, * $p < 0.05$, *** $p < 0.001$). The KC/CXCL-1 chemokine is homologous to the human growth regulated oncogene alpha (GRO-alpha), which is regulated by lysophosphatidic acid (Lee et al) and associated with cancer progression (Loukinova et al). Since chemokines are often significantly upregulated during tumorigenesis and melanoma tumor cells are known to secrete KC/CXCL-1 (Richmond et al), which also serve to exert signaling effects on endothelial cells, this chemokine may be a biomarker for the *in vivo* activity of autotaxinab in this model.

We then sectioned and stained tumor specimens with hematoxylin and eosin for pathology analysis of the tissues. Intriguingly, the percent of necrotic tissue within the tumor of the animals treated at the highest concentration of autotaxinab (40-50 mg/kg) had significantly more necrosis than control (** $p < 0.01$) and 20 mg/kg treated animals (* $p < 0.05$) (**Figure 6.2D**). In addition, the endothelial cells and state of the tumor

specimens were examined. One hundred percent of the control specimens contained viable endothelial cells. This was in contrast to 20 mg/kg treated animals, of which 50% contained only viable endothelial cells present and the other 50% of specimens displayed mixed areas with viable endothelial cells and also necrotic endothelial cells (**Figure 6.3E**). Most interesting was that 100% of specimens from animals treated with 40-50 mg/kg of autaxinib contained necrotic endothelial cells in close proximity to necrotic malignant cells. Taken together, the data suggests an anti-angiogenesis mechanism of action for autotaxinab. In support of this idea, we stained tumor sections with Ki-67 and detected no significant differences between specimens (**Figure 6.3**).

In order to help infer whether the autotaxinab compound was able to inhibit its target in vivo, we isolated RNA from tumor specimens for analysis using quantitative real time PCR. Indeed, we observed that tumors from animals treated with 20 mg/kg of autotaxinab had approximately 50% of the autotaxin compared to the control group (** $p < 0.01$). More importantly, tumors from animals treated with 40-50 mg/kg of autotaxinab showed a significant reduction in comparison to controls (~75%, *** $p < 0.001$). We also examined the expression of receptors that are involved in angiogenesis, including CXCR2, VEGFR1 and VEGFR2, but did not observe any significant changes. This suggests that treated tumors manifested significant reduction in the expression of autotaxin.

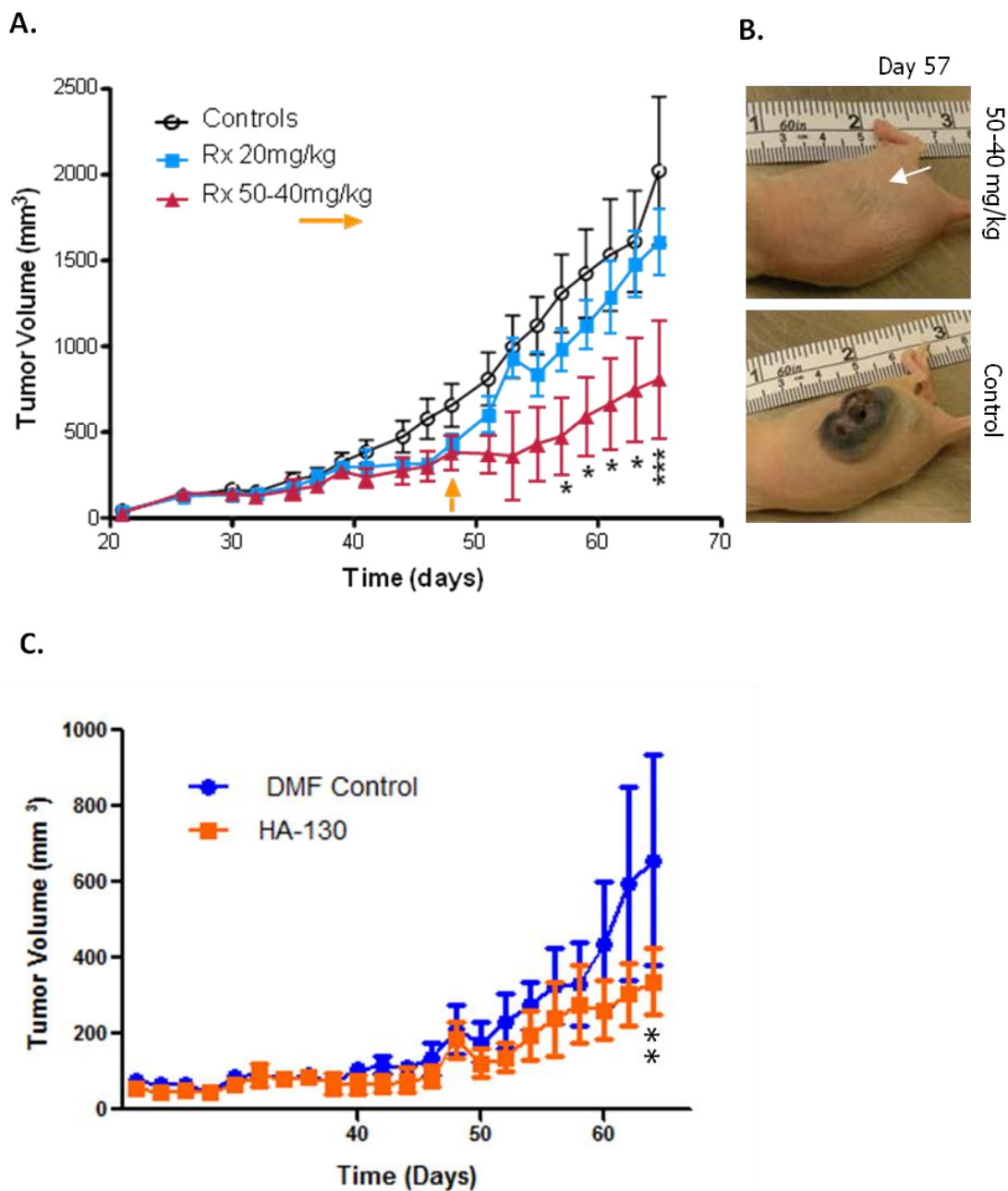


Figure 6.1. Autotaxinab inhibits tumor progression in a melanoma mouse model. Autotaxinab blunts tumor progression by inhibiting angiogenesis in a melanoma mouse model. (A) Animals with melanoma tumors were treated with the indicated concentrations of autotaxinab and established tumors were measured with calipers every other day. The arrow indicates the reduction of dosage from 50 mg/kg to 40 mg/kg on day 47 (see text for details). * $p < 0.05$ and *** $p < 0.0001$, control vs. 50-40 mg/kg. Means are \pm SEM. (B) Images of tumors on day 57 from control and treated animals. (C) Animals were treated with a commercial inhibitor of autotaxin HA130 at a dosage of 30 mg/kg as a positive control and comparison. ** $p < 0.001$, error bars are \pm SEM.

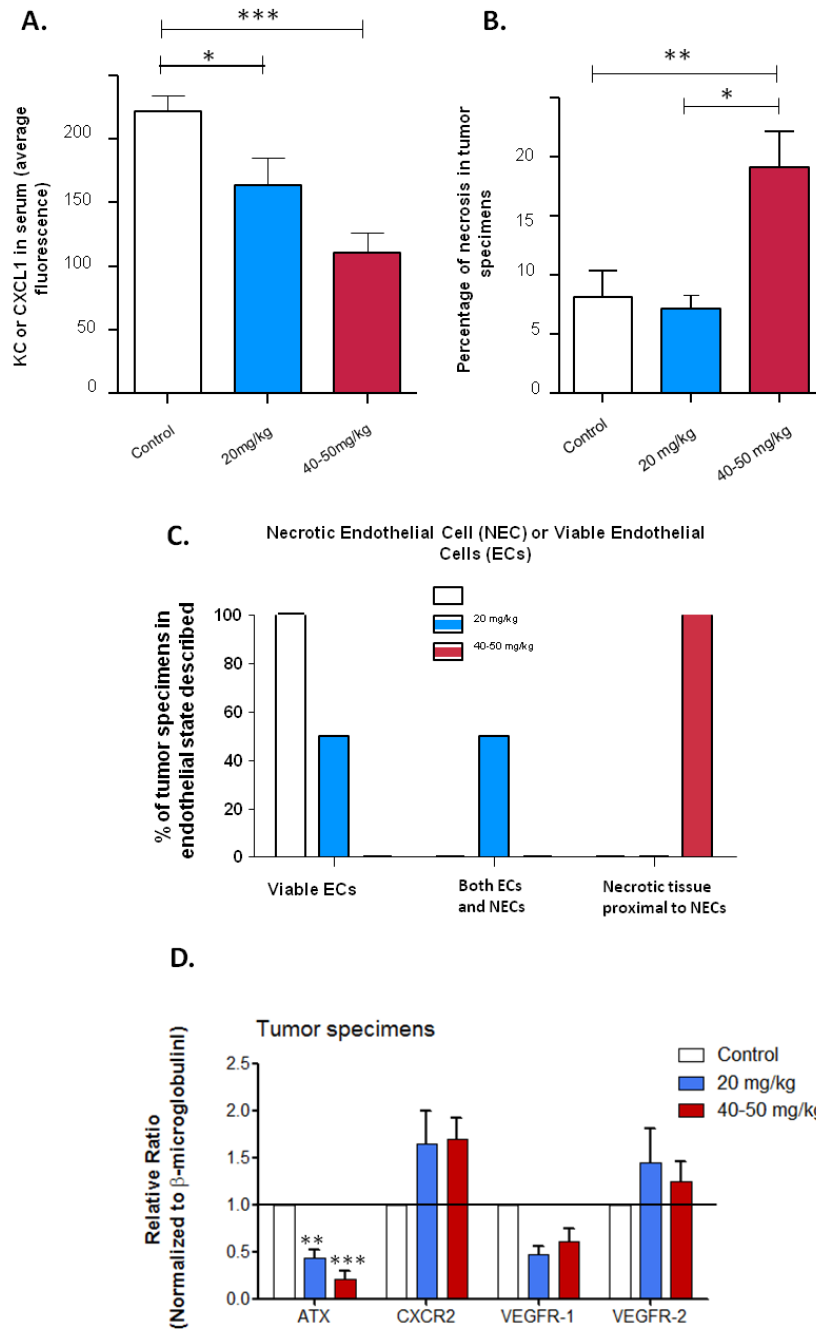


Figure 6.2. Autotaxinab inhibits angiogenesis and serum autotaxin levels. (A) Serum was collected and analyzed for KC/CXCL1. * $p < 0.05$, control vs. 20 mg/kg and *** $p < 0.001$, control vs. 50-40 mg/kg. (B) Quantification of specimens in the pathology report indicates the increase in tumor necrosis among animals treated with 50-40 mg/kg of **10b**. ** $p < 0.01$, control vs. 40-50 mg/kg and * $p < 0.05$, 20 mg/kg vs. 40-50 mg/kg. (C) Analysis of tumor specimens for regions with endothelial cells present indicates differences among the groups. (D) Animals treated with **10b** displayed reduced amounts of autotaxin mRNA in tumors. ** $p < 0.01$ and *** $p < 0.001$, comparing drug treated animals to controls using ANOVA followed by the Bonferroni multiple comparison test.

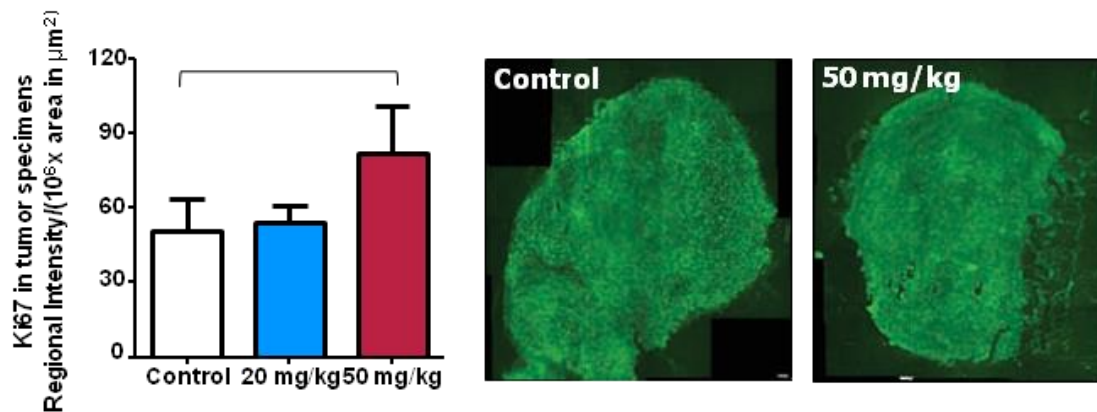


Figure 6.3. Immunofluorescence staining of Ki-67 positive cells in MeWo tumors treated with autotaxinab. Proliferation of tumor specimens was not significant, comparing control and treated animals. Tumors were sectioned and stained for Ki-67. Shown is the bar graph of average regional intensity of Ki-67 fluorescence and representative images of the stained sections.

Discussion

Herein we report the *in vivo* characterization of a vinyl sulfone analog autotaxinab, which we demonstrate is a novel inhibitor of autotaxin with activity against melanoma *in vitro* and *in vivo*. Our lab observed the *in vitro* activity of the vinyl sulfone against viability and migration among multiple cancer cell types (data not shown). Most importantly, we observed the inhibition of tumor progression using an *in vivo* model of melanoma. Taken together, our data suggests that the vinyl sulfone autotaxinab is a potent small molecule inhibitor of autotaxin with biological activity against its target, which reduces viability of cancer cells.

The vinyl sulfone compound compares very favorably against other compounds synthesized to inhibit autotoxin such as the commercial inhibitor HA130. The first known inhibitor of autotaxin was L-histidine, but this molecule was limited in its application due to the millimolar concentrations of L-histidine required to inhibit the lysophospholipase D activity of autotaxin (Clair et al). However, this report was the first to provide a proof-of-concept study that spawned other ideas for future innovation. Using a chemical library screening approach and ~40,000 drug-like small molecules, other groups have identified thiazolidinediones as autotaxin inhibitors that could be enhanced after the addition of a boronic acid moiety to achieve lower IC₅₀ levels (Albers et al). Our approach avoided the necessity to screen tens of thousands of compounds and was achieved through the rationale design.

We, and other groups, have also taken advantage of cyclic phosphatidic acid, a naturally occurring molecule that inhibits autotaxin and is an analogue of lysophosphatidic acid. Manipulating the compound structure to yield 3-carba analogues

of cyclic phosphatidic acid produced potent inhibitors of autotaxin that were effective *in vivo* (Baker et al). Similarly, a phosphonothionate analogue of carba cyclic phosphatidic acid also yielded a compound that inhibited the lysophospholipase D activity of autotaxin, the viability of melanoma cells and reduced melanoma metastasis *in vivo* (Altman et al). A recent study reported the evaluation of the stereoisomers of 3-carba cyclic phosphatidic acid, which are agonists of the LPA5 receptor, yet inhibits melanoma metastasis *in vivo* (Gupte et al).

There are several differences between these reports and our most recent report discussed here. Foremost, the vinyl sulfone is a novel inhibitor of autotaxin. Secondly, in previous studies we focused exclusively on advanced, metastatic models of melanoma (Altman et al , Baker et al). Herein, we established a solid melanoma tumor at one primary site, which is ideal for assessing the effects of angiogenesis. In this melanoma model, the tumors were highly pigmented, allowing for ease of visualization and measurements.

Through this tumor model, we discovered that the mechanism of action of autotaxinab *in vivo* is angiogenesis, which is not what we had predicted based on the data cultivated from our *in vitro* studies. Since we detected reduced viability in the presence of autotaxinab, we hypothesized that autotaxinab had a direct effect against tumor cells, possibly an inhibition of mitogenesis. However, mitogenesis inhibition is not what we discerned in animals, rather it was angiogenesis inhibition. Interestingly, the angiogenic response of autotaxin was previously described as “comparable to that elicited by VEGF” (Nam et al). Thus, our data is consistent with the known properties of autotaxin.

It is highly likely that 50 mg/kg (or very close to) is the MTD for autotaxinab, certainly without supportive therapy for the animals. One treated mouse (50 mg/kg) died, presumably to the unspecified side effects of autotaxinab since it had only a miniscule-sized tumor and no obvious signs of metastases. The fact that a mouse possibly succumbed to side effects is consistent with the harsh adverse drug events manifested by angiogenesis inhibitors used in treating patients with cancer. For example, bevacizumab contains several black-box warnings, which includes: fatal hemorrhage, increased arterial thromboembolic events (myocardial infarction and stroke), gastrointestinal perforation and complications to wound healing which requires discontinuation of the drug at least 28 days before surgery (Genentech). These black-box warnings are in addition to the other known drug toxicities of bevacizumab including hypertension, proteinuria and central nervous system events (e.g. dizziness, depression, headaches, seizure, lethargy, visual disturbances, etc.) (Chu and DeVita).

Although autotaxinab (40-50 mg/kg) was capable of sustaining an inhibition on tumor volume for approximately 53 days after the injection of tumor cells, the sizes of tumors in the highest treated group of animals started to increase on day 54. This was 6 days after we had reduced the dosage in this group from 50 mg/kg to 40 mg/kg. We cannot be certain whether this shift from static to growing tumors was due to the dosage reduction, chemoresistance or another factor. However, it is reasonable given the fact that autotaxin works similarly to VEGF, that inhibiting both would be required to sustain a long-term response against tumor angiogenesis.

Nevertheless, it was very exciting to observe the ability of autotaxinab to prevent melanoma tumor progression in animals. Advanced melanoma is a particularly difficult

type of cancer to treat because it is unresponsive to traditional chemotherapy; therefore, immunotherapy is typically administered even though responses are achieved in less than 20% of patients. In 2011, several new therapeutics for melanoma were approved for the first time in over a decade and these included a BRAF inhibitor, which can achieve remission for a short period of time. Although these new therapeutics should be considered a major breakthrough, they do not achieve cure. Thus, more research is desperately needed in this area. Besides melanoma, the compound was also effective against the viability and migration of MDA-MB-231 breast cells *in vitro*. This is very intriguing considering this cell line was isolated from the pleural effusion of a patient and represents a highly invasive triple-negative breast cancer, which is a clinically challenging subtype to treat. Taken together, our data supports the use of autotaxin inhibitors as a possible combination approach of anticancer therapeutics against the progression of melanoma.

CHAPTER 7

SUMMARY AND FUTURE DIRECTIONS

The goal of this research was to identify novel features among signaling pathways that mediate cell survival and tumor biology in chemoresistant cancers. Specifically, my research focused on understanding the novel role RGS proteins play in growth and survival mechanisms that are involved in the development of chemoresistance in ovarian cancer. Another focus of my research was to further characterize a novel therapeutic target for malignant melanoma. My research findings help to fill gaps in knowledge in understanding signaling pathways involved in the development of chemoresistance and how these pathways can be manipulated to overcome chemoresistance in cancer.

In chapter 2, we set out to determine what RGS proteins potential functions are in ovarian cancer cell survival. Based on our previous studies examining computational bioinformatics, we demonstrated that reduced RGS gene expression develops with the occurrence of drug resistance in ovarian cancer cell lines. Specifically, we showed that silencing of RGS10 and RGS17 proteins increases viability of ovarian cancer cells in the presence of cell cycle arrest compounds such as paclitaxel. We further examined the role of modulating RGS expression on cell differentiation, proliferation, and survival. Our studies showed that reducing levels of RGS10 and RGS 17 proteins enhances ovarian cancer cell viability (Hooks et al 2010). This could be instrumental in ovarian cancer cells' ability to survive in the presence of first line chemotherapeutics.

In Chapter 3, we showed that silencing RGS10 in ovarian cancer cell lines increases phosphorylation of eukaryotic initiation factor (eIF) 4E, the mRNA 5' cap-binding protein (phosphorylated-4E-BP1). Phosphorylation of 4E-BP1 has been shown to be a hallmark of more aggressive cancer phenotypes in prostate cancer and ovarian cancer (Castellvi et al 2006, Hsieh et al 2012). We established that upstream activation of 4E-BP1 (phosphorylated-Thr37/46) was through mTOR (phosphorylated-Ser-2448). Based on knowledge of the mTOR pathway, we hypothesized that these phosphorylation events and observed differences in cell size were occurring through activation of Rheb, a small G-protein. Based on our experimental results, we have elucidated a novel role of RGS10 in the growth and survival signaling pathways involved in the development of chemoresistance in ovarian cancer.

In chapter 4, we set out to clarify the extent to which RGS5 expression regulates tumor progression—whether it plays a pathogenic or protective role in ovarian tumor biology. RGS5 has been previously characterized for its role in angiogenesis during metastasis as well as its ability to promote apoptosis in hypoxic environments; however, little was known about its role in tumor growth. To investigate the role of RGS5 in tumor biology, we constructed an inducible gene expression system to achieve RGS5 expression in HeyA8-MDR ovarian cancer cells. Through this we observed that inducing RGS5 expression significantly reduces cell proliferation in HeyA8-MDR cells. Interestingly, RGS5 expression did not correlate with a reduction in tumor volume observed using an *in vivo* mouse model of ovarian cancer; however, the mice bearing RGS5-expressing tumors demonstrated an increase in survival compared with controls, which might be attributed to the vast regions of necrosis observed by pathological examination. Additionally, mice

bearing RGS5-expressing tumors were less likely to have ulcerated tumors. Note that although survival was increased, this was a modest increase. Too many single agent chemotherapies are thought to be successful, when in actuality they are not. This study supports the idea that temporal expression and stabilization of RGS5 could be a valuable tactic within the context of a multi-component approach for modulating tumor progression (Altman et al 2012).

In chapter 5, the importance of LPA stimulated G-protein coupled receptor signaling in melanoma growth and viability is discussed in the context of developing a new inhibitor of autotoxin the enzyme that produces LPA. Autotaxin is an enzyme that is found in the media of cultured melanoma cells. Autotaxin is known to promote cell motility and it is implicated in malignant progression and more aggressive cancer phenotypes (Baker et al 2006). We demonstrated the ability of thio-ccPA 18:1, a stabilized phosphonothionate analogue of carba cyclic phosphatidic acid, to induce a reduction in viability of metastatic melanoma cells compared to PBS control treated cells. The investigational phosphonothionate analogue serves a dual purpose as an autotaxin inhibitor and LPA1/3 receptor antagonist. Interestingly, transfecting melanoma cells with siRNA specific to LPA3 (siLPA3), but not other LPA receptors, simulated the effects of thio-ccPA 18:1 on viability (Altman et al 2010). Our observations required further exploration and led us to conduct another study looking at autotaxin inhibition in melanoma, which was addressed in chapter 6.

In chapter 6, we looked at the effects of a vinyl sulfone analogue of lysophosphatidylcholine, autotaxinab, which functions to inactivate autotaxin activity. We demonstrated the novel compound autotaxinab functions *in vivo* to reduce tumor

progression in melanoma. Notably, our most valuable observation with the compound autotaxinab was its ability to reduce tumor progression *in vivo* in a primary xenograft model of melanoma in correlation with a reduction in markers of angiogenesis, as compared to another autotaxin inhibitor, HA130. This study further supported our findings that novel inhibitors of autotaxin are promising cancer therapeutics.

Limitations and future directions

Limitations of the RGS10 and RGS17 study looking at cellular viability include transient transfections despite a >80% transfection efficiency. It is possible that endogenous levels of RGS10 and RGS17 in ovarian cancer are not completely silenced by siRNA and are still able to induce effects. Transfection efficiency is not always consistent and long-term duration studies of the consequence of RGS10 suppression are limited because of transient transfections. Initially, we were able to stably transfect shRNA for RGS proteins and induce gene suppression. However, we were unable to passage cells with stable suppression beyond a certain point limiting reliable and consistent knockdown in ovarian cancer cells. Another issue with stable transfection was incorporation of the shRNA in the genome. It was not tested to see where incorporation occurred to ensure that the insert was not in a gene or promoter region of a gene effecting its expression. Given a delivery vector, stable transfections can be dependent on the promoter region that is used in the vector. CMV promoters have been shown to be silent in some cell types, so use of the alternative promoters, such as CAG or U6, have been shown to be less likely silenced in mammalian cells (Qin et al 2010).

Animal studies looking at the effects of RGS10 and RGS17 suppression in ovarian cancer are needed to further investigate their role in chemoresistance. As we have shown the effects of RGS protein modulation are cell type specific. There are RGS10 knock-out mice that result in a severe osteopetrosis phenotype in mice, characterized by shortened limbs and stature (Yang and Li 2007). RGS10 is expressed abundantly in the immune system and broad regions within the brain including microglia. RGS10-null mice also show increased microglia burden and immune response in the CNS (Lee et al 2011). However, the RGS10 null mutation doesn't result in spontaneous formation of cancers or even increased likelihood of developing cancer in these mice. The fact that RGS10 does have a function in the immune system in addition to its role in G-protein signaling could lend to its effects seen in chemoresistant ovarian cancer cells.

Another method of gene silencing that has been recently developed is the CRISPR-Cas system that uses nuclease RNA-guided genome editing to rapidly, easily and efficiently maximize endogenous gene of interest knockout (Sander and Joung 2014). It has been useful in previously difficult to transfect cells and can be used in microinjections or to create transgenic animal models. The CRISPR-Cas system might be a great alternative for our laboratory to develop a stable ovarian cancer cell line with reduced RGS10 and RGS17 expression to use in an *in vivo* xenograft model. However, even the CRISPR-Cas system has limitations. There are off-target effects of using Cas9 nucleases. Currently, researchers are working to determine if there are modifications that can be made to the Cas9 nucleases to reduce these off-target effects (Sander and Joung 2014).

We were able to reduce the off-target gene silencing effects in our *in vitro* studies by using SMARTpool technology (Dharmacon). The off-target activity of siRNAs can lead to difficulty in interpreting observed phenotypes. Previous studies using microarray gene expression profiling support the concept that induction of siRNA would specifically silence the intended target but it is now recognized that off-target activity can occur and is not ameliorated by reducing the siRNA concentration (Jackson and Linsley 2010). In our *in vitro* studies, we cannot rule out the possibility that siRNA of the LPA3 receptor (or siRNA for ATX or any other LPA receptor, or RGS protein) may have off-target effects through microRNA-like down regulation. However, we are using pooled siRNA reagents which reduces the overall number of off-targets through competition among siRNAs.

The exact evolutionary mechanisms by which cancer cells are able to silence or reduce RGS expression in response to chemotherapy are not fully understood. To investigate this further, epigenetic studies of RGS gene expression regulation are needed. Researchers have already made great progress in further elucidating epigenetic gene regulation of RGS proteins in ovarian cancer. Ali et al found that the RGS10-1 transcript is enriched in CpG dinucleotides and that DNA methyl-transferases (DNMTs) increased RGS10 expression in ovarian cancer cells. In the chemoresistant ovarian cancer line, A2780-AD, there are DNA hypermethylated regions in the promoter compared to parental cells (Ali et al 2013). In addition, in this cell line there are decreases in histone H3 acetylation corresponding to an increase in histone deacetylase (HDAC) enzymes (Ali et al 2013, Cacan et al 2014). Furthermore, pharmacological inhibition of DNMTs and HDAC increases RGS10 expression and cisplatin-induced cytotoxicity in chemoresistant

ovarian cancer cells. These findings support the role of using targets for epigenetic mechanisms of gene regulation in combination therapy to overcome chemoresistance in ovarian cancer (Cacan et al 2014).

In our studies with the immunoprecipitation (IP) of RGS10, we show involvement or what we believe to be colocalization of RGS10 and Rheb proteins. However, it is unclear exactly how RGS10 is affecting Rheb activation either as an effector antagonist or a guanine nucleotide exchange inhibitor (GDI). To determine this exact interaction, structural inhibition of protein-protein interactions or FRET based assays would be useful (Arkin et al 2004). It would be beneficial to collaborate with another group to perform these definitive experiments.

For our immunofluorescent experiments, the cellomics machine and its High Throughput Content (HTC) software are powerful tools, however, even data collected using these methods/tools must be carefully interpreted. The assay within the software that you choose to measure your cellular feature of interest (i.e. cell size, nascent protein synthesis) needs to have set parameters between experiments to maintain consistency and allow for reproducible and reliable results. Our measures of cell size (i.e. average cell area and parameter) are also affected by cell density. It is important to ensure ideal cell density consistently between experiments. Overcrowding or sparse cells can influence their susceptibility to drugs/inhibitors and stimulus growth factors like LPA as well as whether cells shrink, expand, or die in response to these stimuli. Another method to determine cell size is flow cytometry. Flow cytometry would be a valuable complement to our cellomics cell size data, it is a way to measure free floating cells as opposed to looking at fixed cells in monolayer. There are studies validating that data collected with

high content imaging correlates well with data assessed using flow cytometry (Trzcinska-Daneluti et al 2009).

In the set of experiments using overexpression constructs, we tested the functional consequences of overexpressing RGS5 protein. We used an inducible pTet Advanced vector system to control the expression of RGS5 in HeyA8 MDR cells. The HeyA8 MDR cell line was chosen for our studies, because after numerous attempts to stably transfect SKOV-3 cells with RGS10, we were unable to successfully create the overexpression construct in this cell line. The SKOV-3 cell line may have some inherent feature that doesn't make them amenable to stable transfections. Cells that are more undifferentiated are more likely to silence the CMV promoter (Saffert and Kalejta 2007). The quantity of transfection reagent necessary to incorporate the DNA plasmid vector killed all of the SKOV-3 cells during our attempts. In contrast, the HeyA8 MDR cells being an inherently aggressive ovarian cancer phenotype resistant to multiple drugs may have acquired features that make the cell line robust enough to tolerate plasmid incorporation and toxicity associated with the transfection reagent. In the future, our laboratory could explore possible alternate means of stably transfecting SKOV-3 cells such as using lentivirus or an alternate promoter region.

In our *in vivo* pilot studies of RGS5, we looked at the functional consequences of overexpressing RGS5 in a xenograft model of ovarian cancer. We chose to use the pTet Advanced vector system with RGS5 gene insertion in HeyA8 MDR ovarian cancer cells to limit our induction of the RGS5 gene to the local tumor. Also, we chose to do xenografts with Extracel because of the ease of tumor formation and 100% take rate. Although orthotopic *in vivo* models of ovarian cancer more closely resemble the disease

state in humans, ours was a proof of concept study. The orthotopic model requires an invasive surgery in which you can lose mice to anesthesia. In the orthotopic model, tumor take rate may be reduced in addition to having an increased time of tumor formation in this model. Human tumor xenograft models are widely used in preliminary anticancer drug studies to study the role of angiogenesis and the microenvironment and can be a valuable predictive model (Kerbel 2003). For all these reasons, our lab chose to use a xenograft model of ovarian cancer.

An important point is made that sectioning tumors creates a cross section of a solid tumor that may not be an accurate representation of the entire heterogeneous tumor. On the periphery of a tumor there will be more actively proliferating tumor cells. In contrast, toward the center of the tumor is where there will be more cells that are distant from functional vasculature that are exposed to more hypoxic conditions resulting in more necrotic tissue regions. Other ways to measure tumor composition *in vivo* would be functional MRI or PET-CT both of which can be expensive and preliminary without the data reported in our study. In PET-FDG used in oncology, a radioisotope of FDG (glucose analog) is used as a biomarker of metabolic activity within a solid gynecological tumor. Diffusion-weighted MRI (DWI) uses imaging of water diffusion molecules to compare differences in diffusion between tissue types to determine their functional composition. Tumors that have vast regions of hypoxia or necrosis may not have functional diffusion detected by this MRI technique, which does not make this method ideal for measuring ovarian lesions. These two methods can often result in false-positives (Alvarez Moreno et al 2012).

During our pilot study with RGS5 we did not administer chemotherapeutic drugs because we had a limited sample size. Since the drugs most commonly administered for ovarian cancer cisplatin and paclitaxel are very toxic, they would need to be administered to the mice via tail vein injections to facilitate systemic circulation. We chose not to add this layer of complexity to our pilot study because we were most interested in determining the contribution of RGS5 modulation alone to tumor biology. In the future it would be very valuable to conduct follow-up *in vivo* studies combining RGS5 modulation with the administration of chemotherapeutic drugs to see if it would result in combined beneficial therapeutic effects. Additionally, it would be interesting to look at combining different RGS proteins that target different G alpha subunits or other signaling molecules to see if this would enhance chemosensitivity in ovarian cancer. Our preliminary data combining RGS protein modulation *in vitro* was inconclusive (data not shown).

In our studies investigating a novel therapeutic target for melanoma, we looked at novel inhibitors of ATX that elicit their effects via angiogenesis inhibition. My discussion will focus on the vinyl sulfone analog autotaxinab that was characterized to have *in vivo* effects on tumor growth in melanoma. Specifically, vinyl sulfone derivatives are widely characterized as irreversible inhibitors of cysteine protease (Kam et al 2004). Cysteine proteinases play a role in numerous physiological processes and their aberrant activity can lead to many pathologies including arthritis, neurological disorders, tumors, and osteoporosis (Rzychon et al 2004). The protein enzymes include caspases, cathepsins, and calpains and they are involved in protein degradation, antigen presentation, fertilization, and cell proliferation to name a few of their functions (Chapman et al 1997). Several studies have characterized the mechanism of action of

vinyl sulfone inhibitors and their ability to make covalent modifications to the active site of a protein, in this case the protein substrate of lysophosphatidylcholine of autotaxin (Kam et al 2004, Kam and Exton 2004) . In this way, our compound is able to inhibit autotaxin through inhibiting its lysophospholipase D activity.

In future studies, it would be valuable to make additional comparisons with our experimental compound autotaxinab to other cysteine proteases inhibitors. For example, the HIV-1 protease inhibitor, nelfinavir is able to reduce glioblastoma tumor growth in nude mice. The mechanism of nelfinavir induced cell death in this model is hypothesized to be through triggering endoplasmic reticulum stress (Pyrko et al 2007). A phase II clinical trial with nelfinavir has been completed by a group that initially looked at the drug *in vitro*. Previously, the group showed that nelfinavir inhibits *in vitro* tumor growth by suppressing aberrant Akt signaling in adenoid cystic carcinoma (ACC) (Hoover et al 2014). Although, this study was done with in a different tissue type, it would be interesting to compare these inhibitors that have presumably different mechanisms of action for their efficacy against melanoma tumor growth *in vivo*. An important point is the efficacy of cysteine protease inhibitors is affected by the presence of serum both *in vitro* and obviously *in vivo*. The presence of serum would cause cysteine protease inhibitors to lose efficacy and therefore increased concentrations of drugs are needed to have beneficial effects. Future studies examining the efficacy of these types of compounds against melanoma cell viability and tumor growth would have to account for this limitation.

Cancer biology and drug design

In the treatment of cancer, convention for patient treatment is moving toward more personalized medicine which has been driven by the use of bioinformatics in tumor analysis and the development of the human cancer genome. It is increasingly important to have a clear picture of the molecular lesions that are present in a particular cancer type in order to choose appropriate treatment options and develop strategies to avoid the inevitable development of chemoresistance. Our studies examining computational bioinformatics demonstrated that reduced RGS gene expression develops with the occurrence of drug resistance in ovarian cancer cell lines. This is an important observation because it may be indicative of a molecular signature associated with chemoresistance in ovarian cancer. Clinically identifying patients with reduced RGS expression within their tumor may reveal patients that are susceptible to developing resistance to first-line chemotherapeutics. This knowledge may help oncologists to develop unique treatment regimens for this subset of patients as well as provide selection criteria for patient candidates in drug trials.

More advanced clinical understanding of the receptors and enzymes involved in chemoresistant malignancies like melanoma is critical to developing therapeutic drug targets. Gene expression array studies in melanoma revealed that there are aberrant LPA3 receptor and ATX enzyme expression levels in a subset of advanced malignant melanomas. This information led to the observation that only a subset of melanomas that have this specific molecular signature may be responsive to novel therapeutics that are aimed at these drug targets. Pre-clinical testing of these novel compounds is necessary to

the successful development of anti-cancer agents that target these specific receptors and exploit their involvement in pathways that are implicated in survival and angiogenesis.

The development of predictive pre-clinical models is highly important to furthering therapeutic development in ovarian cancer and melanoma. As discussed earlier, there were limitations to our studies with reduced RGS expression because of the inability to maintain stable knockdown in ovarian cancer cells to develop an animal model. In contrast, our studies working to develop an *in vivo* model of malignant melanoma and to test novel compounds in this animal model were more successful. Our *in vivo* melanoma xenograft model was representative of primary skin lesions with metastatic potential that are seen in patients that present with malignant melanoma. The development of a successful pre-clinical animal model greatly aided the testing of our novel compounds' efficacy against melanoma. The data that was collected from these studies further solidified that autotaxin inhibitors are viable therapeutic targets for melanoma that have potential in other cancers as well (Altman et al 2010).

Identifying molecular targets in signaling pathways involved with growth, survival, and angiogenesis has been central in developing anti-cancer therapeutics. The common thread in many cancers is the ability of cancer cells to rapidly divide and proliferate, leading to the fact that standard chemotherapeutic drugs target mechanisms that allow cancer cells to do this. Our observations that modulated RGS protein expression counterbalances the effects of cell cycle arrest compounds to influence survival and proliferation provides evidence that RGS proteins contribute to survival signaling pathways. Coupled to the fact that many ovarian cancer patients develop

resistance to initially effective chemotherapy, these observations lend to the idea that RGS proteins should be further investigated as potential therapeutic targets.

The signaling network comprised of PI3K, AKT, and mTOR influences most of the hallmarks in cancer, including growth, survival, and angiogenesis (Fruman and Rommel 2014). Appreciated as a master regulator in many cellular processes, mTOR is recognized as an attractive anti-cancer target. However, inhibitors of mTOR have been used in the clinic with varying levels of success in ovarian cancer, glioblastoma, and basal cell carcinoma mainly due to genetic mutations that affect the sensitivity of these cancers to mTOR inhibitors (Gini et al 2013, Jardim et al 2014). Based on the genetic make-up of a particular cancer, using mTOR inhibitors in combination with other anti-cancer therapeutics may be advantageous (Fruman and Rommel 2014). The rationale for targeting the mTOR signaling network is rooted in the foundation of cancer genetics and molecular cell biology studies. Despite some of the challenges in using mTOR inhibitors, such as their effects on the immunity and metabolism, noticeable advances have been made in the clinic. Alternative targets within the PI3K, AKT, mTOR pathway are being investigated in preclinical studies that target cap-dependent translation in cancer cells (Lindqvist and Pelletier 2009). Therefore, our observations that RGS10 suppression in ovarian cancer cells increases phosphorylation of 4EBP1 and has effects on cell growth via the mTOR pathway could be important in developing combinatorial treatments for ovarian cancer.

The standard drug development path for a targeted anti-cancer drug requires confirming single-agent efficacy before testing the drug in combination. It has been observed in the clinic in several malignancies that endothelial cells within solid tumor

neovasculature are particularly sensitive to radiotherapy (Rao et al 2014). These observations are also leading to the awareness that certain chemotherapies may target these sensitive neovascular endothelial cells in tumors and enhance treatment (Rao et al 2014). There is increasing evidence for changing the single-agent testing paradigm to examine the efficacy of anti-cancer agents in rational combinations based on the genetic make-up of a tumor. Our data provides preliminary evidence for combining anti-cancer therapeutics that target angiogenesis and growth factor receptor pathways in ovarian cancer and melanoma.

The over arching theme behind the findings in these chapters was the idea of better understanding how signaling pathways contribute to the tumor biology and the development of chemoresistance in cancer. More effective treatment of chemoresistant cancers relies on combining therapeutic approaches that have been discussed in this thesis. Strategies include targeting cell surface growth receptors such as LPA receptors or enzymes involved in growth factor production such as autotaxin in melanoma. In addition, targeting the interaction site of proteins like the small G-protein Rheb or over-expressing specific proteins like RGS5 in tumors may offer other options for combination therapy in chemoresistant ovarian cancer.

Survival is the key to understanding the biological complexity of cancer cells. The re-wiring that occurs in tumor cells assaulted with chemotherapy is happening to enhance cell survival. Evolutionary pre-programming for survival that seems to be in place in cancer cells is a major pharmacological challenge to overcome. The problem that lies in the biological complexity of cancer is that tumor cells are able to adapt to their environments to become resistant and survive in the presence of chemotherapeutic

agents. Ultimately, my thesis research findings might result in a better understanding of the signaling pathways involved in chemoresistance and lead to the development of more targeted therapy for patients.

REFERENCES

- Albers HM, Dong A, van Meeteren LA, Egan DA, Sunkara M, van Tilburg EW *et al* (2010). Boronic acid-based inhibitor of autotaxin reveals rapid turnover of LPA in the circulation. *Proc Natl Acad Sci U S A* **107**: 7257-7262.
- Albers HM, Ovaa H (2012). Chemical evolution of autotaxin inhibitors. *Chem Rev* **112**: 2593-2603.
- Ali MW, Cacan E, Liu Y, Pierce JY, Creasman WT, Murph MM *et al* (2013). Transcriptional suppression, DNA methylation, and histone deacetylation of the regulator of G-protein signaling 10 (RGS10) gene in ovarian cancer cells. *PLoS One* **8**: e60185.
- Altman MK, Gopal V, Jia W, Yu S, Hall H, Mills GB *et al* (2010). Targeting melanoma growth and viability reveals dualistic functionality of the phosphonothionate analogue of carba cyclic phosphatidic acid. *Mol Cancer* **9**: 140.
- Altman MK, Nguyen DT, Patel SB, Fambrough JM, Beedle AM, Hardman WJ *et al* (2012). Regulator of G-Protein Signaling 5 Reduces HeyA8 Ovarian Cancer Cell Proliferation and Extends Survival in a Murine Tumor Model. *Biochem Res Int* **2012**: 518437.
- Alvarez Moreno E, Jimenez de la Pena M, Cano Alonso R (2012). Role of New Functional MRI Techniques in the Diagnosis, Staging, and Followup of Gynecological Cancer: Comparison with PET-CT. *Radiol Res Pract* **2012**: 219546.
- An S, Bleu T, Hallmark OG, Goetzl EJ (1998). Characterization of a novel subtype of human G protein-coupled receptor for lysophosphatidic acid. *J Biol Chem* **273**: 7906-7910.
- Anderson AR, Weaver AM, Cummings PT, Quaranta V (2006). Tumor morphology and phenotypic evolution driven by selective pressure from the microenvironment. *Cell* **127**: 905-915.
- Apanovitch DM, Slep KC, Sigler PB, Dohlman HG (1998). Sst2 is a GTPase-activating protein for Gpa1: purification and characterization of a cognate RGS-Galpha protein pair in yeast. *Biochemistry* **37**: 4815-4822.
- Arkin MR, Glicksman MA, Fu H, Havel JJ, Du Y (2004). Inhibition of Protein-Protein Interactions: Non-Cellular Assay Formats.

Bagnato A, Tecce R, Moretti C, Di Castro V, Spergel D, Catt KJ (1995). Autocrine actions of endothelin-1 as a growth factor in human ovarian carcinoma cells. *Clin Cancer Res* **1**: 1059-1066.

Baker DL, Fujiwara Y, Pigg KR, Tsukahara R, Kobayashi S, Murofushi H *et al* (2006). Carba analogs of cyclic phosphatidic acid are selective inhibitors of autotaxin and cancer cell invasion and metastasis. *J Biol Chem* **281**: 22786-22793.

Bandoh K, Aoki J, Hosono H, Kobayashi S, Kobayashi T, Murakami-Murofushi K *et al* (1999). Molecular cloning and characterization of a novel human G-protein-coupled receptor, EDG7, for lysophosphatidic acid. *J Biol Chem* **274**: 27776-27785.

Bansal G, Druey KM, Xie Z (2007). R4 RGS proteins: regulation of G-protein signaling and beyond. *Pharmacol Ther* **116**: 473-495.

Bast RC, Jr., Hennessy B, Mills GB (2009). The biology of ovarian cancer: new opportunities for translation. *Nat Rev Cancer* **9**: 415-428.

Beeram M, Tan QT, Tekmal RR, Russell D, Middleton A, DeGraffenried LA (2007). Akt-induced endocrine therapy resistance is reversed by inhibition of mTOR signaling. *Annals of oncology : official journal of the European Society for Medical Oncology / ESMO* **18**: 1323-1328.

Berger M, Bergers G, Arnold B, Hammerling GJ, Ganss R (2005). Regulator of G-protein signaling-5 induction in pericytes coincides with active vessel remodeling during neovascularization. *Blood* **105**: 1094-1101.

Birnbaumer L (2007). Expansion of signal transduction by G proteins. The second 15 years or so: from 3 to 16 alpha subunits plus betagamma dimers. *Biochim Biophys Acta* **1768**: 772-793.

Blaho VA, Hla T (2011). Regulation of mammalian physiology, development, and disease by the sphingosine 1-phosphate and lysophosphatidic acid receptors. *Chem Rev* **111**: 6299-6320.

Bohm A, Gaudet R, Sigler PB (1997). Structural aspects of heterotrimeric G-protein signaling. *Curr Opin Biotechnol* **8**: 480-487.

Bondjers C, Kalen M, Hellstrom M, Scheidl SJ, Abramsson A, Renner O *et al* (2003). Transcription profiling of platelet-derived growth factor-B-deficient mouse embryos identifies RGS5 as a novel marker for pericytes and vascular smooth muscle cells. *Am J Pathol* **162**: 721-729.

Brown JM, Wilson WR (2004). Exploiting tumour hypoxia in cancer treatment. *Nat Rev Cancer* **4**: 437-447.

- Buys TP, Chari R, Lee EH, Zhang M, MacAulay C, Lam S *et al* (2007). Genetic changes in the evolution of multidrug resistance for cultured human ovarian cancer cells. *Genes Chromosomes Cancer* **46**: 1069-1079.
- Cacan E, Ali MW, Boyd NH, Hooks SB, Greer SF (2014). Inhibition of HDAC1 and DNMT1 modulate RGS10 expression and decrease ovarian cancer chemoresistance. *PLoS One* **9**: e87455.
- Callihan P, Mumaw J, Machacek DW, Stice SL, Hooks SB (2011). Regulation of stem cell pluripotency and differentiation by G protein coupled receptors. *Pharmacol Ther* **129**: 290-306.
- Campbell DB, Lange LA, Skelly T, Lieberman J, Levitt P, Sullivan PF (2008). Association of RGS2 and RGS5 variants with schizophrenia symptom severity. *Schizophr Res* **101**: 67-75.
- Capaccione KM, Pine SR (2013). The Notch signaling pathway as a mediator of tumor survival. *Carcinogenesis* **34**: 1420-1430.
- Carmeliet P, Jain RK (2000). Angiogenesis in cancer and other diseases. *Nature* **407**: 249-257.
- Castellano E, Santos E (2011). Functional specificity of ras isoforms: so similar but so different. *Genes Cancer* **2**: 216-231.
- Castellvi J, Garcia A, Rojo F, Ruiz-Marcellan C, Gil A, Baselga J *et al* (2006). Phosphorylated 4E binding protein 1: a hallmark of cell signaling that correlates with survival in ovarian cancer. *Cancer* **107**: 1801-1811.
- Chang YP, Liu X, Kim JD, Ikeda MA, Layton MR, Weder AB *et al* (2007). Multiple genes for essential-hypertension susceptibility on chromosome 1q. *Am J Hum Genet* **80**: 253-264.
- Chapman HA, Riese RJ, Shi GP (1997). Emerging roles for cysteine proteases in human biology. *Annu Rev Physiol* **59**: 63-88.
- Chen C, Zheng B, Han J, Lin SC (1997). Characterization of a novel mammalian RGS protein that binds to Galpha proteins and inhibits pheromone signaling in yeast. *J Biol Chem* **272**: 8679-8685.
- Cho H, Kozasa T, Bondjers C, Betsholtz C, Kehrl JH (2003). Pericyte-specific expression of Rgs5: implications for PDGF and EDG receptor signaling during vascular maturation. *FASEB J* **17**: 440-442.

Cho H, Park C, Hwang IY, Han SB, Schimel D, Despres D *et al* (2008). Rgs5 targeting leads to chronic low blood pressure and a lean body habitus. *Mol Cell Biol* **28**: 2590-2597.

Chu E, DeVita VT (2011). *Physicians' Cancer Chemotherapy Drug Manual*. Jones and Bartlett Publishers: Sudbury, MA.

Clair T, Aoki J, Koh E, Bandle RW, Nam SW, Ptaszynska MM *et al* (2003). Autotaxin hydrolyzes sphingosylphosphorylcholine to produce the regulator of migration, sphingosine-1-phosphate. *Cancer Res* **63**: 5446-5453.

Clair T, Koh E, Ptaszynska M, Bandle RW, Liotta LA, Schiffmann E *et al* (2005). L-histidine inhibits production of lysophosphatidic acid by the tumor-associated cytokine, autotaxin. *Lipids Health Dis* **4**: 5.

Conn PJ, Christopoulos A, Lindsley CW (2009). Allosteric modulators of GPCRs: a novel approach for the treatment of CNS disorders. *Nat Rev Drug Discov* **8**: 41-54.

Cotton M, Claing A (2009). G protein-coupled receptors stimulation and the control of cell migration. *Cell Signal* **21**: 1045-1053.

Damiano JS, Hazlehurst LA, Dalton WS (2001). Cell adhesion-mediated drug resistance (CAM-DR) protects the K562 chronic myelogenous leukemia cell line from apoptosis induced by BCR/ABL inhibition, cytotoxic drugs, and gamma-irradiation. *Leukemia* **15**: 1232-1239.

Dean M, Fojo T, Bates S (2005). Tumour stem cells and drug resistance. *Nat Rev Cancer* **5**: 275-284.

Dohlman HG, Song J, Apanovitch DM, DiBello PR, Gillen KM (1998). Regulation of G protein signalling in yeast. *Semin Cell Dev Biol* **9**: 135-141.

Durgam GG, Virag T, Walker MD, Tsukahara R, Yasuda S, Liliom K *et al* (2005). Synthesis, structure-activity relationships, and biological evaluation of fatty alcohol phosphates as lysophosphatidic acid receptor ligands, activators of PPARgamma, and inhibitors of autotaxin. *J Med Chem* **48**: 4919-4930.

East JE, Kennedy AJ, Tomsig JL, De Leon AR, Lynch KR, Macdonald TL (2010). Synthesis and structure-activity relationships of tyrosine-based inhibitors of autotaxin (ATX). *Bioorg Med Chem Lett* **20**: 7132-7136.

Efeyan A, Sabatini DM (2010). mTOR and cancer: many loops in one pathway. *Curr Opin Cell Biol* **22**: 169-176.

Eisen MB, Spellman PT, Brown PO, Botstein D (1998). Cluster analysis and display of genome-wide expression patterns. *Proc Natl Acad Sci U S A* **95**: 14863-14868.

- Faruque MU, Chen G, Doumatey A, Huang H, Zhou J, Dunston GM *et al* (2011). Association of ATP1B1, RGS5 and SELE polymorphisms with hypertension and blood pressure in African-Americans. *J Hypertens* **29**: 1906-1912.
- Ferry G, Moulharat N, Pradere JP, Desos P, Try A, Genton A *et al* (2008). S32826, a nanomolar inhibitor of autotaxin: discovery, synthesis and applications as a pharmacological tool. *J Pharmacol Exp Ther* **327**: 809-819.
- Fruman DA, Rommel C (2014). PI3K and cancer: lessons, challenges and opportunities. *Nat Rev Drug Discov* **13**: 140-156.
- Garattini S (2007). Pharmacokinetics in cancer chemotherapy. *Eur J Cancer* **43**: 271-282.
- Genentech I (2011). U.S. BL 125085 Supplement: Bevacizumab. In: Genentech I (ed): South San Francisco. pp 1-23.
- Genentech I (2013). Avastin (bevacizumab) full prescribing information. In: Group AMotR (ed): South San Francisco. p 26.
- Gerlinger M, Rowan AJ, Horswell S, Larkin J, Endesfelder D, Gronroos E *et al* (2012). Intratumor heterogeneity and branched evolution revealed by multiregion sequencing. *N Engl J Med* **366**: 883-892.
- Gierse J, Thorarensen A, Beltey K, Bradshaw-Pierce E, Cortes-Burgos L, Hall T *et al* (2010). A novel autotaxin inhibitor reduces lysophosphatidic acid levels in plasma and the site of inflammation. *J Pharmacol Exp Ther* **334**: 310-317.
- Gini B, Zanca C, Guo D, Matsutani T, Masui K, Ikegami S *et al* (2013). The mTOR kinase inhibitors, CC214-1 and CC214-2, preferentially block the growth of EGFRvIII-activated glioblastomas. *Clin Cancer Res* **19**: 5722-5732.
- Gold SJ, Ni YG, Dohlman HG, Nestler EJ (1997). Regulators of G-protein signaling (RGS) proteins: region-specific expression of nine subtypes in rat brain. *J Neurosci* **17**: 8024-8037.
- Goorden SM, Hoogeveen-Westerveld M, Cheng C, van Woerden GM, Mozaffari M, Post L *et al* (2011). Rheb is essential for murine development. *Mol Cell Biol* **31**: 1672-1678.
- Grunwald V, DeGraffenried L, Russel D, Friedrichs WE, Ray RB, Hidalgo M (2002). Inhibitors of mTOR reverse doxorubicin resistance conferred by PTEN status in prostate cancer cells. *Cancer research* **62**: 6141-6145.
- Guo Y, Kwiatkowski DJ (2013). Equivalent benefit of rapamycin and a potent mTOR ATP-competitive inhibitor, MLN0128 (INK128), in a mouse model of tuberous sclerosis. *Mol Cancer Res* **11**: 467-473.

- Gupte R, Siddam A, Lu Y, Li W, Fujiwara Y, Panupinthu N *et al* (2010). Synthesis and pharmacological evaluation of the stereoisomers of 3-carba cyclic-phosphatidic acid. *Bioorg Med Chem Lett* **20**: 7525-7528.
- Gupte R, Patil R, Liu J, Wang Y, Lee SC, Fujiwara Y *et al* (2011a). Benzyl and Naphthalene Methylphosphonic Acid Inhibitors of Autotaxin with Anti-invasive and Anti-metastatic Activity. *ChemMedChem*.
- Gupte R, Patil R, Liu J, Wang Y, Lee SC, Fujiwara Y *et al* (2011b). Benzyl and naphthalene methylphosphonic acid inhibitors of autotaxin with anti-invasive and anti-metastatic activity. *ChemMedChem* **6**: 922-935.
- Hama K, Aoki J, Fukaya M, Kishi Y, Sakai T, Suzuki R *et al* (2004). Lysophosphatidic acid and autotaxin stimulate cell motility of neoplastic and non-neoplastic cells through LPA1. *J Biol Chem* **279**: 17634-17639.
- Hamzah J, Jugold M, Kiessling F, Rigby P, Manzur M, Marti HH *et al* (2008). Vascular normalization in Rgs5-deficient tumours promotes immune destruction. *Nature* **453**: 410-414.
- Hanahan D, Weinberg RA (2011). Hallmarks of cancer: the next generation. *Cell* **144**: 646-674.
- Hardman JG, Robison GA, Sutherland EW (1971). Cyclic nucleotides. *Annu Rev Physiol* **33**: 311-336.
- Hasegawa Y, Erickson JR, Goddard GJ, Yu S, Liu S, Cheng KW *et al* (2003). Identification of a phosphothionate analogue of lysophosphatidic acid (LPA) as a selective agonist of the LPA3 receptor. *J Biol Chem* **278**: 11962-11969.
- Hasegawa Y, Murph M, Yu S, Tigyi G, Mills GB (2008). Lysophosphatidic acid (LPA)-induced vasodilator-stimulated phosphoprotein mediates lamellipodia formation to initiate motility in PC-3 prostate cancer cells. *Mol Oncol* **2**: 54-69.
- Hausmann J, Kamtekar S, Christodoulou E, Day JE, Wu T, Fulkerson Z *et al* (2011). Structural basis of substrate discrimination and integrin binding by autotaxin. *Nat Struct Mol Biol* **18**: 198-204.
- Hecht JH, Weiner JA, Post SR, Chun J (1996). Ventricular zone gene-1 (vzg-1) encodes a lysophosphatidic acid receptor expressed in neurogenic regions of the developing cerebral cortex. *J Cell Biol* **135**: 1071-1083.
- Heximer SP, Watson N, Linder ME, Blumer KJ, Hepler JR (1997). RGS2/G0S8 is a selective inhibitor of Gqalpha function. *Proc Natl Acad Sci U S A* **94**: 14389-14393.

Higashijima T, Ferguson KM, Sternweis PC, Ross EM, Smigel MD, Gilman AG (1987). The effect of activating ligands on the intrinsic fluorescence of guanine nucleotide-binding regulatory proteins. *J Biol Chem* **262**: 752-756.

Hocker T, Tsao H (2007). Ultraviolet radiation and melanoma: a systematic review and analysis of reported sequence variants. *Hum Mutat* **28**: 578-588.

Hoeglund AB, Bostic HE, Howard AL, Wanjala IW, Best MD, Baker DL *et al* (2010). Optimization of a pipemidic acid autotaxin inhibitor. *J Med Chem* **53**: 1056-1066.

Hollinger S, Hepler JR (2002a). Cellular regulation of RGS proteins: modulators and integrators of G protein signaling. *Pharmacol Rev* **54**: 527-559.

Hollinger S, Hepler JR (2002b). Cellular Regulation of RGS Proteins: Modulators and Integrators of G Protein Signaling. *Pharmacological Reviews* **54**: 527-559.

Hooks SB, Callihan P, Altman MK, Hurst JH, Ali MW, Murph MM (2010). Regulators of G-Protein signaling RGS10 and RGS17 regulate chemoresistance in ovarian cancer cells. *Mol Cancer* **9**: 289.

Hoover AC, Milhem MM, Anderson CM, Sun W, Smith BJ, Hoffman HT *et al* (2014). Efficacy of nelfinavir as monotherapy in refractory adenoid cystic carcinoma: Results of a Phase II clinical trial. *Head Neck*.

Hsieh AC, Liu Y, Edlind MP, Ingolia NT, Janes MR, Sher A *et al* (2012). The translational landscape of mTOR signalling steers cancer initiation and metastasis. *Nature* **485**: 55-61.

Hunt TW, Fields TA, Casey PJ, Peralta EG (1996). RGS10 is a selective activator of G alpha i GTPase activity. *Nature* **383**: 175-177.

Hurst-Kennedy J, Zhong M, Gupta V, Boyan BD, Schwartz Z (2010). 24R,25-Dihydroxyvitamin D3, lysophosphatidic acid, and p53: a signaling axis in the inhibition of phosphate-induced chondrocyte apoptosis. *J Steroid Biochem Mol Biol* **122**: 264-271.

Hurst JH, Henkel PA, Brown AL, Hooks SB (2008). Endogenous RGS proteins attenuate Galpha(i)-mediated lysophosphatidic acid signaling pathways in ovarian cancer cells. *Cell Signal* **20**: 381-389.

Hurst JH, Hooks SB (2009). Lysophosphatidic acid stimulates cell growth by different mechanisms in SKOV-3 and Caov-3 ovarian cancer cells: distinct roles for Gi- and Rho-dependent pathways. *Pharmacology* **83**: 333-347.

Hurst JH, Mendpara N, Hooks SB (2009). Regulator of G-protein signalling expression and function in ovarian cancer cell lines. *Cell Mol Biol Lett* **14**: 153-174.

- Inoki K, Li Y, Xu T, Guan KL (2003). Rheb GTPase is a direct target of TSC2 GAP activity and regulates mTOR signaling. *Genes & development* **17**: 1829-1834.
- Jackson AL, Linsley PS (2010). Recognizing and avoiding siRNA off-target effects for target identification and therapeutic application. *Nat Rev Drug Discov* **9**: 57-67.
- Jackson DB, Sood AK (2011). Personalized cancer medicine--advances and socio-economic challenges. *Nat Rev Clin Oncol* **8**: 735-741.
- James MA, Lu Y, Liu Y, Vikis HG, You M (2009). RGS17, an overexpressed gene in human lung and prostate cancer, induces tumor cell proliferation through the cyclic AMP-PKA-CREB pathway. *Cancer Res* **69**: 2108-2116.
- Jardim DL, Wheler JJ, Hess K, Tsimberidou AM, Zinner R, Janku F *et al* (2014). FBXW7 mutations in patients with advanced cancers: clinical and molecular characteristics and outcomes with mTOR inhibitors. *PLoS One* **9**: e89388.
- Jemal A, Thomas A, Murray T, Thun M (2002). Cancer statistics, 2002. *CA Cancer J Clin* **52**: 23-47.
- Jemal A, Siegel R, Ward E, Hao Y, Xu J, Murray T *et al* (2008). Cancer statistics, 2008. *CA Cancer J Clin* **58**: 71-96.
- Jemal A, Siegel R, Xu J, Ward E (2010). Cancer statistics, 2010. *CA Cancer J Clin* **60**: 277-300.
- Jemal A, Simard EP, Dorell C, Noone AM, Markowitz LE, Kohler B *et al* (2013). Annual Report to the Nation on the Status of Cancer, 1975-2009, featuring the burden and trends in human papillomavirus(HPV)-associated cancers and HPV vaccination coverage levels. *J Natl Cancer Inst* **105**: 175-201.
- Jia W, Eneh JO, Ratnaparkhe S, Altman MK, Murph MM (2011). MicroRNA-30c-2* expressed in ovarian cancer cells suppresses growth factor-induced cellular proliferation and downregulates the oncogene BCL9. *Mol Cancer Res* **9**: 1732-1745.
- Jiang G, Xu Y, Fujiwara Y, Tsukahara T, Tsukahara R, Gajewiak J *et al* (2007). Alpha-substituted phosphonate analogues of lysophosphatidic acid (LPA) selectively inhibit production and action of LPA. *ChemMedChem* **2**: 679-690.
- Jiang H, Vogt PK (2008). Constitutively active Rheb induces oncogenic transformation. *Oncogene* **27**: 5729-5740.
- Jin Y, An X, Ye Z, Cully B, Wu J, Li J (2009). RGS5, a hypoxia-inducible apoptotic stimulator in endothelial cells. *J Biol Chem* **284**: 23436-23443.

- Kam CM, Gotz MG, Koot G, McGuire M, Thiele D, Hudig D *et al* (2004). Design and evaluation of inhibitors for dipeptidyl peptidase I (Cathepsin C). *Arch Biochem Biophys* **427**: 123-134.
- Kam Y, Exton JH (2004). Role of phospholipase D1 in the regulation of mTOR activity by lysophosphatidic acid. *FASEB journal : official publication of the Federation of American Societies for Experimental Biology* **18**: 311-319.
- Kamat AA, Kim TJ, Landen CN, Jr., Lu C, Han LY, Lin YG *et al* (2007). Metronomic chemotherapy enhances the efficacy of antivasular therapy in ovarian cancer. *Cancer Res* **67**: 281-288.
- Kamrava M, Simpkins F, Alejandro E, Michener C, Meltzer E, Kohn EC (2005). Lysophosphatidic acid and endothelin-induced proliferation of ovarian cancer cell lines is mitigated by neutralization of granulip-epithelin precursor (GEP), a prosurvival factor for ovarian cancer. *Oncogene* **24**: 7084-7093.
- Kerbel RS (2003). Human tumor xenografts as predictive preclinical models for anticancer drug activity in humans: better than commonly perceived-but they can be improved. *Cancer Biol Ther* **2**: S134-139.
- Keunen O, Johansson M, Oudin A, Sanzey M, Rahim SA, Fack F *et al* (2011). Anti-VEGF treatment reduces blood supply and increases tumor cell invasion in glioblastoma. *Proc Natl Acad Sci U S A* **108**: 3749-3754.
- Kimple AJ, Bosch DE, Giguere PM, Siderovski DP (2011). Regulators of G-protein signaling and their Galpha substrates: promises and challenges in their use as drug discovery targets. *Pharmacol Rev* **63**: 728-749.
- Kishi Y, Okudaira S, Tanaka M, Hama K, Shida D, Kitayama J *et al* (2006). Autotaxin is overexpressed in glioblastoma multiforme and contributes to cell motility of glioblastoma by converting lysophosphatidylcholine to lysophosphatidic acid. *J Biol Chem* **281**: 17492-17500.
- Kotarsky K, Boketoft A, Bristulf J, Nilsson NE, Norberg A, Hansson S *et al* (2006). Lysophosphatidic acid binds to and activates GPR92, a G protein-coupled receptor highly expressed in gastrointestinal lymphocytes. *J Pharmacol Exp Ther* **318**: 619-628.
- Labuda M, Laberge S, Briere J, Berube D, Krajcinovic M (2013). RGS5 gene and therapeutic response to short acting bronchodilators in paediatric asthma patients. *Pediatr Pulmonol* **48**: 970-975.
- Lappano R, Maggiolini M (2011). G protein-coupled receptors: novel targets for drug discovery in cancer. *Nat Rev Drug Discov* **10**: 47-60.

Lee CW, Rivera R, Gardell S, Dubin AE, Chun J (2006a). GPR92 as a new G12/13- and Gq-coupled lysophosphatidic acid receptor that increases cAMP, LPA5. *J Biol Chem* **281**: 23589-23597.

Lee JK, McCoy MK, Harms AS, Ruhn KA, Gold SJ, Tansey MG (2008a). Regulator of G-protein signaling 10 promotes dopaminergic neuron survival via regulation of the microglial inflammatory response. *The Journal of neuroscience : the official journal of the Society for Neuroscience* **28**: 8517-8528.

Lee JK, Chung J, McAlpine FE, Tansey MG (2011). Regulator of G-protein signaling-10 negatively regulates NF-kappaB in microglia and neuroprotects dopaminergic neurons in hemiparkinsonian rats. *J Neurosci* **31**: 11879-11888.

Lee SJ, Chan TH, Chen TC, Liao BK, Hwang PP, Lee H (2008b). LPA1 is essential for lymphatic vessel development in zebrafish. *FASEB J* **22**: 3706-3715.

Lee Z, Swaby RF, Liang Y, Yu S, Liu S, Lu KH *et al* (2006b). Lysophosphatidic acid is a major regulator of growth-regulated oncogene alpha in ovarian cancer. *Cancer Res* **66**: 2740-2748.

Lefkowitz RJ, Kobilka BK, Caron MG (1989). The new biology of drug receptors. *Biochem Pharmacol* **38**: 2941-2948.

Li M, Balch C, Montgomery JS, Jeong M, Chung JH, Yan P *et al* (2009). Integrated analysis of DNA methylation and gene expression reveals specific signaling pathways associated with platinum resistance in ovarian cancer. *BMC Med Genomics* **2**: 34.

Lindqvist L, Pelletier J (2009). Inhibitors of translation initiation as cancer therapeutics. *Future Med Chem* **1**: 1709-1722.

Liu S, Murph M, Panupinthu N, Mills GB (2009a). ATX-LPA receptor axis in inflammation and cancer. *Cell Cycle* **8**: 3695-3701.

Liu S, Umez-Goto M, Murph M, Lu Y, Liu W, Zhang F *et al* (2009b). Expression of autotaxin and lysophosphatidic acid receptors increases mammary tumorigenesis, invasion, and metastases. *Cancer Cell* **15**: 539-550.

Long J, Darroch P, Wan KF, Kong KC, Ktistakis N, Pyne NJ *et al* (2005a). Regulation of cell survival by lipid phosphate phosphatases involves the modulation of intracellular phosphatidic acid and sphingosine 1-phosphate pools. *Biochem J* **391**: 25-32.

Long X, Lin Y, Ortiz-Vega S, Yonezawa K, Avruch J (2005b). Rheb binds and regulates the mTOR kinase. *Current biology : CB* **15**: 702-713.

Loukinova E, Dong G, Enamorado-Ayalya I, Thomas GR, Chen Z, Schreiber H *et al* (2000). Growth regulated oncogene-alpha expression by murine squamous cell carcinoma

promotes tumor growth, metastasis, leukocyte infiltration and angiogenesis by a host CXC receptor-2 dependent mechanism. *Oncogene* **19**: 3477-3486.

Lu CH, Wyszomierski SL, Tseng LM, Sun MH, Lan KH, Neal CL *et al* (2007). Preclinical testing of clinically applicable strategies for overcoming trastuzumab resistance caused by PTEN deficiency. *Clinical cancer research : an official journal of the American Association for Cancer Research* **13**: 5883-5888.

Mabuchi S, Kawase C, Altomare DA, Morishige K, Sawada K, Hayashi M *et al* (2009). mTOR is a promising therapeutic target both in cisplatin-sensitive and cisplatin-resistant clear cell carcinoma of the ovary. *Clinical cancer research : an official journal of the American Association for Cancer Research* **15**: 5404-5413.

Mansfield AS, Markovic SN (2013). Inhibition of angiogenesis for the treatment of metastatic melanoma. *Curr Oncol Rep* **15**: 492-499.

Manzur M, Hamzah J, Ganss R (2008). Modulation of the "blood-tumor" barrier improves immunotherapy. *Cell Cycle* **7**: 2452-2455.

Manzur M, Hamzah J, Ganss R (2009). Modulation of g protein signaling normalizes tumor vessels. *Cancer Res* **69**: 396-399.

Mao H, Zhao Q, Daigle M, Ghahremani MH, Chidiac P, Albert PR (2004). RGS17/RGSZ2, a novel regulator of Gi/o, Gz, and Gq signaling. *J Biol Chem* **279**: 26314-26322.

Marinissen MJ, Gutkind JS (2001). G-protein-coupled receptors and signaling networks: emerging paradigms. *Trends Pharmacol Sci* **22**: 368-376.

Masuda A, Nakamura K, Izutsu K, Igarashi K, Ohkawa R, Jona M *et al* (2008). Serum autotaxin measurement in haematological malignancies: a promising marker for follicular lymphoma. *Br J Haematol* **143**: 60-70.

Mazzoletti M, Bortolin F, Brunelli L, Pastorelli R, Di Giandomenico S, Erba E *et al* (2011). Combination of PI3K/mTOR inhibitors: antitumor activity and molecular correlates. *Cancer Res* **71**: 4573-4584.

McCoy KL, Hepler JR (2009). Regulators of G protein signaling proteins as central components of G protein-coupled receptor signaling complexes. *Prog Mol Biol Transl Sci* **86**: 49-74.

McIntyre TM, Pontsler AV, Silva AR, St Hilaire A, Xu Y, Hinshaw JC *et al* (2003). Identification of an intracellular receptor for lysophosphatidic acid (LPA): LPA is a transcellular PPARgamma agonist. *Proc Natl Acad Sci U S A* **100**: 131-136.

Mills GB, Moolenaar WH (2003). The emerging role of lysophosphatidic acid in cancer. *Nat Rev Cancer* **3**: 582-591.

Minchinton AI, Tannock IF (2006). Drug penetration in solid tumours. *Nat Rev Cancer* **6**: 583-592.

Mitchell TS, Bradley J, Robinson GS, Shima DT, Ng YS (2008). RGS5 expression is a quantitative measure of pericyte coverage of blood vessels. *Angiogenesis* **11**: 141-151.

Mitchell TS BJ, Robinson GS, Shima DT, Ng YS. (2008). RGS5 expression is a quantitative measure of pericyte coverage of blood vessels. *Angiogenesis* **11**: 141-151.

Mu H, Calderone TL, Davies MA, Prieto VG, Wang H, Mills GB *et al* (2012). Lysophosphatidic acid induces lymphangiogenesis and IL-8 production in vitro in human lymphatic endothelial cells. *Am J Pathol* **180**: 2170-2181.

Mukai M, Iwasaki T, Tatsuta M, Togawa A, Nakamura H, Murakami-Murofushi K *et al* (2003). Cyclic phosphatidic acid inhibits RhoA-mediated autophosphorylation of FAK at Tyr-397 and subsequent tumor-cell invasion. *Int J Oncol* **22**: 1247-1256.

Murakami-Murofushi K, Shioda M, Kaji K, Yoshida S, Murofushi H (1992). Inhibition of eukaryotic DNA polymerase alpha with a novel lysophosphatidic acid (PHYLPA) isolated from myxoamoebae of *Physarum polycephalum*. *J Biol Chem* **267**: 21512-21517.

Murakami M, Shiraishi A, Tabata K, Fujita N (2008). Identification of the orphan GPCR, P2Y(10) receptor as the sphingosine-1-phosphate and lysophosphatidic acid receptor. *Biochem Biophys Res Commun* **371**: 707-712.

Murph M, Tanaka T, Liu S, Mills GB (2006). Of spiders and crabs: the emergence of lysophospholipids and their metabolic pathways as targets for therapy in cancer. *Clin Cancer Res* **12**: 6598-6602.

Murph M, Mills GB (2007). Targeting the lipids LPA and S1P and their signalling pathways to inhibit tumour progression. *Expert Rev Mol Med* **9**: 1-18.

Murph MM, Hurst-Kennedy J, Newton V, Brindley DN, Radhakrishna H (2007). Lysophosphatidic acid decreases the nuclear localization and cellular abundance of the p53 tumor suppressor in A549 lung carcinoma cells. *Mol Cancer Res* **5**: 1201-1211.

Murph MM, Liu W, Yu S, Lu Y, Hall H, Hennessy BT *et al* (2009). Lysophosphatidic acid-induced transcriptional profile represents serous epithelial ovarian carcinoma and worsened prognosis. *PLoS One* **4**: e5583.

Nakai Y, Ikeda H, Nakamura K, Kume Y, Fujishiro M, Sasahira N *et al* (2011). Specific increase in serum autotaxin activity in patients with pancreatic cancer. *Clin Biochem*.

Nam SW, Clair T, Kim YS, McMarlin A, Schiffmann E, Liotta LA *et al* (2001). Autotaxin (NPP-2), a metastasis-enhancing motogen, is an angiogenic factor. *Cancer Res* **61**: 6938-6944.

Nguyen D, Nguyen O, Zhang H, Prestwich GD, Murph MM (2011). A Bromophosphonate Analogue of Lysophosphatidic Acid Surpasses Dacarbazine in Reducing Cell Proliferation and Viability of MeWo Melanoma Cells. In: Murph MM (ed). *Research on Melanoma - A Glimpse into Current Directions and Future Trends*. InTech.

Nishimasu H, Okudaira S, Hama K, Mihara E, Dohmae N, Inoue A *et al* (2011). Crystal structure of autotaxin and insight into GPCR activation by lipid mediators. *Nat Struct Mol Biol* **18**: 205-212.

Noguchi K, Ishii S, Shimizu T (2003). Identification of p2y9/GPR23 as a novel G protein-coupled receptor for lysophosphatidic acid, structurally distant from the Edg family. *J Biol Chem* **278**: 25600-25606.

Nunn C, Mao H, Chidiac P, Albert PR (2006). RGS17/RGSZ2 and the RZ/A family of regulators of G-protein signaling. *Semin Cell Dev Biol* **17**: 390-399.

Ovens K, Naugler C (2012). Preliminary evidence of different selection pressures on cancer cells as compared to normal tissues. *Theor Biol Med Model* **9**: 44.

Oyesanya RA, Greenbaum S, Dang D, Lee Z, Mukherjee A, Wu J *et al* (2010). Differential requirement of the epidermal growth factor receptor for G protein-mediated activation of transcription factors by lysophosphatidic acid. *Mol Cancer* **9**: 8.

Papandreou I, Cairns RA, Fontana L, Lim AL, Denko NC (2006). HIF-1 mediates adaptation to hypoxia by actively downregulating mitochondrial oxygen consumption. *Cell Metab* **3**: 187-197.

Pasternack SM, von Kugelgen I, Al Aboud K, Lee YA, Ruschendorf F, Voss K *et al* (2008). G protein-coupled receptor P2Y5 and its ligand LPA are involved in maintenance of human hair growth. *Nat Genet* **40**: 329-334.

Perrakis A, Moolenaar WH (2014). Autotaxin: structure-function and signaling. *J Lipid Res*.

Prestwich GD, Gajewiak J, Zhang H, Xu X, Yang G, Serban M (2008). Phosphatase-resistant analogues of lysophosphatidic acid: agonists promote healing, antagonists and autotaxin inhibitors treat cancer. *Biochim Biophys Acta* **1781**: 588-594.

Ptaszynska MM, Pendrak ML, Bandle RW, Stracke ML, Roberts DD (2008). Positive feedback between vascular endothelial growth factor-A and autotaxin in ovarian cancer cells. *Mol Cancer Res* **6**: 352-363.

Ptaszynska MM, Pendrak ML, Stracke ML, Roberts DD (2010). Autotaxin signaling via lysophosphatidic acid receptors contributes to vascular endothelial growth factor-induced endothelial cell migration. *Mol Cancer Res* **8**: 309-321.

Pyrko P, Kardosh A, Wang W, Xiong W, Schonthal AH, Chen TC (2007). HIV-1 protease inhibitors nelfinavir and atazanavir induce malignant glioma death by triggering endoplasmic reticulum stress. *Cancer Res* **67**: 10920-10928.

Qin JY, Zhang L, Clift KL, Huler I, Xiang AP, Ren BZ *et al* (2010). Systematic comparison of constitutive promoters and the doxycycline-inducible promoter. *PLoS One* **5**: e10611.

Qin M, Huang H, Wang T, Hu H, Liu Y, Cao H *et al* (2012). Absence of Rgs5 prolongs cardiac repolarization and predisposes to ventricular tachyarrhythmia in mice. *J Mol Cell Cardiol* **53**: 880-890.

Rao SS, Thompson C, Cheng J, Haimovitz-Friedman A, Powell SN, Fuks Z *et al* (2014). Axitinib sensitization of high Single Dose Radiotherapy. *Radiother Oncol*.

Rhodes DR, Yu J, Shanker K, Deshpande N, Varambally R, Ghosh D *et al* (2004). ONCOMINE: a cancer microarray database and integrated data-mining platform. *Neoplasia* **6**: 1-6.

Richmond A, Yang J, Su Y (2009). The good and the bad of chemokines/chemokine receptors in melanoma. *Pigment Cell Melanoma Res* **22**: 175-186.

Riker AI, Enkemann SA, Fodstad O, Liu S, Ren S, Morris C *et al* (2008). The gene expression profiles of primary and metastatic melanoma yields a transition point of tumor progression and metastasis. *BMC Med Genomics* **1**: 13.

Rivero G, Gabilondo AM, Garcia-Sevilla JA, La Harpe R, Morentin B, Javier Meana J (2010). Characterization of regulators of G-protein signaling RGS4 and RGS10 proteins in the postmortem human brain. *Neurochem Int* **57**: 722-729.

Rosano L, Spinella F, Bagnato A (2013). Endothelin 1 in cancer: biological implications and therapeutic opportunities. *Nat Rev Cancer* **13**: 637-651.

Ross EM, Gilman AG (1977). Reconstitution of catecholamine-sensitive adenylate cyclase activity: interactions of solubilized components with receptor-replete membranes. *Proc Natl Acad Sci U S A* **74**: 3715-3719.

Rossmann KL, Der CJ, Sondek J (2005). GEF means go: turning on RHO GTPases with guanine nucleotide-exchange factors. *Nat Rev Mol Cell Biol* **6**: 167-180.

Rzychon M, Chmiel D, Stec-Niemczyk J (2004). Modes of inhibition of cysteine proteases. *Acta Biochim Pol* **51**: 861-873.

- Saffert RT, Kalejta RF (2007). Human cytomegalovirus gene expression is silenced by Daxx-mediated intrinsic immune defense in model latent infections established in vitro. *J Virol* **81**: 9109-9120.
- Samadi N, Gaetano C, Goping IS, Brindley DN (2009). Autotaxin protects MCF-7 breast cancer and MDA-MB-435 melanoma cells against Taxol-induced apoptosis. *Oncogene* **28**: 1028-1039.
- Sambi BS, Hains MD, Waters CM, Connell MC, Willard FS, Kimple AJ *et al* (2006). The effect of RGS12 on PDGFbeta receptor signalling to p42/p44 mitogen activated protein kinase in mammalian cells. *Cell Signal* **18**: 971-981.
- Sancho-Martinez SM, Prieto-Garcia L, Prieto M, Lopez-Novoa JM, Lopez-Hernandez FJ (2012). Subcellular targets of cisplatin cytotoxicity: an integrated view. *Pharmacol Ther* **136**: 35-55.
- Sander JD, Joung JK (2014). CRISPR-Cas systems for editing, regulating and targeting genomes. *Nat Biotechnol* **32**: 347-355.
- Saponaro C, Malfettone A, Ranieri G, Danza K, Simone G, Paradiso A *et al* (2013). VEGF, HIF-1alpha expression and MVD as an angiogenic network in familial breast cancer. *PLoS One* **8**: e53070.
- Saunders LP, Ouellette A, Bandle R, Chang WC, Zhou H, Misra RN *et al* (2008). Identification of small-molecule inhibitors of autotaxin that inhibit melanoma cell migration and invasion. *Mol Cancer Ther* **7**: 3352-3362.
- Schewe DM, Aguirre-Ghiso JA (2008). ATF6alpha-Rheb-mTOR signaling promotes survival of dormant tumor cells in vivo. *Proceedings of the National Academy of Sciences of the United States of America* **105**: 10519-10524.
- Seki N, Sugano S, Suzuki Y, Nakagawara A, Ohira M, Muramatsu M *et al* (1998). Isolation, tissue expression, and chromosomal assignment of human RGS5, a novel G-protein signaling regulator gene. *J Hum Genet* **43**: 202-205.
- Sethakorn N, Yau DM, Dulin NO (2010). Non-canonical functions of RGS proteins. *Cell Signal* **22**: 1274-1281.
- Shah BH, Baukal AJ, Shah FB, Catt KJ (2005). Mechanisms of extracellularly regulated kinases 1/2 activation in adrenal glomerulosa cells by lysophosphatidic acid and epidermal growth factor. *Mol Endocrinol* **19**: 2535-2548.
- Shao M, Hollar S, Chambliss D, Schmitt J, Emerson R, Chelladurai B *et al* (2012). Targeting the insulin growth factor and the vascular endothelial growth factor pathways in ovarian cancer. *Mol Cancer Ther* **11**: 1576-1586.

Shor B, Zhang WG, Toral-Barza L, Lucas J, Abraham RT, Gibbons JJ *et al* (2008). A new pharmacologic action of CCI-779 involves FKBP12-independent inhibition of mTOR kinase activity and profound repression of global protein synthesis. *Cancer research* **68**: 2934-2943.

Siderovski DP, Willard FS (2005). The GAPs, GEFs, and GDIs of heterotrimeric G-protein alpha subunits. *Int J Biol Sci* **1**: 51-66.

Siegel R, Naishadham D, Jemal A (2013). Cancer statistics, 2013. *CA Cancer J Clin* **63**: 11-30.

Silini A, Ghilardi C, Figini S, Sangalli F, Fruscio R, Dahse R *et al* (2012). Regulator of G-protein signaling 5 (RGS5) protein: a novel marker of cancer vasculature elicited and sustained by the tumor's proangiogenic microenvironment. *Cell Mol Life Sci* **69**: 1167-1178.

Singh AD, Sisley K, Xu Y, Li J, Faber P, Plummer SJ *et al* (2007). Reduced expression of autotaxin predicts survival in uveal melanoma. *Br J Ophthalmol* **91**: 1385-1392.

Smith EN, Bloss CS, Badner JA, Barrett T, Belmonte PL, Berrettini W *et al* (2009). Genome-wide association study of bipolar disorder in European American and African American individuals. *Mol Psychiatry* **14**: 755-763.

Sorensen G, Emblem K, Polaskova P, Jennings D, Kim H, Ancukiewicz M *et al* (2012). Increased Survival of Glioblastoma Patients Who Respond to Antiangiogenic Therapy with Elevated Blood Perfusion. *Cancer Res* **72**: 402-408.

Spencer SL, Gerety RA, Pienta KJ, Forrest S (2006). Modeling somatic evolution in tumorigenesis. *PLoS Comput Biol* **2**: e108.

St-Coeur PD, Ferguson D, Morin P, Jr., Touaibia M (2013). PF-8380 and closely related analogs: synthesis and structure-activity relationship towards autotaxin inhibition and glioma cell viability. *Arch Pharm (Weinheim)* **346**: 91-97.

Sternweis PC, Northup JK, Smigel MD, Gilman AG (1981). The regulatory component of adenylate cyclase. Purification and properties. *J Biol Chem* **256**: 11517-11526.

Stracke ML, Krutzsch HC, Unsworth EJ, Arestad A, Cioce V, Schiffmann E *et al* (1992). Identification, purification, and partial sequence analysis of autotaxin, a novel motility-stimulating protein. *J Biol Chem* **267**: 2524-2529.

Tabata K, Baba K, Shiraishi A, Ito M, Fujita N (2007). The orphan GPCR GPR87 was deorphanized and shown to be a lysophosphatidic acid receptor. *Biochem Biophys Res Commun* **363**: 861-866.

- Tanaka M, Okudaira S, Kishi Y, Ohkawa R, Iseki S, Ota M *et al* (2006). Autotaxin stabilizes blood vessels and is required for embryonic vasculature by producing lysophosphatidic acid. *J Biol Chem* **281**: 25822-25830.
- Tannock IF (2001). Tumor physiology and drug resistance. *Cancer Metastasis Rev* **20**: 123-132.
- Tee AR, Manning BD, Roux PP, Cantley LC, Blenis J (2003). Tuberous sclerosis complex gene products, Tuberin and Hamartin, control mTOR signaling by acting as a GTPase-activating protein complex toward Rheb. *Current biology : CB* **13**: 1259-1268.
- Tee AR, Blenis J, Proud CG (2005). Analysis of mTOR signaling by the small G-proteins, Rheb and RhebL1. *FEBS Lett* **579**: 4763-4768.
- Tesmer JJ, Sunahara RK, Gilman AG, Sprang SR (1997). Crystal structure of the catalytic domains of adenylyl cyclase in a complex with G α .GTP γ S. *Science* **278**: 1907-1916.
- Tibes R, Qiu Y, Lu Y, Hennessy B, Andreeff M, Mills GB *et al* (2006). Reverse phase protein array: validation of a novel proteomic technology and utility for analysis of primary leukemia specimens and hematopoietic stem cells. *Molecular cancer therapeutics* **5**: 2512-2521.
- Tokumura A, Kume T, Fukuzawa K, Tahara M, Tasaka K, Aoki J *et al* (2007). Peritoneal fluids from patients with certain gynecologic tumor contain elevated levels of bioactive lysophospholipase D activity. *Life Sci* **80**: 1641-1649.
- Tredan O, Galmarini CM, Patel K, Tannock IF (2007). Drug resistance and the solid tumor microenvironment. *J Natl Cancer Inst* **99**: 1441-1454.
- Trzcinska-Daneluti AM, Ly D, Huynh L, Jiang C, Fladd C, Rotin D (2009). High-content functional screen to identify proteins that correct F508del-CFTR function. *Mol Cell Proteomics* **8**: 780-790.
- Tsao H, Atkins MB, Sober AJ (2004). Management of cutaneous melanoma. *N Engl J Med* **351**: 998-1012.
- Tsurutani J, West KA, Sayyah J, Gills JJ, Dennis PA (2005). Inhibition of the phosphatidylinositol 3-kinase/Akt/mammalian target of rapamycin pathway but not the MEK/ERK pathway attenuates laminin-mediated small cell lung cancer cellular survival and resistance to imatinib mesylate or chemotherapy. *Cancer research* **65**: 8423-8432.
- Uchiyama A, Mukai M, Fujiwara Y, Kobayashi S, Kawai N, Murofushi H *et al* (2007). Inhibition of transcellular tumor cell migration and metastasis by novel carba-derivatives of cyclic phosphatidic acid. *Biochim Biophys Acta* **1771**: 103-112.

- Ueda K, Yoshihara M, Nakao M, Tanaka T, Sano S, Fukuzawa K *et al* (2010). Evaluation of inhibitory actions of flavonols and related substances on lysophospholipase D activity of serum autotaxin by a convenient assay using a chromogenic substrate. *J Agric Food Chem* **58**: 6053-6063.
- Umezū-Goto M, Kishi Y, Taira A, Hama K, Dohmae N, Takio K *et al* (2002). Autotaxin has lysophospholipase D activity leading to tumor cell growth and motility by lysophosphatidic acid production. *J Cell Biol* **158**: 227-233.
- Valentine WJ, Fujiwara Y, Tsukahara R, Tigyi G (2008). Lysophospholipid signaling: beyond the EDGs. *Biochim Biophys Acta* **1780**: 597-605.
- van Meeteren LA, Ruurs P, Christodoulou E, Goding JW, Takakusa H, Kikuchi K *et al* (2005). Inhibition of autotaxin by lysophosphatidic acid and sphingosine 1-phosphate. *J Biol Chem* **280**: 21155-21161.
- van Meeteren LA, Ruurs P, Stortelers C, Bouwman P, van Rooijen MA, Pradere JP *et al* (2006). Autotaxin, a secreted lysophospholipase D, is essential for blood vessel formation during development. *Mol Cell Biol* **26**: 5015-5022.
- Vezina C, Kudelski A, Sehgal SN (1975). Rapamycin (AY-22,989), a new antifungal antibiotic. I. Taxonomy of the producing streptomycete and isolation of the active principle. *The Journal of antibiotics* **28**: 721-726.
- Wagle N, Emery C, Berger MF, Davis MJ, Sawyer A, Pochanard P *et al* (2011). Dissecting therapeutic resistance to RAF inhibition in melanoma by tumor genomic profiling. *J Clin Oncol* **29**: 3085-3096.
- Wang X, Seed B (2003). A PCR primer bank for quantitative gene expression analysis. *Nucleic Acids Res* **31**: e154.
- Warburg O (1956). On respiratory impairment in cancer cells. *Science* **124**: 269-270.
- Watanabe N, Ikeda H, Nakamura K, Ohkawa R, Kume Y, Aoki J *et al* (2007). Both plasma lysophosphatidic acid and serum autotaxin levels are increased in chronic hepatitis C. *J Clin Gastroenterol* **41**: 616-623.
- Wei Q, St Clair JB, Fu T, Stratton P, Nieman LK (2009). Reduced expression of biomarkers associated with the implantation window in women with endometriosis. *Fertil Steril* **91**: 1686-1691.
- Weinberg R (2014). *The Biology of Cancer, Second Edition*. Garland Science.
- Weinberg RA (2007a). *The biology of cancer*. Garland Science: New York.

- Weinberg RA (ed) (2007b) *The Biology of Cancer*. Garland Science, Taylor & Francis Group: New York, NY, 796pp.
- Weis SM, Cheresh DA (2005). Pathophysiological consequences of VEGF-induced vascular permeability. *Nature* **437**: 497-504.
- Willars GB (2006). Mammalian RGS proteins: multifunctional regulators of cellular signalling. *Semin Cell Dev Biol* **17**: 363-376.
- Xiao B, Zhang Y, Niu WQ, Gao PJ, Zhu DL (2009). Haplotype-based association of regulator of G-protein signaling 5 gene polymorphisms with essential hypertension and metabolic parameters in Chinese. *Clin Chem Lab Med* **47**: 1483-1488.
- Xu X, Yang G, Zhang H, Prestwich GD (2009). Evaluating dual activity LPA receptor pan-antagonist/autotaxin inhibitors as anti-cancer agents in vivo using engineered human tumors. *Prostaglandins Other Lipid Mediat* **89**: 140-146.
- Xu X, Prestwich GD (2010). Inhibition of tumor growth and angiogenesis by a lysophosphatidic acid antagonist in an engineered three-dimensional lung cancer xenograft model. *Cancer* **116**: 1739-1750.
- Xu Y, Jiang G, Tsukahara R, Fujiwara Y, Tigyi G, Prestwich GD (2006). Phosphonothioate and fluoromethylene phosphonate analogues of cyclic phosphatidic acid: Novel antagonists of lysophosphatidic acid receptors. *J Med Chem* **49**: 5309-5315.
- Yang S, Li YP (2007). RGS10-null mutation impairs osteoclast differentiation resulting from the loss of [Ca²⁺]_i oscillation regulation. *Genes Dev* **21**: 1803-1816.
- Yau DM, Sethakorn N, Taurin S, Kregel S, Sandbo N, Camoretti-Mercado B *et al* (2008). Regulation of Smad-mediated gene transcription by RGS3. *Mol Pharmacol* **73**: 1356-1361.
- Ye X, Fukushima N, Kingsbury MA, Chun J (2002). Lysophosphatidic acid in neural signaling. *Neuroreport* **13**: 2169-2175.
- Ye X, Hama K, Contos JJ, Anliker B, Inoue A, Skinner MK *et al* (2005). LPA3-mediated lysophosphatidic acid signalling in embryo implantation and spacing. *Nature* **435**: 104-108.
- Ye X (2008). Lysophospholipid signaling in the function and pathology of the reproductive system. *Hum Reprod Update* **14**: 519-536.
- Yu S, Murph MM, Lu Y, Liu S, Hall HS, Liu J *et al* (2008). Lysophosphatidic acid receptors determine tumorigenicity and aggressiveness of ovarian cancer cells. *J Natl Cancer Inst* **100**: 1630-1642.

Zastre J, Anantha M, Ramsay E, Bally M (2007). Irinotecan-cisplatin interactions assessed in cell-based screening assays: cytotoxicity, drug accumulation and DNA adduct formation in an NSCLC cell line. *Cancer Chemother Pharmacol* **60**: 91-102.

Zhang H, Xu X, Gajewiak J, Tsukahara R, Fujiwara Y, Liu J *et al* (2009). Dual activity lysophosphatidic acid receptor pan-antagonist/autotaxin inhibitor reduces breast cancer cell migration in vitro and causes tumor regression in vivo. *Cancer Res* **69**: 5441-5449.

Zhang Y, Gao X, Saucedo LJ, Ru B, Edgar BA, Pan D (2003). Rheb is a direct target of the tuberous sclerosis tumour suppressor proteins. *Nature cell biology* **5**: 578-581.

Zhao P, Nunn C, Ramineni S, Hepler JR, Chidiac P (2013). The Ras-binding domain region of RGS14 regulates its functional interactions with heterotrimeric G proteins. *J Cell Biochem* **114**: 1414-1423.

Zhou J, Moroi K, Nishiyama M, Usui H, Seki N, Ishida J *et al* (2001). Characterization of RGS5 in regulation of G protein-coupled receptor signaling. *Life Sci* **68**: 1457-1469.

APPENDICES

